Machinability of Polypropylene Biocomposites Reinforced With Natural Fibers and Biocarbon Particles

by

Dinh Son TRAN

MANUSCRIPT-BASED THESIS PRESENTED TO ÉCOLE DE TECHNOLOGIE SUPÉRIEURE IN PARTIAL FULFILLMENT FOR THE DEGREE OF DOCTOR OF PHILOSOPHY
Ph.D.

MONTREAL, DECEMBER 16, 2020

ÉCOLE DE TECHNOLOGIE SUPÉRIEURE
UNIVERSITÉ DU QUÉBEC

BOARD OF EXAMINERS

THIS THESIS HAS BEEN EVALUATED

BY THE FOLLOWING BOARD OF EXAMINERS

Mr. Victor Songmene, Thesis Supervisor
Department of Mechanical Engineering at École de Technologie Supérieure

Mr. Anh Dung Ngo, Thesis Co-supervisor
Department of Mechanical Engineering at École de Technologie Supérieure

Mr. Simon Joncas, President of the Board of Examiners
Department of Systems Engineering at École de Technologie Supérieure

Mr. Marek Balazinski, External Evaluator
Department of Mechanical Engineering at École Polytechnique Montréal

Mr. Mouhab Meshreki, Independent External Evaluator
Aerospace Research Centre, National Research Council Canada

THIS THESIS WAS PRENSENTED AND DEFENDED

IN THE PRESENCE OF A BOARD OF EXAMINERS AND PUBLIC

ON DECEMBER 08th, 2020

AT ÉCOLE DE TECHNOLOGIE SUPÉRIEURE

ACKNOWLEDGMENT

I would like to express my deep gratitude to my Supervisor, Professor Victor Songmene, who supports me a lot in both academic and financial aids. He assists me in correcting manuscripts submitted in scientific journals. He also helps me throughout my Ph.D. study. Without his support and encouragement, this thesis could not be completed.

I would like to be grateful to my Co-supervisor, Professor Anh Dung Ngo, who accepted me as his Ph. D. student at ETS. He provides financial aids and helps me understand more about composite materials. This thesis could not be completed without his extreme support and assistance.

I would like to give my gratitude to the Vietnam Ministry of Education and Training for the scholarship grant to facilitate my study in Canada. I cannot say enough words to thank my colleagues at the University of Danang – University of Science and Technology, who support me a lot in my Ph.D. study.

I would like to thank Dr. Jules Kouam and the technical team at LIPPS laboratory (ETS) for assisting me in carrying out the experiments.

I would like to send my gratitude to the Bioproducts Discovery and Development Centre at the University of Guelph, Ontario, Canada, for donating biocomposite materials used for this research project.

I am very happy to express my appreciation to my wife, Nguyen Thi Dieu, and to my two daughters, Tran Nguyen Thuc Uyen and Tran Nguyen Thuc Anh, who always encourage and support me in the most difficult times. I could not finish my Ph.D. study without their sacrifices and hardships while I am away from home.

I am very happy to extend my gratitude to my mother, my father, my mother-in-law, my father-in-law, my brothers, and my relatives, who constantly encourage and motivate me while away from home to continue my research work. The completion of my thesis is indispensable for their encouragement.

L'utilisabilité du Bio-composite Polypropylène Renforcé Par les Fibres Naturelles et les Particules de Biocarbone

Dinh Son TRAN

RÉSUMÉ

Les bio-composites sont de plus en plus développés et appliqués dans de nombreux domaines de l'ingénierie. La plus part des pièces en bio-composite sont produites tout près de leur forme finale. Cependant, l'opération d'usinage secondaire est nécessaire pour obtenir la précision dimensionnelle et l'état fini de surface usinée. L'usinabilité du bio-composite est significativement affectée par la méthode d'usinage, le renforcement et la matrice utilisés dans le bio-composite. Par conséquent, il est nécessaire de comprendre le comportement d'usinage d'un bio-composite particulier. Il peut ainsi aider à choisir les paramètres de coupe appropriés pour obtenir la qualité de surface souhaitée lors de l'usinage.

Cette recherche est pour but d'étudier les facteurs clés qui affectent les indicateurs d'usinabilité lors du perçage à sec de nouveaux bio-composites. Ces bio-composites sont constitués de la même matrice (PP/POE/MAPP) renforcée avec différentes teneurs en poids des fibres de miscanthus courtes et des particules de bicarbone : le bio-composite M1 (30wt% de biocarbone), le bio-composites M2 (30wt% de miscanthus) et le bio-composite hybride M3 (15wt% de miscanthus, 15wt% de biocarbone). Un plan factoriel complet a été utilisé comme le plan expérimental pour étudier le comportement d'usinage lors du perçage des bio-composites. Les effets des paramètres d'usinage sur les indicateurs d'usinabilité des bio-composites sont mesurés et analysés.

Les résultats obtenus dans cette recherche ont montré que les paramètres de coupe et le diamètre du foret affectent significativement les indicateurs de performance du processus d'usinage (la force axiale, l'énergie spécifique de coupe, la rugosité de surface, et l'émission de poussières fines) à tous bio-composites considérés. Le type (nature et forme) et la teneur en poids du renfort utilisé dans le bio-composite ont l'influence significative sur les indicateurs d'usinabilité. Les paramètres du perçage ne sont pas statistiquement significatifs pour l'émission des particules ultrafines. La rugosité de surface (Ra) et la force axiale lors du perçage des bio-composites sont prédites en utilisant l'analyse de régression et les modèles basés sur l'ANFIS. Les résultats ont montré la haute précision des modèles prédictifs.

Mots-clés : usinabilité, bio-composite, force axiale, rugosité de surface, émission des poussières fines, renforcement naturel.

Machinability of Polypropylene Biocomposites Reinforced With Natural fibers and Biocarbon Particles

Dinh Son TRAN

ABSTRACT

Biocomposites are increasingly being developed and applied in many engineering fields. Parts made of biocomposites are mostly produced close to their final shape. However, the secondary machining operation is required to achieve dimensional accuracy and surface finish. The machinability of biocomposite is significantly affected by the processing method, the reinforcement, and the matrix used in the biocomposite. Therefore, it is necessary to understand the machining behavior of a particular biocomposite. It could thereby help to choose suitable cutting parameters to obtain the desired surface quality during machining.

This study investigates the key factors that affect the machinability indicators during the dry drilling of new biocomposites. These biocomposites are made of the same matrix (PP/POE/MAPP) reinforced with different weight ratios of chopped miscanthus fibers and biocarbon particles: biocomposite M1 (30wt% biocarbon), biocomposite M2 (30wt % miscanthus), and hybrid biocomposite M3 (15wt% miscanthus, 15wt% biocarbon). A full factorial design was used for the experimental design to study machining behavior during the drilling of biocomposites. The effects of the drilling parameters on the machinability indicators of biocomposites are measured and analyzed.

The results from this research work demonstrated that the cutting parameters and the tool diameters significantly affect the machining process performance indicators (thrust force, specific cutting energy for thrust force, surface roughness, and fine particle emission) for all biocomposites. The type (nature and shape) and the weight ratio of reinforcement used in biocomposite have a significant effect on the machinability indicators. The drilling parameters are not statistically significant for ultrafine particle emission. Surface roughness (R_a) and thrust force in the drilling of biocomposites were predicted using regression analysis and ANFIS-based models. The results showed that predictive models have high predicted accuracy.

Keywords: machinability, biocomposite, thrust force, surface roughess, fine dust emission, natural reinforcements.

TABLE OF CONTENTS

LIST OF TABLES

Page

LIST OF FIGURES

Page

LIST OF ABREVIATIONS

ANFIS	Adaptive Neuro-Fuzzy Inference System
ANN	Artificial Neural Network
ANOVA	Analysis of Variance
APS	Aerodynamic Particles Sizer
BFRP	Banana Fiber Reinforced Polyester
CFRP	Carbon Fiber Reinforced Polymer
CNC	Computer Numerical Control
DMA	Differential Mobility Analyzer
DOE	Design of Experiments
FP	Fine Particles
GA	Genetic Algorithm
GFRP	Glass Fiber Reinforced Polyester
HFRP	Hemp Fiber Reinforced Polyester
HSS	High-Speed Steel
JFRP	Jute Fiber Reinforced Polyester
MA	Maleic Anhydride
MAPE	Mean Absolute Percentage Error
MAPP	Maleic Anhydride grafted Polypropylene
MDF	Medium Density Fiberboard
MF	Membership Function
MQL	Minimum Quantity of Lubrication
MRA	Multivariate Regression Analysis
MRR	Material Removal Rate
NFRP	Natural Fiber Reinforced Polymer
PA	Polyamide
PBAT	Poly(butylene adipate-co- terephthalate)
PBS	Poly(butylene succinate)
PHBV	Poly(3-hydroxybutyrate-co-3-hydroxyvalerate)

PLA	Poly(lactic acid)
PLLA	Poly(L-lactic acid)
POE	Polyolefin elastomer
PP	Polypropylene
RMSE	Root Mean Square Error
RSM	Response Surface Methodology
SEM	Scanning Electron Microscopy
SFRPs	Synthetic Fiber Reinforced Polymer Composites
SMPS	Scanning Mobility Particles Sizer
UFP	Ultrafine Particles

LIST OF SYMBOLS AND UNITS OF MEASUREMENT

d	Drill bit diameter (mm)
f	Feed rate (mm/rev)
F_t	Thrust force (N)
K_t	Specific cutting energy for thrust force (N/mm^2)
R_a	Arithmetic average roughness (μm)
R_t	Maximum height of the profile (μm)
s	Spindle speed (rpm)
v	Cutting speed (m/min)
v_f	Linear feed rate (mm/min)
wt	The weight ratio (%)

INTRODUCTION

In recent years, natural fiber reinforced polymer (NFRP) composites are rapidly being developed and applied in many technical fields such as automotive, aerospace, sports, construction, etc. (Peças et al., 2018). The wide range of their applications is due to the advantages such as low density, abundance in nature, good mechanical properties, low cost, biodegradability, less abrasive damage, less toxic manufacturing process. NFRP composites have many outstanding advantages to replace composite reinforced with synthetic fibers for manufacturing automotive parts to reduce the weight of the vehicles (Chauhan et al., 2019).

NFRP composites reinforced with natural fibers such as flax, jute, hemp, sisal, and kenaf, are commonly used to manufacture automotive parts. They are used to produce internal and external parts of automobiles such as seat pads, door panels, visor skin, luggage compartments, spare tire cover, floor panels, packet tray skin, etc. (Akampumuza et al., 2017). The NFRP composites used in the automotive parts are expected to increase rapidly to significantly reduce the vehicles' weight, which directly leads to a reduction in fuel consumption, thereby reducing carbon dioxide (CO_2) emission and environmental impact. The environmental concerns have driven automakers to invest in developing lightweight-sustainable materials for their products (Faruk et al., 2014).

Parts made of NFRP composites are mostly produced close to the final shape by manufacturing methods such as hand layup, compression molding, extrusion, resin transfer molding. However, a secondary machining operation (e.g., drilling, milling, and turning) is essential to obtain dimensional accuracy and surface finish for products (Lotfi et al., 2019). It is found that there are many studies on the machining of synthetic fiber reinforced polymer composites (SFRPs), while little investigation has been done on the machining of NFRPs. Besides, the results obtained from the machining of SFRPs could not be applied to the machining of NFRPs due to the significant differences in mechanical and thermal properties between synthetic and natural fibers (Nassar et al., 2017). Therefore, the investigation on the machining of a particular NFRP is essential to understand its machining behaviors.

Based on the literature, the machinability of NFRPs depends on many factors such as machining process, tool material and geometry, machining condition, cutting parameters, reinforcements and matrix used in NFRP composite, etc. The choice of cutting tools and parameters for the machining process should be taken into account with the type of reinforcement used in the biocomposite (Nassar et al., 2017). Debnath et al. (2017) have stated that a specific geometry of drill bit is only suitable for cutting a particular composite. Ismail et al. (Ismail, Dhakal, Dimla, et al., 2016) have observed that the poor cutting behavior (higher surface roughness and greater delamination-induced damage) was obtained during the drilling hemp fiber reinforced polycaprolactone as a result of an increase in fiber aspect ratio. Pailoor et al. (2019) have also shown that the machinability during the drilling of jute/PP is greatly affected by the type of fiber (chopped or long fiber), coupling agent, and the weight ratio of fibers used in NFRP composite.

Fine dust generated during the machining process is considered an indicator of machinability and is of interest to some researchers. Several studies of fine dust emitted during machining have been done in recent years. It is shown that the majority of fine dust generated is less than 2.5 microns in size for various materials (Djebara et al., 2013; Haddad et al., 2014). These fine dust particles are easily inhaled into the deepest part of the lung and thereby affecting the machine operator's health (Songmene et al., 2008a). In addition, the fine particles created during machining are significantly influenced by factors such as workpiece material, machining process, tool (material, coating, and geometry), cutting parameters, and cutting conditions. According to the literature, the research on fine dust generated during the machining process mainly focuses on metal and metal matrix composites. In contrast, no publication of fine dust generated when machining biocomposites. Therefore, this is also an issue to consider during the machining of biocomposites.

New biocomposites have been rapidly developed, but manufacturers still need to understand their machining behaviors to meet production needs quickly. In recent years, ANFIS-based models have been applied to predict the machinability indicators during the machining of materials. ANFIS (adaptive neuro-fuzzy inference system) is a soft computing technique that combines the advantages of an artificial neural network and a fuzzy inference system. The

limited empirical data is used to develop an ANFIS-based model, which is highly effective in predicting the factors that affect the machining process performance indicators. It is shown that the ANFIS-based model has slightly better predictive accuracy than the regression analysis model in predicting surface roughness during the turning of high-strength steel (Abbas et al., 2017). Sen et al. (2017) observed that ANFIS-based models produced the predicted values that are more consistent with the actual values than that of the ANN (artificial neural network) based models in terms of surface roughness, cutting force, and cutting temperature. ANFIS model is considered to be a better option for predicting machinability during the milling of Inconel alloy. Samanta et al. (2008) showed that the ANFIS model has the best predictive accuracy compared to ANN and MRA (multivariate regression analysis) models in predicting surface roughness during milling of aluminum alloy. Marani et al. (2019) demonstrated that the predictive accuracy of the ANFIS model was significantly affected by the type and number of membership functions used. The predicted values obtained are in good agreement with the empirical values.

In the present research work, the dry drilling process was applied to investigate the machinability of new biocomposites. These new biocomposites are made of the same matrix (PP/POE/MAPP) are randomly reinforced with chopped miscanthus fibers and biocarbon particles. The tested ones were: biocomposite M1 (PP/POE/MAPP + 30wt% biocarbon), biocomposite M2 (PP/POE/MAPP + 30wt% miscanthus), and hybrid biocomposite M3 (PP/POE/MAPP + 15wt% miscanthus, and 15wt% biocarbon). These biocomposites have been developed for making automotive parts and provided by the Bioproducts Discovery and Development Centre at the University of Guelph, Ontario, Canada.

A full factorial design was used for the experimental design to carry out the dry drilling of biocomposites. The influence of tested factors and their interaction on the machining process performance indicators (thrust forces, specific cutting energy for thrust force, surface roughness, fine dust emission) were measured and analyzed. The regression-based models and ANFIS-based models are developed to predict surface roughness (Ra) and thrust force. The empirical models are used as the objective functions of the genetic algorithm (GA) to

identify optimal drilling parameters to obtain the minimum values of surface roughness (Ra) and thrust force.

Thesis objectives

The goal of the thesis is to understand the machinability of new biocomposites. There are three main objectives summarized as follows.

(1) To study the influence of the drilling parameters (feed rate, spindle speed, and drill diameter) on the machining process performance indicators (thrust force, specific cutting energy for thrust force, surface roughness, and fine dust emission) during the drilling of new biocomposites.

(2) To investigate the effects of reinforcement types used in biocomposite on the machinability indicators during the machining of biocomposites.

(3) To develop predictive models for predicting thrust force and surface roughness during the drilling of biocomposites.

Thesis outline

The thesis content is presented in six chapters as a manuscript-based thesis. Chapter 1 reviews recent publications related to the content of the thesis. Chapter 2 presents the methodology and the experimental procedures used to accomplish the declared objectives.

Chapter 3 presents the first article, published in Materials (Tran et al., 2020). The first article presents the results of investigation on the effects of the machining parameters and tool diameter on the machining process performance indicators (thrust force, surface roughness, specific cutting energy for thrust force, and fine dust emissions) during dry drilling of a new hybrid biocomposite (PP/POE/MAPP + 15wt% miscanthus fibers + 15wt% biocarbon

particles). It is found that the drilling parameters significantly affect the machining performance of hybrid biocomposites.

Chapter 4 presents the second article, published in The International Journal of Advanced Manufacturing Technology (https://doi.org/10.1007/s00170-020-06070-7). The result showed that the machinability of biocomposite is significantly affected by the drilling parameters and the nature and shape of the reinforcements in biocomposites; the effects of the drilling parameters on the machining process performance indicators are considerably for biocomposite containing 30wt% miscanthus fibers and for the one 30wt% biocarbon particles.

Chapter 5 presents the third article, submitted to Neural Computing and Applications (Manuscript Number: NCAA-D-20-02512). In this chapter, surface roughness (Ra) and thrust force in the drilling of biocomposites were predicted using regression analysis and ANFIS-based models. The predictive models were established based on empirical data. It was shown that regression analysis models and ANFIS-based models have good predicted accuracy for thrust force and surface roughness (Ra). However, the predicted values of the ANFIS-based models are in better agreement with the actual values compared to those of the regression models. In addition, optimal drilling parameters were established to obtain the minimum values of thrust force and surface roughness using Genetic Algorithm.

Chapter 6 presents the effects of cutting speed, material removal rate, and reinforcements on the machining process performance indicators. Finally, the conclusions, contributions, and recommendations for future research works are presented in an additional section at the end of the thesis.

CHAPTER 1

LITERATURE REVIEW

This chapter provides a brief review of the machinability of NFRP composites. The machinability of the NFRPs is influenced by the key factors (machining parameters, tools, reinforcements, matrix, etc.) in the machining process is presented. In addition, fine dust generated during the machining processes is succinctly described. The ANFIS-based models for predicting the machining process performance indicators of other materials are also mentioned.

1.1 Natural fiber reinforced polymer composite

Biocomposites are made by combining two or more distinct materials having different properties. Most biocomposites are made of two components. One is a matrix that surrounds and binds together the second material which can be either fibers or particles and are called reinforcements. Depending on the nature of the constituents, the biocomposites can be classified either partly eco- friendly or green as shown in Figure 1.1 (Peças et al., 2018)

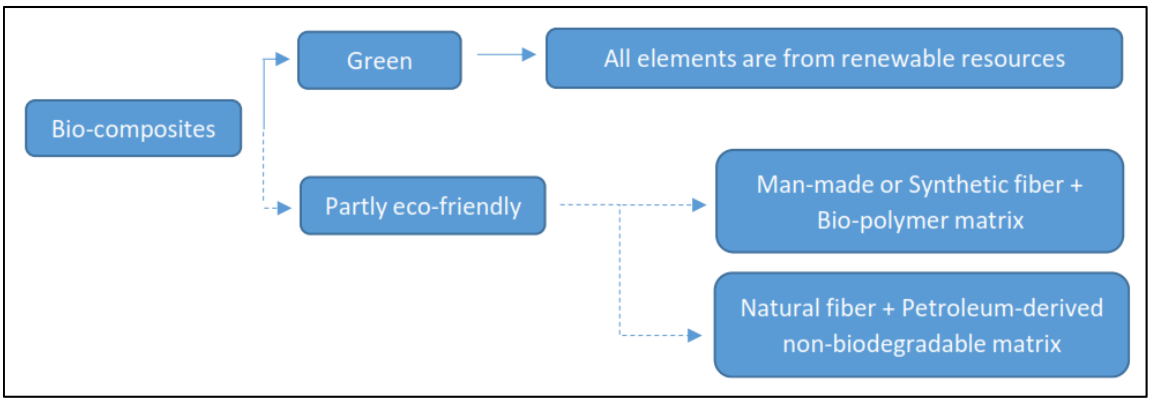

Figure 1.1 Classification of biocomposites (Peças et al., 2018)

The main components of biocomposites are natural fibers and matrix. Biocomposites based on natural fibers have many advantages such as low density, good mechanical properties, and positive environmental impact. Biocomposites are applied in different fields depending on the production costs of biocomposites and their functional properties (Nassar et al., 2017).

1.1.1 Natural fibers

Natural fibers can be classified based on their origin: animal, mineral, and plant. Plant-based fibers are most commonly used in many technical fields. Plant fibers have complicated cell structures. The main constituents of the plant fibers are cellulose, hemicellulose, and lignin. Figure 1.2 shows images of typical plant fibers (Salit et al., 2015). The mechanical properties of plant fibers depend mainly on the plant species, the growth conditions, the age of the plant, and the method of fiber extraction (Ho et al., 2012). Natural fibers used in biocomposite directly affect the machinability of biocomposite, so it is necessary to understand the properties of natural fibers such as mechanical, thermal, physical, and chemical properties. Table 1.1 summarizes the mechanical properties of the plant-based fibers.

Figure 1.2 Images of plant-based fibers (Salit et al., 2015)

Table 1.1 Mechanical properties of natural fibers and particles used in biocomposites

Fiber	Density (g/cm^3)	Elongation at break (%)	Tensile strength (MPa)	Young's modulus (GPa)	Reference
Cotton	1.5 – 1.6	7.0 – 8.0	287 – 800	5.5 - 12.6	(Mohanty et al., 2000)
Jute	1.3 – 1.45	1.16 – 1.5	393 – 773	13 – 26.5	
Flax	1.5	2.7 – 3.2	345 – 1100	27.6	
Remie	1.5	1.2 – 3.8	400 – 938	61.4 – 128	
Sisal	1.45	3 – 7	468 – 640	9.4 – 22.0	
Coir	1.15	15 – 40	131 – 175	4 – 6	
Bamboo	1.158	1.3	441	35.9	(Nassar et al., 2017)
Banana	1.4	3	529 – 914	27 – 32	
Date Palm	0.92	5 – 10	170 – 275	5 – 12	
Hemp	1.14	1.6	690	30 – 60	
Kenaf	1.4	1.5	930	53	
Nettle	0.72	1.7 – 2.11	650 – 1594	87	
Roselle	1.45	2	170 – 350	10 – 17	
Vetiver	1.5	1.6 – 2.4	247 – 723	12 – 49.8	
Abaca	1.5	2.9	430 – 813	31.1 – 33.6	(Peças et al., 2018)
Pineapple	1.5	1 – 3	170 – 1627	60 – 82	
Biocarbon	1.3 – 1.4	-	-	5 – 11	(E.O. Ogunsona et al., 2019)

1.1.2 Biocomposites reinforced with miscanthus fibers

Miscanthus is part of the grass family of the Poaceae with possible cultivation in a variety of climates. The chemical compositions of miscanthus included 40 – 60% cellulose, 20 – 40% hemicellulose, and 10 – 30% lignin. However, its chemical compositions are greatly

influenced by the weather conditions of the growth period, the soil quality, and the harvesting time, etc. (Moll et al., 2020).

Figure 1.3 shows images of chopped miscanthus fibers (Chen et al., 2017). The shape and size of the miscanthus fibers are varied. Therefore, the sieving is required to produce the regular size of the fibers. Figures 1.3 a and b show the chopped fiber of 0-2 mm and 2-4 mm in size, respectively. Figure 1.3c presents miscanthus powder.

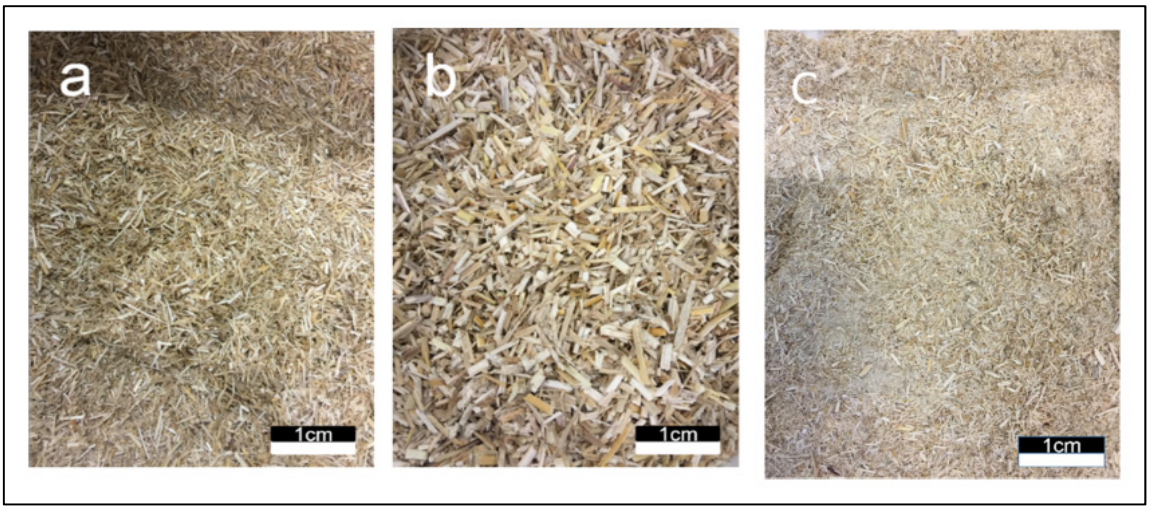

Figure 1.3 Images of the raw miscanthus (Chen et al., 2017)

According to the literature, chopped miscanthus fibers less than 5 mm in size are commonly used and mixed with a polymer matrix to produce biocomposites using injection molding and compression molding process. Table 1.2 shows several biocomposites reinforced with miscanthus fibers. Bourmaud and Pimbert (2008) showed that the improvement of the tensile modulus of PP and PLLA was significant with the addition of miscanthus fibers. Nagarajan et al. (2013) showed that miscanthus fiber-based biocomposite improved the tensile strength and Young's modulus of the matrix (PHBV/PBAT) and exhibited higher thermal stability.

Muthuraj et al. (2016) studied the effects of processing parameters on the impact strength of the PBS/PBAT biocomposite reinforced with miscanthus fibers. It is showed that the

stiffness and flexural strength of the blend matrix (PBS/PBAT) is improved with the addition of miscanthus fibers. The results also showed that the fiber length has the highest statistical significance for the impact strength of biocomposite compared to other processing parameters. Biocomposite reinforced with shorter miscanthus fiber has higher impact strength.

Muthuraj et al. (2017) studied the blend matrix (PBS/PBAT) reinforced with chopped miscanthus fibers. They showed that the tensile and flexural modulus of the biocomposites increased with increasing the miscanthus fiber content from 30wt% to 50wt%. However, the tensile and impact strength of the biocomposite (PBS/PBAT/miscanthus) is lower than that of the blend matrix (PBS/PBAT). It is because of the lack of interfacial interaction between the components. In order to improve this issue, an interactive compatibilizer (MAHgPBS / PBAT) was added to the biocomposite. They also stated that miscanthus fibers reinforced PBS/PBAT biocomposite could contribute significantly to economic and functional performance.

Table 1.2 Biocomposites reinforced with miscanthus fibers

Process	Matrix	Compatibilizer	Reference
Injection molding	PVA	-	(Kirwan et al., 2007)
Injection molding	PLLA, and PP	MA	(Bourmaud & Pimbert, 2008)
Injection molding	PHBV/PBAT	-	(Nagarajan et al., 2013)
Injection molding	PP	MA	(Girones et al., 2016)
Injection molding	PBS/PBAT	MA	(Muthuraj et al., 2017)
Co-Injection molding	PBS/PHBV	-	(Zhang et al., 2014)
Thermo-compression	PP/PLA	-	(Ragoubi et al., 2012)
Injection molding	PBS/PBAT	-	(Muthuraj et al., 2016)

1.1.3 Biocomposites reinforced with biocarbon particles

Biocarbon is produced from the pyrolysis of plant-based fibers. According to the literature, the pyrolysis temperature is used in the range of 500^0C to 900^0C. The temperature of the pyrolysis process greatly affects the mechanical properties of biocarbon. The biocarbon particles produced have various sizes depending on the milling (ball milling, and hammer milling) and sieving process. Figure 1.4 shows the SEM images of biocarbon particles (Behazin et al., 2017b).

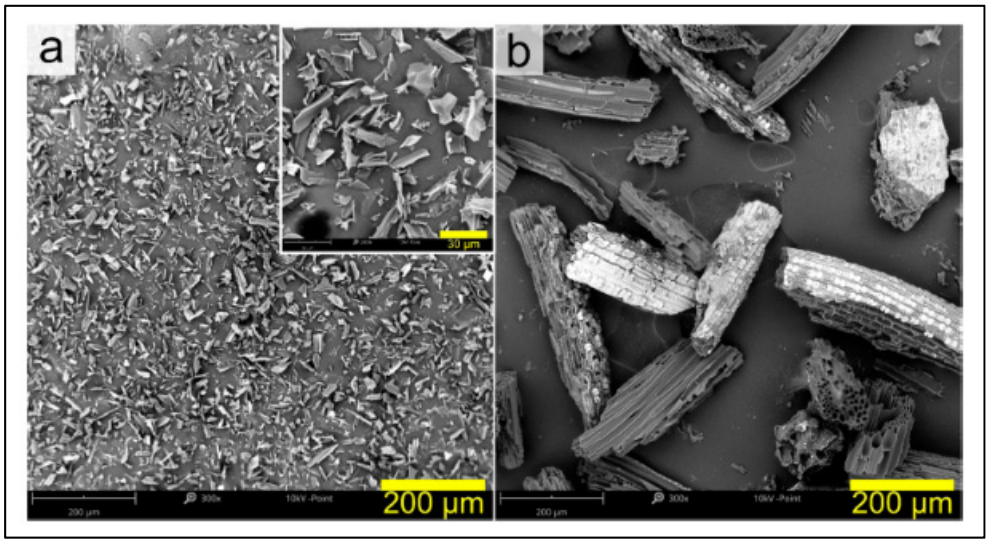

Figure 1.4 SEM images of biocarbon particles (Behazin et al., 2017b)

Biocarbon particles are mixed with a matrix or blend matrix to produce biocomposites from the injection molding or compression molding process. Table 1.3 shows some biocomposites containing biocarbon particles. The size and the weight ratio of the biocarbon particles used in biocomposite significantly affect the mechanical properties of composites.

Behazin et al. (2017b) showed that biocomposites with smaller particles have better strength and modulus and lower impact toughness than those with larger particle sizes. Emmanuel O. Ogunsona et al. (2017b) stated that the shape and size of the biocarbon particles have a significant effect on the biocomposite properties. The better impact strength with a reduction in particle size. They also claimed that biocarbon has great potential as a replacement for

other reinforcing fillers in the near future. Codou et al. (2018) showed that a decrease in the size of biocarbon particles leads to an increase in the mechanical properties, especially the material strength of biocomposite.

Li et al. (2020) found that Young's modulus of the matrix (PHBV) increased with the addition of biocarbon particles, but decreased tensile and flexural strength. They also showed that with the addition of biocarbon particles, the heat deflection temperature increased, and the coefficient of linear thermal expansion decreased and thereby improved the dimensional stability of the matrix.

Behazin et al. (2017a) investigated biocomposites reinforced with biocarbon particles that were produced from the pyrolysis of chopped miscanthus fibers with different temperatures (LTBioC at 500^0C, and HTBioC at 900^0C). They showed that the pyrolysis temperature greatly affects the surface characteristics and the interaction between the biocarbon and the matrix. Biocomposite reinforced with the high temperature pyrolyzed biocarbon (HTBioC) has better stiffness-toughness balance compared to that with the low temperature pyrolyzed biocarbon (LTBioC).

Wang et al. (2018) stated that a reduction in biocarbon particle size by increasing milling time, and then smaller particle size used in biocomposite contribute to improved impact strength. The impact strength of biocarbon/PP composite reaching the same level as that of the Talc/PP composite. Thus, biocarbon/PP composite could help achieve the automotive industry's goal of reducing vehicle weight.

Table 1.3 Biocomposites reinforced with biocarbon particles

Process	Matrix	Compatibilizer	Reference
Injection molding	PA6	-	(Emmanuel O. Ogunsona et al., 2017a)
Injection molding	PA 6,10	-	(Emmanuel O. Ogunsona et al., 2017b)
Compression molding	PLA	-	(Snowdon et al., 2019)
Injection molding	PHBV	-	(Li et al., 2020)
Injection molding	PP	-	(Abdelwahab et al., 2019)
Co-Injection molding	PA6/PP	MAPP	(Codou et al., 2018)
Injection molding	PP/POE	MAPP	(Behazin et al., 2017b)
Injection molding	PP/POE	-	(Behazin et al., 2017a)
Injection molding	PP	-	(Wang et al., 2018)

1.2 Drilling of NFRPs (Natural fiber reinforced polymer composites)

Hole-making is one of the most important machining operations for NFPRs to obtain dimensional accuracy, surface finish, and thereby to facilitate the assembly operation of components. The machinability of NFRPs differs from metallic materials due to the anisotropic and heterogeneous properties of natural fibers, as well as the diversity of fibers in nature. The cutting forces and temperature generated from the cutting process significantly affect machining-induced failures such as debonding, fibers pull-out, delamination, thermal damage, etc. Thus it is considered to investigate the factors involved in the drilling process carefully.

1.2.1 Drilling

Drilling is the most common material removal operation in the machining of the composite. It is used to make holes for assembly. The drilling process involves two basic motions: the

primary rotary motion and the auxiliary linear feed motion. The spindle speed provides the primary rotational motion to the drill bit to perform the main cutting motion. The feed into the workpiece is provided through the linear movement of the spindle axis. Figure 1.5 presents the cutting geometry of the twist drill. It can be seen that a two-flute twist drill has two major cutting edges forming the point angle of the drill bit. Each major cutting edge acts as a single point cutting tool.

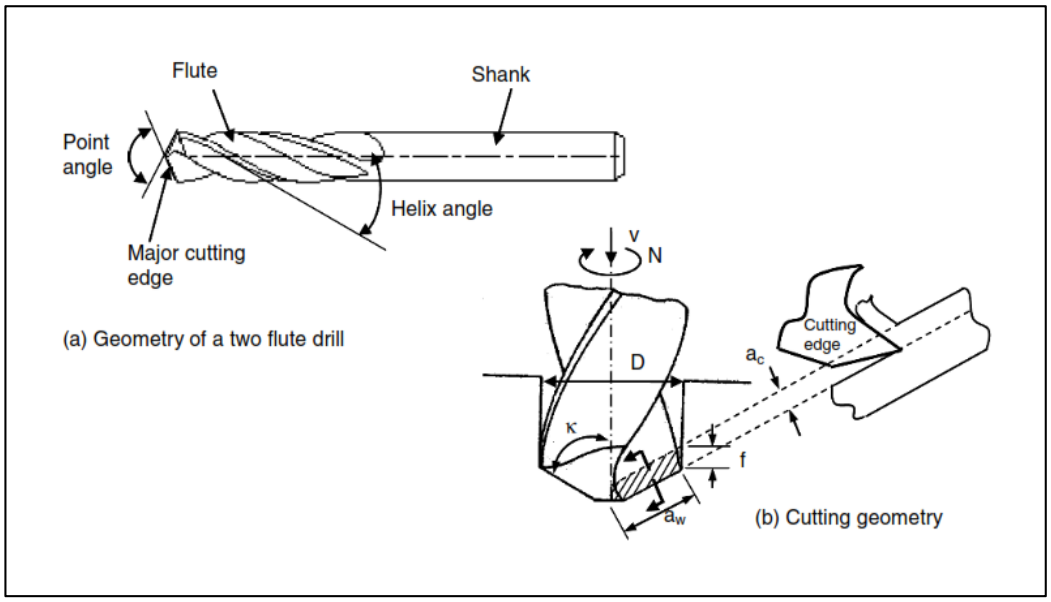

Figure 1.5 Cutting geometry in drilling (Sheikh-Ahmad, 2009)

1.2.2 Effects of reinforcement and matrix of NFRPs

Natural fibers and matrix used in composite significantly affect the machinability of NFRPs. Ismail et al. (Ismail, Dhakal, Popov, et al., 2016) investigated the drilling of CFRP (carbon fiber reinforced polymer) and HFRP (hemp fiber reinforced polymer). It was observed that the drilling parameters significantly affect the damage of the machined surface of two composites. CFRP showed more damage occurred than HFRP under the same cutting conditions. CFRP exhibited lower surface roughness and higher delamination than that of HFRP. The chip shapes formed are different for both composites. The discontinuous and powder-like chips are generated from CFRP. However, the continuous, coiled, and long chips

are formed from HFRP. When drilling both composites using an HSS twist drill under the same cutting condition, there is almost no tool wear for HFRP, whereas there is a clear sign of tool wear for CFRP.

Pailoor et al. (2019) studied the effects of fiber type, coupling agent, and the weight ratio of fibers used in biocomposite on thrust force and delamination during the drilling of two types of jute/PP (chopped and long fibers reinforced polypropylene). They have shown that chopped jute fibers reinforced polypropylene have higher delamination drilling-induced damage. The delamination increased with the weight ratio of fibers used in composites without a coupling agent. Thrust force was higher in drilling long jute fiber reinforced polypropylene. Thrust force was larger obtained from the drilling of composite with fibers of 30wt%. Ismail et al. (Ismail, Dhakal, Dimla, et al., 2016) stated that the fiber aspect ratio (ratio of length to diameter of fiber) significantly affects the machinability during drilling of HFRP (hemp fiber reinforced polycaprolactone). The delamination factor and surface roughness increase with the fiber aspect ratio.

Chegdani et al. (2020) investigated the influence of fiber orientation with respect to the cutting direction on machinability in the orthogonal cutting of UDF/PP (polypropylene reinforced with unidirectional flax fibers). It is observed that fiber orientation has a significant effect on the machined surface. The surface roughness achieved the smallest and highest values for the fiber orientation of 45^0 and 0^0, respectively. Besides, the lowest and largest cutting energy generated corresponding to the fiber orientation of 45^0 and 90^0. The better machinability of UDF/PP obtained with the fiber orientation of 45^0. Debnath et al. (2014) studied the machinability of drilling two NFRPs (sisal/PP and sisal/epoxy) using three drill geometry (parabolic, four-facet, and step drill). They showed that the formed chips were continuous and discontinuous for sisal/PP and sisal/epoxy, respectively. It could be due to the difference in the polymer matrix used in the NFRP composite. The damage caused by the drilling of sisal/PP is less than that of sisal/epoxy. The thrust force generated from sisal/PP is larger than that of sisal/epoxy when drilling using a step drill. However, the lowest thrust force obtained during drilling of sisal/PP using a parabolic drill. It may be due to the differences in the interaction of drill geometry and NFRP composite.

1.2.3 Effects of machining parameters

Machining parameters are the main factors that directly affect the machinability of NFRPs, which have been studied by several studies. Abilash and Sivapragash (2016) studied the machinability in the drilling of bamboo/polyester composite. The result showed that the drill diameter and feed rate contribute to delamination induced failure. The delamination factor obtains low value when using a small drill diameter and low feed rate. It is also showed that the rise of the delamination factor is the result of an increase in feed rate and spindle speed during drilling of banana/epoxy composite (Venkateshwaran & ElayaPerumal, 2013).

Manickam and Gopinath (2017) investigated the machinability of sisal/glass fibers reinforced polymer composite. They showed that the feed rate has the highest impact on thrust force, followed by spindle speed and drill diameter. The increase in thrust force results from an increase in the drill diameter and feed rate and the decrease in the spindle speed. Jayabal et al. (2011) have shown that the feed rate has the most effect on thrust force and torque, while the drill diameter has the most significant impact on tool wear when drilling glass-coir-polyester hybrid composite using HSS twist drill.

Roy Choudhury et al. (2018) studied the influence of drilling parameters on the machinability of the woven nettle/epoxy composite using different tool geometry. It is observed that an increase in feed rate results in an increase in thrust force, torque, delamination, and surface roughness. An increase in spindle speed leads to an increase in drilling temperature, surface roughness, and results in a reduction in thrust force. Vinayagamoorthy (2017) stated that the cutting parameters significantly affect the machinability in drilling jute-steel-polyester hybrid composite. It was found that thrust force increases with increasing feed rate and drill diameter. The increase in feed rate leads to an increase in surface roughness and machined-surface damage. However, the decrease in spindle speed increases thrust force and surface roughness and reduces machined-surface damage. The increase in thrust force and torque as a result of the increase in feed rate during drilling of woven nettle/PP composite using different drill geometries (Debnath et al., 2017).

Maleki et al. (Hadi Rezghi Maleki et al., 2019) showed that the feed rate has the most significant impact on thrust force. The increase in feed rate leads to an increase in thrust force when drilling jute/epoxy composite using different drill geometries. This result is similar to that obtained from the drilling of flax/epoxy composite (H. Rezghi Maleki et al., 2019). Chaudhary and Gohil (2016) investigated drilling cotton-polyester composite. They showed that thrust force is significantly affected by feed rate, and thrust force increases with increasing feed rate. Palanikumar and Valarmathi (2016) investigated the influence of cutting parameters on the thrust force during drilling of wood composite MDF (Medium Density Fiberboard). It was found that thrust force was significantly affected by feed rate, and the reduction of thrust force as a result of the reduced feed rate, while spindle speed is not statistically significant for thrust force.

1.2.4 Effects of tool material and geometry

Some researchers studied the influence of tool material and geometry on the machinability of NFRP composite. Debnath et al. (2014) showed that the thrust force and torque generated by the parabolic drill are lower than that of the step and four-facet drill during drilling of sisal/PP and sisal/epoxy. In which the step drill created the thrust force and torque is of greater value. The influence of the tool geometry on the machinability of nettle/PP composite presented the same result as mentioned above (Debnath et al., 2017). In addition, the drill geometry is more statistically significant than feed rate and spindle speed for thrust force and torque. It is recommended to use a parabolic drill to drill NFRP composite. Yallew et al. (2016) investigated the machinability when drilling woven jute/PP using different drill geometry (twist, step, and parabolic drill). They indicated that the tool geometry has a significant effect on thrust force, torque, and delamination. Parabolic drill exhibited better-cutting behavior than other drills in terms of smaller drilling force and better-machined surface quality.

Roy Choudhury et al. (2018) investigated drilling woven nettle/epoxy composite using different drill geometry (dagger, 4-facet, 8-facet, step, and parabolic drill). They observed that thrust force, drilling temperature, surface roughness, and drilling-induced damage

generated by 8-facet and dagger drill are lower than other drills. Drilling using a step drill leads to high drilling temperatures, high surface roughness, and large drilling-induced damage. The hollow drill has shown better cutting behavior compared to the twist drill, and the lower thrust force generated during drilling sisal/PP composite (Bajpai & Singh, 2013). The machinability of the NFRP is significantly affected by the drill's point angle. The increased thrust force leading to drilling-induced damage is the result of an increase in the drill's point angle (Vinayagamoorthy, 2017; Palanikumar & Valarmathi, 2016).

Chegdani and El Mansori (2018) investigated drilling flax/PP composite using the same drill geometry with different coating materials (uncoated, TiB2 coated, and diamond coated). They showed that the specific cutting energy increases in drilling with coated tools. The diamond-coated drill has a higher specific cutting energy than other drill bits under the same cutting conditions. It is because the coating thickness increases the cutting edge radius and changes the drill's intrinsic friction by changing the surface morphology.

The study (H. Rezghi Maleki et al., 2019) stated that smaller thrust force, lower drilling temperature, and less delamination are obtained with an HSS twist drill during drilling flax/epoxy composite as compared to other carbide drills (CoroDrill 854 and CoroDrill 856). It could be due to the cutting edge radius of the HSS twist drill, it is smaller than that of the carbide drills, resulting in a sharper cutting edge. Therefore, it can easily cut soft and non-abrasive materials. Another study has shown that the HSS twist drill has better cutting behavior than carbide drills (CoroDrill 854 and CoroDrill 856) in terms of smaller thrust force and lower delamination in drilling jute/epoxy composite (Hadi Rezghi Maleki et al., 2019).

1.2.5 Cutting parameters used for drilling of biocomposites

Drilling parameters and tools significantly affect the machining process performance indicators. The selection of cutting parameters must be taken into account with the reinforcements and matrix of the biocomposite to avoid damages during drilling biocomposite materials.

Table 1.4 shows the cutting parameters used for the drilling of various biocomposites, which were conducted by several studies. Table 1.5 presents the optimal drilling parameters used for the drilling of some biocomposites. These drilling parameters are useful for reference to select cutting parameters when drilling new biocomposite materials.

Table 1.4 Cutting parameters for drilling of various biocomposites (Nassar et al., 2017)

No	Biocomposite	Tool material	Cutting parameters
1	Banana/Epoxy	HSS twist	d = 10 mm s = 500, 1000, 1500, 2000 rpm f = 0.1, 0.2, 0.3 mm/rev
2	Sisal/(PLA/S and PLA/G)	Twist, Jo, and Parabolic drill	d = 8 mm s = 900, 1800, 2800 rpm, f = 0.05, 0.12, 0.19 mm/rev
3	Banana/Polyester	HSS twist	d = 8 mm s = 1000, 2000, 3000 rpm f = 0.1, 0.2, 0.3 mm/rev
4	Sisal/Epoxy-Polypropylene	4-facets, Parabolic, and step solid carbide	d = 8 mm s = 900, 1800, 2700 rpm, f = 0.05, 0.08, 0.12, 0.09, 0.3 mm/rev
5	Coir/Polyester	HSS twist	d = 6, 8, 10 mm s = 600, 1200, 1800 rpm, f = 0.1, 0.2, 0.3 mm/rev
6	Jute/Polypropylene	Twist drill, Jo, and Parabolic drill	d = 6, 8, 10 mm s = 900, 1800, 2800 rpm f = 0.05, 0.12, 0.19 mm/rev
7	Basalt and sisal/Epoxy	HSS twist	d = 3, 4, 5 mm, s = 300, 600, 900 rpm, f = 0.1, 0.2, 0.3 mm/rev
8	Hemp/Polyester	Two fluted solid carbide	d = 5 mm s = 1000, 1500, 2000 rpm f = 100, 200, 300 mm/min
9	Vetiver, jute, and glass/Vinyl ester	HSS twist	d = 10 mm, s = 500, 1000, 1500, 2000 rpm f = 0.1, 0.2, 0.3, 0.4 mm/rev
10	Jute/Epoxy	HSS twist	d = 6, 8, 10 mm s = 1000, 2000, 3000 rpm f = 50, 150, 250 mm/min
d: drill diameters, s: spindle speed, f: feed rate			

Table 1.5 Optimal drilling parameters of some NFRP composites (Rajmohan et al., 2019)

No	Fibers used	Responses explored	Optimal conditions
1	Sisal-jute	Thrust force, torque and delamination	d = 6 mm, s = 3000 rpm, f = 0.04 mm/rev
2	Jute-steel	Thrust force, surface roughness and damage	d = 8 mm, s = 1070 rpm, f = 0.1 mm/rev, point angle = 90^0
3	Jute	Delamination	s = 500 - 970 rpm, f = 0.1 mm/rev, point angle = 90^0-120^0
4	Hemp	Delamination	s = 2000 rpm, f = 100 mm/min
5	Sisal-banana	Delamination	d = 3 mm, s = 1200 rpm, f = 0.1 mm/rev
6	Coir-glass	Thrust force, torque and tool wear	d = 8 mm, s = 1500 rpm, f = 0.2 mm/rev
7	Medium density fiber boards	Delamination entry and exit	d = 4 mm, s = 2950 rpm, f = 100 mm/min
d: drill diameters, s: spindle speed, f: feed rate			

1.3 Milling of NFRP composites

Parts made of NFRP composites are usually manufactured close to the final shape. However, secondary processing is required to achieve dimensional accuracy and surface finish for assembly and finishing of the product. Milling is a typical machining process widely used for making slot, pocket, and trimming to achieve geometric and dimensional accuracy (Nassar et al., 2017). Several studies have observed that the machinability in milling NFRP composite is significantly affected by the cutting parameters, tool geometry and materials, the reinforcement and the matrix, and the NFRP composite's processing method (Rajmohan et al., 2019).

Babu et al. (2013) investigated the influence of cutting parameters on the machinability in slot milling of GFRP (glass fiber reinforced polyester) and various NFRP composites, including hemp, jute, and banana fibers reinforced polyester composite (HFRP, JFRP, BFRP). It is observed that feed rate and spindle speed are statistically significant for delamination and surface roughness. The increase in delamination and surface roughness is a

result of an increase in feed rate. Conversely, an increase in spindle speed leads to a reduction in delamination and surface roughness. It is also found that NFRP composites have better cutting behavior than GRRP in terms of less delamination and lower surface roughness.

Balasubramanian et al. (2016) stated that the spindle speed and depth of cut are statistically significant for cutting force during milling of woven jute/polyester composite. They noticed that cutting force increases with increasing feed rate and depth of cut and decreases with increasing spindle speed. Azmi et al. (2018) showed that the feed is the highest effect on surface roughness, followed by spindle speed during the milling of kenaf/epoxy composite. The increased surface roughness results from an increase in feed rate and a decrease in spindle speed. Another study has noticed that the helix angle of end mill cutter significantly affects the machined surface quality in profile milling of woven flax/PP composite. The uncut fiber induced damage leading to an increase in surface roughness as a result of an increase of helix angle used (Faissal Chegdani et al., 2016).

Çelik et al. (2019) studied the influence of cutting parameters, the number of flutes in end mill, and the fiber orientation angle on the machinability in slot milling of jute/epoxy composite. They showed that the lowest cutting force, the smallest delamination factor, and the highest surface roughness obtained from the milling of composite having $\pm 45^0$ orientation angle. A larger feed rate leads to higher delamination factor, cutting force, and surface roughness. The increased spindle speed leads to reduced cutting force and surface roughness and results in increased delamination factor. An increase in the number of flutes in the milling cutter contributes to a reduction in cutting force, lower surface roughness, and smaller delamination factor.

Çelik and Alp (2020) conducted an investigation on slot milling of jute/epoxy and flax/epoxy composite using different end mill (HSS, TiN coated HSS, and WC). It is observed that lower delamination factor, smaller surface roughness, and higher cutting force were obtained from jute/epoxy than that from flax/epoxy during milling under the same cutting conditions. It is also showed that the cutting parameters and milling tools significantly affect the

machinability of jute/epoxy and flax/epoxy. An increase in feed rate leads to increased surface roughness, cutting force, and delamination factor. Lower cutting force and surface roughness, and higher delamination factor result from the higher spindle speed. Besides, the cutting force, delamination factor, and surface roughness are the lowest obtained with WC end mill. In contrast, the cutting force, delamination factor, and surface roughness are the highest obtained with HSS end mill.

1.4 Dust emission during machining

1.4.1 Dust formation during drilling

Songmene et al. (2008a) studied dust formation during drilling of metal. The drilling process is described in Figure 1.6. Sources of dust generation are presented as follows.

- Q1 is the amount of dust generated in the primary deformation zone, which is the shearing plane where the materials undergo high deformation.
- Q2 is the amount of dust created in the secondary deformation zone at the chip-tool interface where the friction between the tool and the chip occurs.
- Q3 is the amount of dust produced by little friction in the workpiece-tool interface.
- Q4 is the amount of dust emitted by compressive bending deformation and chip breaking in the chip's outer surface.
- Q5 is the amount of dust created by the friction, deformation, and segmentation of the cut chip in the drill's helical surface.
- Q6 is the amount of dust produced by the chisel edge of the drill rubbing on the workpiece

The total amount of dust emitted (Q) is calculated as follows.

$$Q = Q1 + Q2 + Q3 + Q4 + Q5 + Q6 \quad (1.1)$$

Songmene et al. (2008a) stated that the fine particles generated were significantly affected by cutting speed, feed rate, and workpiece material. A higher amount of fine dust generated as a result of an increase in feed rate and cutting speed. Ductile materials generated more fine dust than brittle materials.

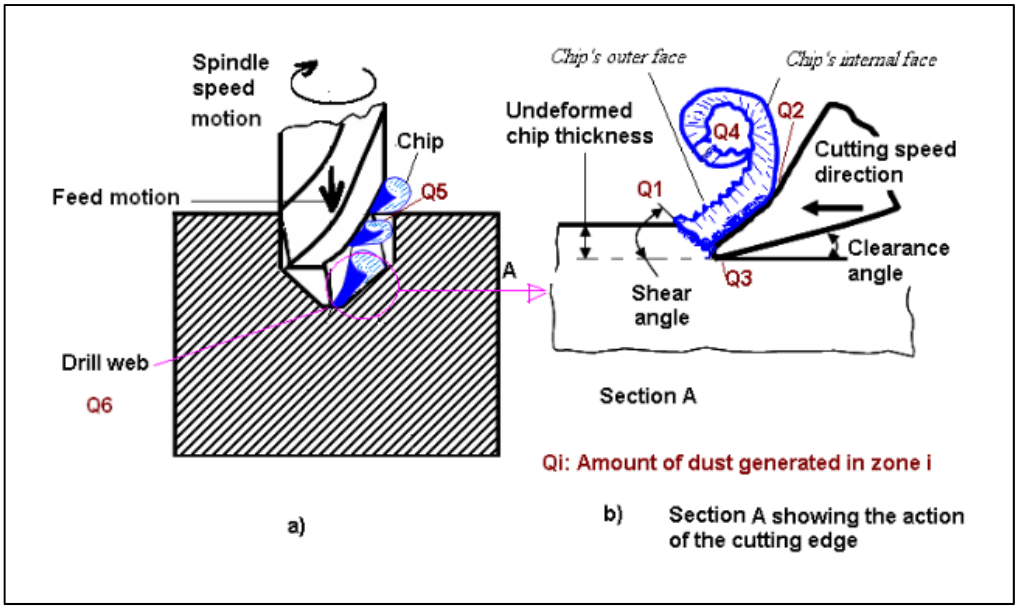

Figure 1.6 Sources of dust formation in drilling (Songmene et al., 2008a)

1.4.2 Particles emission during machining of metallic workpiece

Several studies have considered fine dust generated during machining because it directly affects the health of machine-tool operators and the environment. Songmene et al. (2008a) have mentioned that fine particles are less than 2.5 microns in diameter ($PM_{2.5}$) could easily be inhaled into the deepest parts of the lungs. The protection of the environment and operators must be taken into consideration, which has become an additional indicator of the machining process performance.

Khettabi et al. (2007) have shown that fine particles ($PM_{2.5}$) produced are significantly affected by the tool geometry and cutting conditions in cutting different metal materials. The dust generated by using a tool having a lead angle of 90^0 is less than that of having a lead angle of 70^0 or 110^0. Khettabi et al. (2010) have studied the influence of workpiece material and cutting parameters on dust emission. It is observed that the dust emission significantly affected by the workpiece material used. An increase in cutting speed results in an increase in dust emission for brittle materials, but the amount of dust is relatively small compared to that of ductile materials. Kamguem et al. (2013) have investigated the effects of the coated

carbide tools on fine dust generated during slot milling of different materials (6061-T6, 2024-T351, and 7075-T6). They have shown that a TiCN coated tool produces less fine dust than a multilayer-coated tool (TiCN + Al_2O_3 + TiN).

Zaghbani et al. (2009) have studied fine dust generated during high-speed milling of aluminum alloy (6061-T6) in dry and wet conditions. They have shown that the primary source of dust emitted during cutting is the shearing zone. The deformation conditions in the chip formation zone have a significant effect on dust emission. Moreover, the lubrication conditions significantly affect the form of particles emitted. The dry milling process produces more particles in the size of 1 to 10 microns than the wet milling process. Nanoparticles emission is not significantly affected by the lubrication and cutting conditions.

Songmene et al. (2008b) investigated the effects of the initial preparation of workpiece, tool condition and geometry, and machining strategies on fine particle emission during drilling of different materials. They demonstrated that friction plays a significant role in dust formation. A worn drill bit produced more fine dust than a sharp drill bit did. The highest amount of dust is generated at the period of drill penetration into the workpiece. In addition, the dust generation is significantly affected by the initial preparation of the workpiece.

1.4.3 Particles emission in machining composites

Saidi et al. (2015) investigated the effects of polishing conditions on particle emission, distribution, and dispersion in the granite polishing process. They showed that the great part of the material was removed from the granite surface during the first period of the polishing process using coarse abrasives, and thereby more fine dust was produced. Increasing the spindle speed results in the increased microparticle generation, and the large concentrations were found far from the region of particle creation. The majority of fine dust produced is less than 2.5 microns in diameter.

Saidi et al. (2019) studied the influence of cutting parameters on the emission and dispersion of fine dust generated during the dry granite polishing process. They noticed that the feed rate and the spindle speed significantly affect fine dust emission. An increase in fine particles

and ultrafine particles results from an increase in spindle speed or decreased feed rate in the two periods of granite polishing. It could be due to an increase in spindle speed leads to an increase in material removal, which increases the dust emission. Moreover, an increase in feed rate results in the rise of the dilution effect, which decreases the dust emission. The concentration of fine particles and ultrafine particles are higher near the polishing tool. They indicated the peak of number concentration for fine particles ranging from 0.626 to 0.777 microns in diameter and the peak of number concentration for ultrafine particles between 14.1 and 34.6 nanometers in size.

Marani et al. (2018) stated that dust emission is greatly affected by the machining conditions and microstructure during the milling of aluminum matrix composite (Al-20Mg_2Si-2Cu) with the addition of bismuth (Bi) and barium (Ba). Dust generation increases as the cutting speed increases within the range of 300 to 700 (m/min), and then decreases with increasing cutting speed to 1100 (m/min). The ultrafine particles emitted from the composites with addition to Bi and Ba smaller than that of the base composite.

Haddad et al. (2014) have studied the effects of cutting conditions and tool geometries (uncoated carbide burr, diamond coated carbide burr, and four-flute diamond coated end mill) on the dust generated during the trimming of carbon fibers reinforced polymer (CFRP). It was observed that the tool geometry greatly influences the generated dust particles. The coating had no significant effect on dust emission. Fine dust generation decreased with decreasing cutting speed or increasing feed rate. The majority of fine dust emitted is less than 2.5 microns in size.

Based on the literature as mentioned above, it could be deduced that fine dust generated during machining depends on machining factors such as the machining process (drilling, milling, and grinding, etc.), cutting parameters, the tools used (geometry, coating, and material), workpiece material, and cutting conditions, etc. Therefore, it is necessary to choose cutting parameters, tools, and machining strategies suitable for each specific machining case to reduce the amount of fine dust generated during the machining process. Moreover, the fine dust generated during the machining of biocomposites has not been interested in research. This issue is investigated in the present research work.

1.5 Adaptive Neuro-Fuzzy Inference System (ANFIS)

ANFIS is an artificial intelligence technique that combines the advantages of both adaptive network and fuzzy inference systems. The adaptive network is a particular case of a neural network with supervised-learning capability. The adaptive network adjusts its parameters (i.e., weights) to meet a specific termination criterion (error tolerance or number of iterations) in correspondence with the training data (input-output data) are provided. The fuzzy inference system allows the presentation of uncertain situations in the form of rules using decision-making mechanisms (Abbas et al., 2017). The learning ability of artificial neural networks and the decision-making mechanism of the fuzzy inference system are combined in ANFIS. One of the significant disadvantages of the artificial neural network is that the weight values obtained could not be explained. This drawback is eliminated by the fuzzy inference system of the ANFIS structure. Therefore, ANFIS is used in solving many practical problems (Kar et al., 2014).

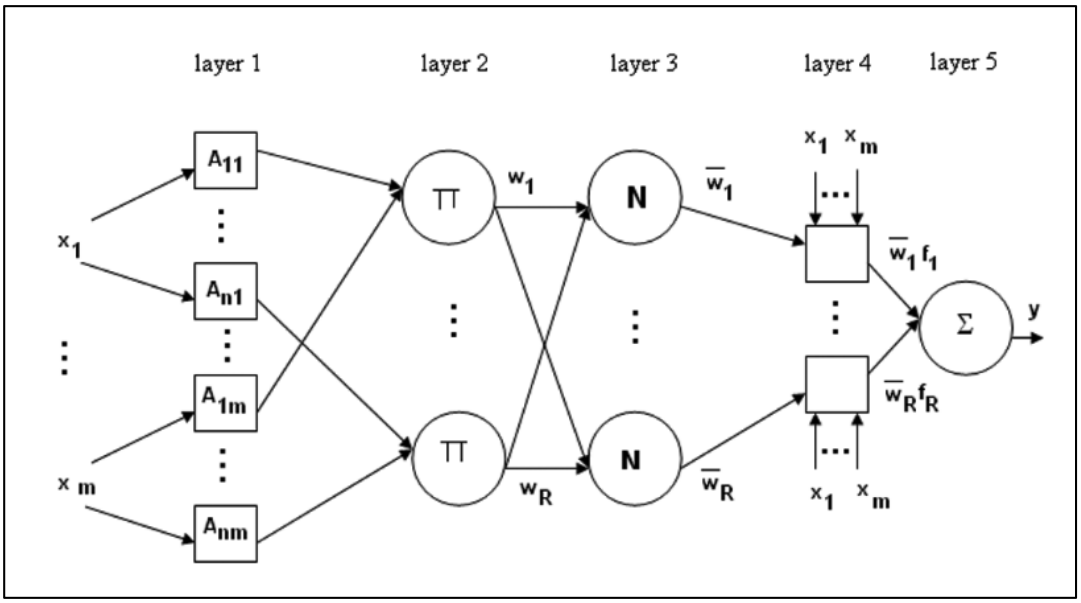

Figure 1.7 The basic structure of ANFIS (Samanta et al., 2008)

Figure 1.7 presents the basic structure of ANFIS with m inputs ($x_1 \ldots x_m$), each input with n membership functions (MFs), a fuzzy rule base of R rules (R = m.n), and one output response (y). The ANFIS structure consisted of five layers and can be briefly described as follows.

- Layer 1 is the fuzzification layer. It transforms the crisp inputs (x_i) into linguistic labels (A_{ij}) with a membership degree. The output of node ij is determined by equations (1.2).

$$O_{ij}^1 = \mu_{ij}(x_i) \; ; \quad i = 1,m; \quad j = 1,n \tag{1.2}$$

Where μ_{ij} (x_i) represents the j^{th} membership functions for the input x_i, typically, the various membership functions are used, such as triangular, generalized bell, etc.

Assuming that gbellmf (general bell membership function) is applied to node ij, the corresponding output determined as follows.

$$\mu_{ij}(x_i) = gbellmf(x; a, b, c) = \frac{1}{1 + \left|\frac{x - c}{a}\right|^{2b}} \tag{1.3}$$

Where a, b, and c are the parameters of the membership function. These parameters are called as premise parameters.

- Layer 2 is the product layer. The output of node r in this layer represents weighting factor (firing strength) of the r^{th} rule. The output (w_r) is the product of all its inputs as follows.

$$O_r^2 = \prod \mu_{ir}(x_i); \quad i = 1, m; \quad r = 1, R \tag{1.4}$$

- Layer 3 is the normalized layer. The output of node r in this layer represents the normalized weighting factor of the r^{th} rule as follows.

$$O_r^3 = \overline{w}_r = \frac{w_r}{\sum_r w_r}; \quad r = 1, R \tag{1.5}$$

- Layer 4 is the defuzzification layer. The defuzzification relationship between the input and output are calculated in equation (1.6).

$$O_r^4 = \overline{w}_r . f_r; \quad f_r = \sum_i p_{ri} x_i + q_r; \quad i = 1, m; \quad r = 1, R \tag{1.6}$$

Where p_{ri} and q_r are called the consequence parameters

- Layer 5 is the output layer. The overall output of ANFIS as a sum of all weighted outputs of the rules

$$O^5 = \sum_{r=1}^{R} \overline{w}_r f_r \tag{1.7}$$

Where R is the number of rules

Sen et al. (2017) used ANN (Artificial Neural Network) and ANFIS to develop predictive models for cutting force, surface roughness, and cutting temperature during milling Inconel alloy (Inconel 690). The result showed that the errors between the experimental values and the predicted values of ANFIS-based models are smaller than those of ANN-based models. Consequently, the use of the ANFIS-based model to predict the machinability of Inconel alloy is most appropriate.

Samanta et al. (2008) developed models for predicting surface roughness during the milling of 6061 aluminum alloy by using MRA (multivariate regression analysis) and soft computing

techniques (ANN and ANFIS). The cutting parameters, namely feed rate, spindle speed, and depth of cut, were used as inputs to model the surface roughness. It was observed that the ANFIS-based model produced the best prediction, followed by ANN and MRA. The predicted values obtained from the ANFIS- and ANN-based approach were quite close to the actual values. Therefore, ANN- and ANFIS-based models can also be used to generate data for different machining conditions within the predefined ranges without the need for additional testing.

Kumar and Hynes (2019) developed the ANFIS-based model to predict surface roughness during the drilling of the galvanized steel sheet. The thermal drilling parameters include the spindle speed, angle of tool, and workpiece thickness, which are used as inputs to the ANFIS-based model to predict the drilled-surface roughness. It is indicated that the predicted values of the ANFIS model are relatively close to the experimental values.

Savkovic et al. (2019) predicted the cutting temperature during turning hardened steel (EN 90MnCrV8) by the ANFIS-based model. The machining parameters (cutting speed, feed, depth of cut, and tool material) were used as inputs to the ANFIS predictive model. By comparing the experimental data and the predicted values, the ANFIS model has shown high predictive accuracy. Shivakoti et al. (2019) developed the ANFIS-based model in the turning of stainless steel 202. The cutting parameters were used as inputs to ANFIS models. The outputs, namely, material removal rate (MMR), and surface roughness (Ra), were predicted. The results show that the ANFIS models have relatively good predictability. The predicted values are in agreement with the actual values.

Marani et al. (2019) established ANFIS-based models to predict the surface roughness and cutting force during milling metal matrix composite (Al-20Mg2Si). The inputs used for the predictive models include feed rate, cutting speed, and particle size. It has been shown that the type and number of membership functions used in the ANFIS structure mainly affect the model’s predictive accuracy. The predicted values obtained are very satisfactory with the empirical values.

Abbas et al. (2017) developed both the regression analysis model and the ANFIS approach to predict surface roughness when turning Grade-H high-strength steel. The cutting parameters (cutting speed, feed rate, and depth of cut) were used as inputs to the ANFIS model. The results showed that high predictive accuracy was obtained from both predictive models. However, the ANFIS model has slightly better accuracy than the regression analysis.

1.6 Summary and conclusive remarks

Some concerned issues in the machining of the NFRP composites are drawn from the published literature as follows.

- The machinability of biocomposites strongly depends on the reinforcements and matrix used in biocomposites. Therefore, it is essential to understand the machining behavior of a particular biocomposite.

- The machining-induced damages are mainly caused by cutting forces and cutting temperatures, so it is necessary to choose appropriate cutting parameters and tools (material, coating, and geometry) to reduce failure occurred.

- Fine dust emitted during the machining of materials directly affects the machine operators' health. However, several studies have focused only on factors affecting fine dust generated from the machining of metal and metal matrix composites. Therefore, the issues of fine dust generated from the machining of polymer composites need to be studied.

- With the rapid development of NFRP composites, it is necessary to build predictive models to identify factors affecting machining performance for new materials quickly. Particular attention should be paid to build the predictive model based on the limited empirical data that have good predictability, such as the ANFIS-based models.

CHAPTER 2

METHODOLOGY AND EXPERIMENTAL PROCEDURE

This chapter presents the methodology and the experimental procedure will be conducted in the research work. The machinability of the three new biocomposites was studied by the dry drilling process. A full factorial design with three factors (feed rate, spindle speed, and drill diameter) at three levels was used for the drilling of the three tested biocomposites. The statistical technique was applied to investigate the influence of the tested factors (drilling parameters and reinforcement type) on the machining process performance indicators (thrust force, specific cutting energy for thrust force, surface roughness, and fine dust emission). The regression analysis and ANFIS-based models were established based on empirical data to predict the machinability indicators (thrust force, and surface roughness) during drilling biocomposites. Optimal drilling parameters for minimizing thrust force and surface roughness R_a are identified by the GA approach.

2.1 Workpiece materials and drill tool

2.1.1 Biocomposites

The new biocomposites were used for the dry drilling process, designated M1, M2, and M3. These biocomposites are made of a common matrix (Polypropylene (PP)/Polyolefin (POE)/Maleic Anhydride grafted Polypropylene (MAPP)) are randomly reinforced with various weight ratios of biocarbon particles and chopped miscanthus fibers.

PP (trade name, 1350N); POE (trade name, Engage 7487); MAPP (trade name, Fusabond 613). The biocarbon resulting from the pyrolysis operation of miscanthus fibers (average length of 4 mm) was invented in Southern Ontario, Canada. The four millimeters long miscanthus fibers used in biocomposites were supplied by Competitive Green Technology.

The press molding process produced the biocomposite can be summarized as the following step. Firstly, the mold platens are preheated to 180°C for 30 minutes. Next, the material components are loaded into the press and preheated with closed platens to melt material before pressing for about 10 minutes. Then, the vacuuming is carried out to degas for 3 minutes, and the mold platens are closed at a pressure of 2 tons for 10 minutes. Finally, the cooling of platens is conducted to below 50°C, and then biocomposite is removed from the press.

The mechanical properties and chemical composition of the biocomposites as described in Table 2.1. Figure 2.1 shows images of biocomposites.

Table 2.1 Chemical composition and mechanical properties of biocomposites

Materials	**Chemical composition**				
	PP (wt %)	POE (wt %)	MAPP (wt %)	Biocarbon (wt %)	miscanthus (wt %)
M1	62	5	3	30	-
M2	62	5	3	-	30
M3 (hybrid)	62	5	3	15	15
Mechanical properties					
	Young's modulus (MPa)	Tensile strength (MPa)	Flexural modulus (MPa)	Flexural strength (MPa)	Impact strength (J/m)
M1	2510	31	2146	52	294.5
M2	3872	37.3	3148	58.5	128.5
M3 (hybrid)	3175	34	2717	55	140

(a) biocomposite M1 (b) biocomposite M2 (c) hybrid biocomposite M3

Figure 2.1 Biocomposites used for experiments

2.1.2 Workpiece samples

Biocomposites are manufactured through the press molding process. The specimen of biocomposites is a rectangular sheet (dimensions of 300 x 120 x 5 mm). These samples are cut from the original sheet with dimensions of 500 x 500 x 5 mm, provided by the Bioproducts Discovery and Development Centre, University of Guelph, Ontario, Canada.

2.1.3 Drill tool

High-speed steel twist drills are selected for experiments with diameters ranging from 6 to 10 mm, right-hand cut, and regular spiral flutes. The drill geometry is described in Table 2.2. The image of twist drills is presented in Figure 2.2.

Table 2.2 The geometric dimensions of drills (Precision twist drill, HSS, Jobber)

Shank type	Length (mm)	Flute length (mm)	Diameter (mm)	Point angle (deg)
Straight	93	57	6	118
Straight	117	75	8	118
Straight	133	87	10	118

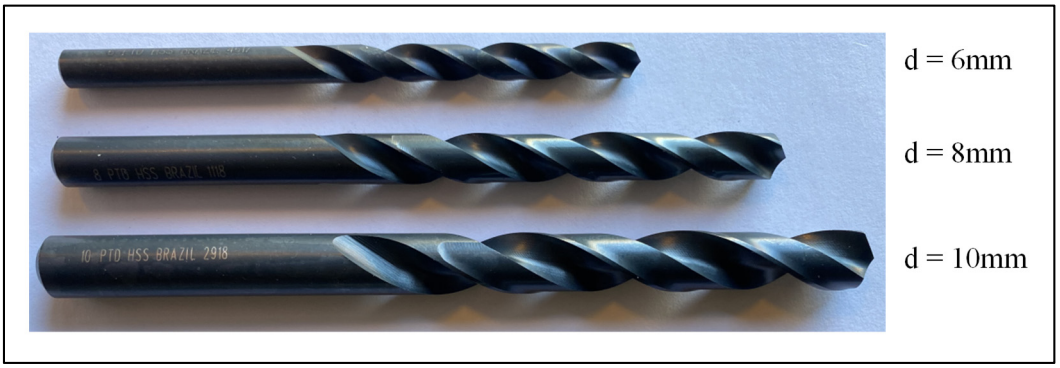

Figure 2.2 Twist drills used for experiments

2.2 Design of experiment

A full factorial was used for the experimental design. The input factors include drill diameter (d), spindle speed (s), feed rate (f), and three biocomposites (M1, M2, and M3). The machining process performance indicators consisted of thrust force, specific cutting energy for thrust force, surface roughness, and fine dust emissions. The drilling parameters and their levels are described in Table 2.3. Table 2.4 presents the combination of the parameters obtained from the factorial design for the drilling of biocomposites. A drilled hole with the same drilling parameters and biocomposite material was carried out three times, and thereby a total of 243 (3^3 x 3 x 3) holes were drilled.

The drilling parameters are chosen for cutting biocomposite based on the tool manufacturer's catalog and the literature (Tables 1.4 and 1.5). In addition, new biocomposites are made of a polypropylene matrix, which has low thermal conductivity and low softening temperature. Therefore, the machined surface damages will have occurred as the increased cutting temperature. According to the literature, the machined parts should be retained at a temperature ranging from 80^0C to 160^0C. So the selection of cutting parameters should be considered to avoid thermal-induced damages during drilling biocomposites.

Table 2.3 Factors and their levels used for experimental design

Factors	Low	Medium	High
d: drill diameter (mm)	6	8	10
s: spindle speed (rpm)	600	1500	2400
f: feed rate (mm/rev)	0.1	0.2	0.3
Biocomposite	M1	M2	M3

Table 2.4 Matrix of experiments used for the drilling of biocomposites

Testing number	Feed rate (mm/rev)	Spindle speed (rpm)	Drill diameter (mm)	Cutting speed (m/min)	Material removal rate (cm^3/min)
1	0.1	600	6	11	1.7
2	0.2	600	6	11	3.4
3	0.3	600	6	11	5.1
4	0.1	1500	6	28	4.2
5	0.2	1500	6	28	8.5
6	0.3	1500	6	28	12.7
7	0.1	2400	6	45	6.8
8	0.2	2400	6	45	13.6
9	0.3	2400	6	45	20.4
10	0.1	600	8	15	3.0
11	0.2	600	8	15	6.0
12	0.3	600	8	15	9.0
13	0.1	1500	8	38	7.5
14	0.2	1500	8	38	15.1
15	0.3	1500	8	38	22.6
16	0.1	2400	8	60	12.1
17	0.2	2400	8	60	24.1
18	0.3	2400	8	60	36.2
19	0.1	600	10	19	4.7
20	0.2	600	10	19	9.4
21	0.3	600	10	19	14.1
22	0.1	1500	10	47	11.8
23	0.2	1500	10	47	23.6
24	0.3	1500	10	47	35.3
25	0.1	2400	10	75	18.8
26	0.2	2400	10	75	37.7
27	0.3	2400	10	75	56.5

2.3 Equipment used for machining and measuring

2.3.1 CNC machine tool

The drilling process was conducted on a 3-axis CNC machine tool (HURON – K2X10). The main characteristics of the machine: maximum power, 50 KW, spindle speed, 28000 rpm, and Torque, 50Nm. Figure 2.3 presents the image of the CNC machine tool.

Figure 2.3 CNC machine tool

2.3.2 Cutting forces

Figure 2.4 describes the devices used to measure cutting forces, which included a dynamometer (Kistler 9255B), a charge amplifier (Kistler 5010, Kistler Instrument Corporation, New York, NY, USA), a data translation card (type DT 9836, Data Translation Inc., Marlborough, MA, USA), and a personal computer.

The workpiece clamping device is placed and screwed on the dynamometer table, which is placed and fixed on the machine table to measure the cutting forces directly. The cutting force signals in X, Y, and Z-axis are directed to the charge amplifiers (Kistler 5010), and next transmitted to a data translation card (DT 9836) and then to a personal computer. The cutting forces are recorded on a personal computer and analyzed with the help of Matlab software.

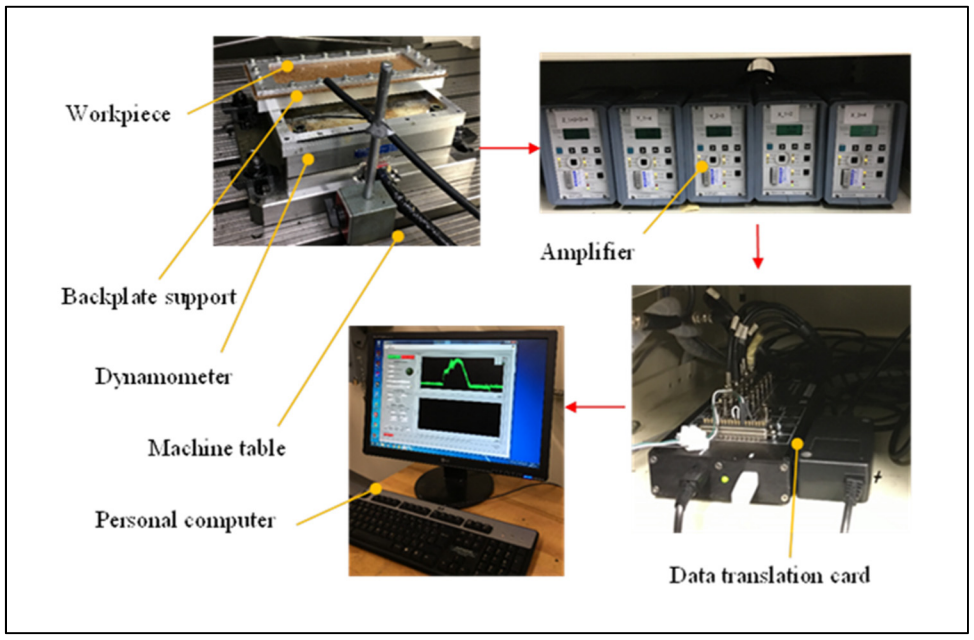

Figure 2.4 Devices used for measuring cutting forces

2.3.3 Surface roughness

The surface roughness is measured by a surface profilometer (model SJ-410, Mitutoyo (Figure 2.5)), which is directly connected to a personal computer. The surface roughness data were recorded and analyzed with the SURFPARK-SJ software package installed on the personal computer.

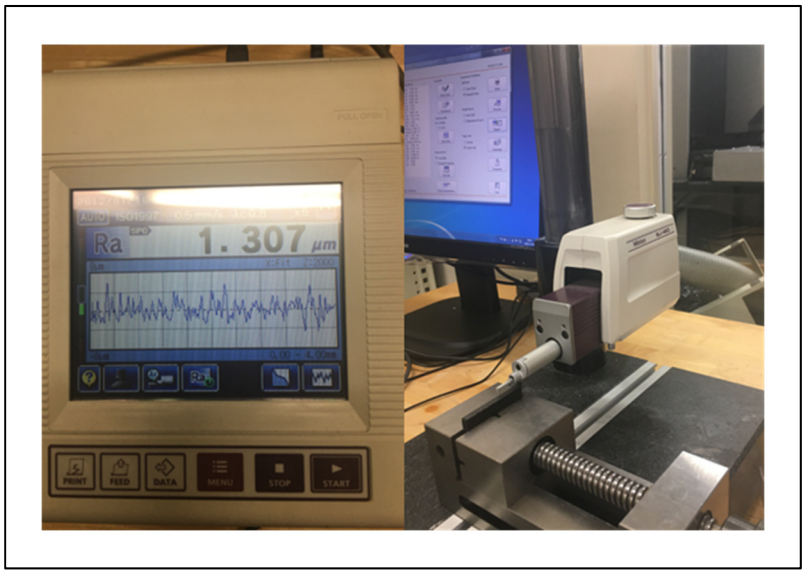

Figure 2.5 Surface profilometer

2.3.4 Fine dust emissions

A system consists of Aerodynamic Particle Sizer (APS, model 3321, TSI Inc., Shoreview, MN, USA) and Scanning Mobility Particle Sizer (SMPS, model 3080, TSI Inc., Shoreview, MN, USA) was used to measure the fine dust emitted during the drilling of biocomposites. APS (Figure 2.6a) was used to measure the fine particles with a diameter ranging from 0.5 to 20 microns. SMPS (Figure 2.6b) was used to measure the ultrafine particles between 7 nm and 100 nm in size.

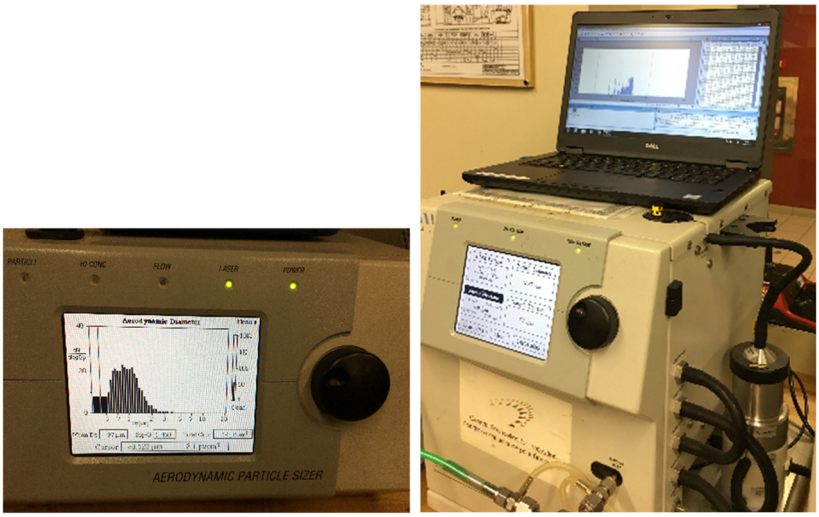

(a) APS (b) SMPS

Figure 2.6 APS (model 3321, TSI, Inc) and SMPS (model 3080, TSI, Inc)

2.3.5 SEM (scanning electron microscope)

The microstructure of the pre-machined and post-machined surface of biocomposite are observed on the Scanning Electron Microscope (SEM, S-3600N, HITACHI), as shown in Figure 2.7.

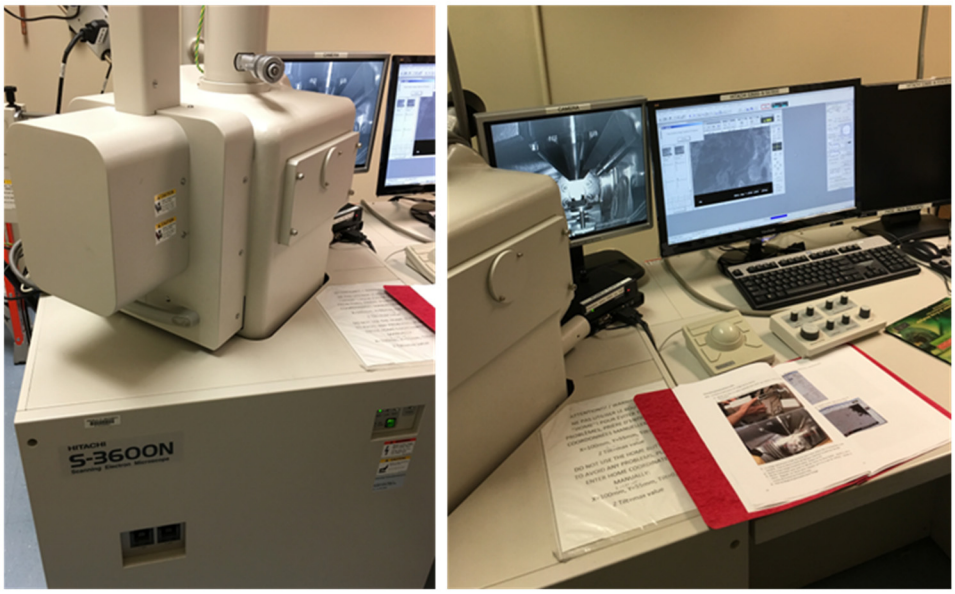

Figure 2.7 Scanning Eletron Microscope (S-3600N, HITACHI)

CHAPTER 3

EXPERIMENTAL INVESTIGATION ON MACHINABILITY OF POLYPROPYLENE REINFORCED WITH MISCANTHUS FIBERS AND BIOCHAR

Dinh Son Tran [1, 2], Victor Songmene [1], Anh Dung Ngo [1], Jules Kouam [1], Arturo Rodriguez-Uribe[3], Manjusri Misra [3] and Amar Kumar Mohanty [3]

[1] Department of Mechanical Engineering, École de technologie supérieure (ÉTS), Montreal, QC, Canada H3C 1K3.
[2] Department of Mechanical Engineering, The University of Danang - University of Science and Technology, 54, Nguyen Luong Bang Street, Danang, Vietnam.
[3] Bioproducts Discovery and Development Centre, Department of Plan Agriculture, Crop Science Building, University of Guelph, Guelph, N1G 2W1, ON, Canada.

Article published in Materials, March 2020

Abstract

The machinability of composite materials depends on reinforcements, matrix properties, cutting parameters, and on the cutting tool used (material, coating, and geometry). For new composites, experimental studies must be performed in order to understand their machinability, and thereby help manufacturers establishing appropriate cutting data. In this study, investigations are conducted to analyze the effects of cutting parameters and drill bit diameter on the thrust force, surface roughness, specific cutting energy, and dust emission during dry drilling of a new hybrid biocomposite consisting of polypropylene reinforced with miscanthus fibers and biochar. A full factorial design was used for the experimental design. It was found that the feed rate, the spindle speed, and the drill bit diameter have significant effects on the thrust force, the surface roughness, and the specific cutting energy. The effects of the machining parameters and the drill bit diameter on ultrafine particles emitted were not statistically significant, while the feed rate and drill bit diameter had significant effects on fine particle emission.

Keywords: Hybrid biocomposite, drilling, machinability, thrust force, specific cutting energy, surface roughness, fine particle, ultrafine particle.

3.1 Introduction

Natural fiber reinforced polymer (NFRP) composites are used in technical area such as construction, automotive parts, and sports' goods due to their many advantages, for instance, low density, high specific strength and stiffness, low hazard manufacturing process, and low cost (Pickering et al., 2016). Manufacturers are expected to use NFRPs as replacement of synthetic fiber reinforced polymer (SFRP) composites when producing automobile parts in order to minimize environmental impacts and reduce vehicle weight (Koronis et al., 2013). Products made with composite materials need to be machined (for example, drilled) in order to obtain the final dimensions or for assembly purposes. Conventional drilling is a popular hole making method, and an indispensable process for creating holes for parts assembly (Sheikh-Ahmad, 2009).

Many publications have covered the machining of SFRPs, while little research work has been done on the machining of NFRPs. Results relating to the machinability of SFRPs cannot be directly applied to NFRPs because of the differences in the mechanical properties of these two composites (Nassar et al., 2017). Debnath et al. (2017) investigated the drilling behavior of nettle/polypropylene composite with various drill bit geometries. They found that a specific drill bit geometry is only suitable for cutting one material, but is not appropriate for cutting others. Consequently, studying the cutting mechanism is necessary so that each material's machinability can be fully understood. Bajpai and Singh (2013) studied the machinability of sisal/polypropylene composite during the drilling process. They observed that the thrust force created with the standard drill tool is significantly bigger than that obtained with the trepanning tool. Maleki et al. (Hadi Rezghi Maleki et al., 2019) carried out an investigation on the machining of woven jute fabric reinforced polymer composite with different drill tool materials. They (Hadi Rezghi Maleki et al., 2019) showed that the delamination factor and thrust force are lower with the HSS drill compared to those obtained with carbide drills (CoroDrill 854 and CoroDrill 856). The surface roughness generated with the CoroDrill 856 was higher than that made with the HSS tool and the carbide CoroDrill 854. They recommended using the HSS twist drill when drilling jute fiber reinforced polymer composites (Hadi Rezghi Maleki et al., 2019).

The type of fibers used in composite materials has a great influence on the machinability of NFRPs since the tool used will cut both the fibers and the matrix. Therefore, in addition to machining parameters, the properties of the fibers must be taken into account when selecting the cutting tool (Nassar et al., 2017). Ismail et al. (Ismail, Dhakal, Popov, et al., 2016) investigated the drilling of sustainable and conventional composites (HFRP - hemp fiber reinforced polycaprolactone, and CFRP - carbon fiber reinforced polymer). They observed that cutting parameters can significantly affect the damage sustained by both composites. The thrust force, the roughness, and delamination increased with feed rate increase for these materials. Their results also showed that CFRP presents a lower surface roughness value, and that HFRP exhibits a smaller delamination factor during drilling process in the same cutting conditions. Abilash and Sivapragash (2016) studied the influence of cutting condition on delamination during drilling of polyester composite reinforced with bamboo fiber. They found that the feed rate and the drill bit diameter play a larger role in delamination failure. Venkateshwaran and ElayaPerumal (2013) presented that an increase in the feed rate and the spindle speed contributed to the rise of the delamination factor during drilling of epoxy composite reinforced with banana fibers. Chegdani and El Mansori (2018) found that the use of coated tools generated an increase in specific cutting energy in the drilling of bidirectional flax fiber reinforced polypropylene. The study (Bajpai et al., 2017) explored the machinability of two types of green composites (Sisal/PLA and Grewia Optiva/PLA). They noticed that drilling with a twist drill and a parabolic drill produces a better surface quality and a lower thrust force than does the Jo drill tool.

Debnath et al. (2014) investigated the drilling of sisal reinforced epoxy and polypropylene composites. They found that the machinability of sisal composite depends not only on the tool geometry, but also on the matrix material. The thrust force and torque generated are lower for the parabolic drill than for the step and four-facet drills. Higher torque values were observed for sisal/epoxy than for sisal/polypropylene at the same cutting condition. No delamination was observed for both materials. Palanikumar and Valarmathi (2016) studied the drilling of MDF (Medium Density Fiberboard, which is a wood-based composite) and discovered that the thrust force increased with the feed rate. Prakash et al. (2014) observed that the roughness increased with the drill bit diameter and feed rate during drilling of MDF.

Szwajka et al. (2019) noted that the tool coating type and the feed rate significantly influenced the thrust force and the roughness when machining MDF.

Hybrid composite materials are made from a common matrix reinforced with more than one type of reinforcements. Fu et al. (2002) defined hybrid composites as having two or more reinforcing materials mixed in a common matrix. Recently, some studies have looked at the machinability of hybrid composites. Jayabal et al. (2011) investigated the machinability during drilling of glass-coir/polyester hybrid composite. They found that the feed rate has a more significant effect on the thrust force than the drill diameter and spindle speed do. Navaneethakrishnan and Athijayamani (2016) observed the effect of cutting conditions on the cutting force during drilling of vinylester reinforced with sisal fiber and coconut shell powder. They discovered the drill point angle and the feed rate have the significant impact on thrust force. Increases in the point angle and the feed rate contribute to increases in the thrust force. Vinayagamoorthy (2017) observed that a decrease in the spindle speed and/or an increase in the feed rate lead to the rise of the thrust force and the roughness during drilling of polyester composite reinforced with jute and steel fiber. They also discovered that the thrust force increases with a drill diameter and drill point angle increase.

The dust generated during machining of metallic materials has been studied by several researchers (R. Khettabi et al., 2007; Songmene et al., 2008a,b; Djebara et al., 2013; Zaghbani et al., 2009; Kamguem et al., 2013; J. Kouam et al., 2012; Riad Khettabi, Songmene, & Masounave, 2010; Balout et al., 2007; Jules Kouam et al., 2015; Riad Khettabi, Songmene, Zaghbani, et al., 2010), who observed that the relationship of the dust emission with cutting conditions such as the workpiece material, tools, and cutting parameters (R. Khettabi et al., 2007; Riad Khettabi, Songmene, & Masounave, 2010; Riad Khettabi, Songmene, Zaghbani, et al., 2010). Small size dust emitted during machining has a significant impact on the environment and on the health of machine operators (Songmene et al., 2008a; Balout et al., 2007). Djebara et al. (2013) observed that during machining, the greatest proportion of dust generated is less than 2.5 microns, for different workpiece materials at different cutting conditions. The quantity of particles emitted is a function of the spindle speed and the feed rate (Songmene et al., 2008a; Kamguem et al., 2013). Kouam et

al. (2012) found that friction has a great impact on dust formation. Zaghbani et al. (2009) noted that the deformation conditions in the chip formation zone greatly influence the dust generated, while the cutting conditions do not significantly affect the nanoparticle generation rate. The result from (Kamguem et al., 2013) indicates that the tool coating materials influence the dust generated during the machining of aluminum alloys. The study (Balout et al., 2007) investigated the effect of the initial temperature of the workpiece material on fine dust emission during dry drilling and found that the initial workpiece temperature greatly affects the dust generation. For pre-cooled workpiece materials, the equivalent generation was low.

To date, only a few studies have focused on dust generated during machining of composites. Marani et al. (2018) found that the cutting parameters and the microstructure of the workpiece material directly affect the dust generated during metal matrix composite milling. Songmene et al. (2018) found that fine dust generation is significantly reduced by using water MQL (Minimum Quantity Lubrication) during polishing of granite, while ultrafine particle generation is insensitive to water use. Kremer and Mansori (Kremer & El Mansori, 2009) observed that a smooth coating tool generates more dust than a rough one during machining of metal matrix composite. The study (Kremer & El Mansori, 2011) showed that the dust created during cutting of metal matrix composite is affected differently depending on the tool type. Haddad et al. (2014) revealed that dust emission is a function of cutting parameters and the tool geometry during the trimming of polymer composite reinforced with carbon fibers.

The aim of this study is to investigate the effects of machining conditions on the machining process performance indicators: Specific cutting energy, thrust force, surface roughness, and fine dust and ultrafine dust emission during dry drilling of a new hybrid biocomposite material made of miscanthus fibers and biochar reinforced polypropylene.

3.2 Experimental setup

3.2.1 Workpiece material

The hybrid biocomposite material used consists of a matrix (polypropylene (PP)/ polyolefin elastomer (POE)) randomly reinforced with biochar and chopped miscanthus fiber, and mixed with a MAPP (Maleic Anhydride grafted Polypropylene) compatibilizer. The composition of the hybrid biocomposite is presented in Table 3.1.

Table 3.1 Composition of hybrid biocomposite

PP (wt%)	POE (wt%)	MAPP (wt%)	Biochar (wt%)	Miscanthus (wt%)
62	5	3	15	15

PP (trade name, 1350N) is produced by Pinnacle Polymers LLC, LA, USA. POE (trade name, Engage 7487); MAPP (trade name, Fusabond 613). The biochar is the result of the pyrolysis operation of natural miscanthus fibers (average length of 4 mm) invented in Southern Ontario, Canada. Competitive Green Technologies supplied four millimeters long miscanthus fibers that were used for the manufacturing of the hybrid composite. Figure 3.1 describes the miscanthus fibers and biochar that were made from miscanthus fibers by pyrolysis (Anstey et al., 2016). The mechanical properties of hybrid biocomposite are described in Table 3.2 (Dhaouadi, 2018).

Table 3.2 Mechanical properties of hybrid biocomposite (Dhaouadi, 2018)

Tensile strength (MPa)	34
Young’s modulus (MPa)	3175
Flexural strength (MPa)	55
Flexural modulus (MPa)	2717
Impact strength (J/m)	140

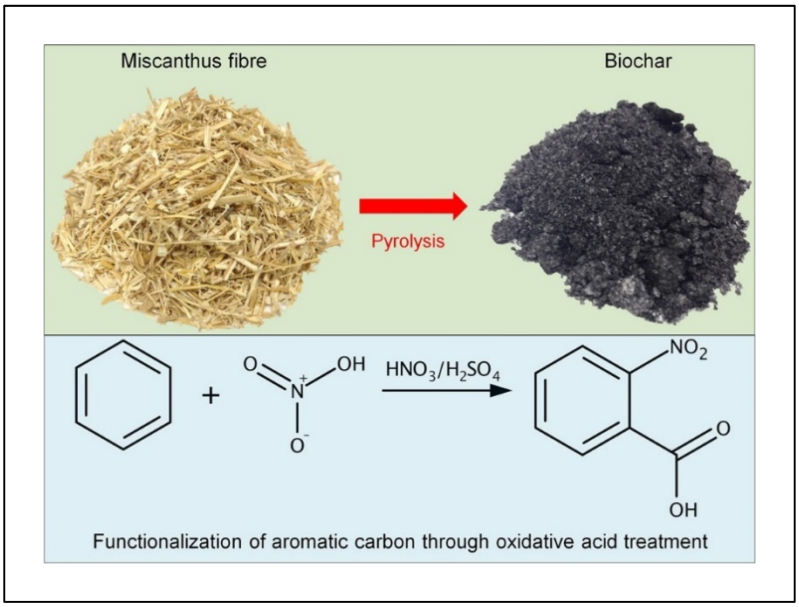

Figure 3.1 Fabrication of biochar (Anstey et al., 2016)

The hybrid biocomposite material was produced through the press molding process, using a French Press USA machine, TMP, Model EHV, max tonnage 57 tons. The following steps represent the process for producing compression-molded materials. Firstly, the mold platens are preheated to 180 °C for 30 min. Then, the material is loaded into the press and pre-heated with closed platens, but without raising the pressure in order to melt material before pressing. This operation takes about 10 minutes. Then vacuuming is conducted to degas for 3 min, and platens are closed at a pressure of 2 tons for 10 min. Finally, the platens are cooled to below 50 °C and then removed from the press.

The hybrid biocomposite material was developed in 2017 by the University of Guelph Bioproducts Discovery and Development Center for internal automobile parts production. The result obtained from (Dhaouadi, 2018) showed this hybrid biocomposite exhibited better stiffness than the matrix (PP/POE). The Young's modulus of the matrix was increased by 70% as reinforced with biochar (15wt%) and miscanthus (15wt%). Hybrid biocomposite has higher tensile and flexural strength than commercial Talc/PP composite (RTP132UV). As a

result, hybrid biocomposite is considered the most likely material to replace the commercial Talc/PP composite.

3.2.2 Experimental procedure

The dry drilling of hybrid biocomposite was conducted on a 3-axis CNC machine-tool (HURON - K2X10) with the following main characteristics: Maximum power, 50 KW; and spindle speed, 28,000 rpm. Standard HSS twist drill bits (6 mm, 8 mm, 10 mm diameters) were used to drill holes on the workpiece. The cutting parameters were selected based on the tool manufacturer's catalogue and literature.

The workpiece sample (300 mm × 120 mm × 5 mm) was screwed to an aluminum back plate support. The support (300 mm × 120 mm × 30 mm) had 80 drilled holes (12 mm diameter). The subsystem (workpiece and back plate support) was placed and tightened onto the dynamometer with screws. The responses measured and analyzed were the drilling force, the surface roughness, and the particle emission. The drilling forces were measured using a dynamometer (type Kistler 9255B) clamped on the machine table and connected to the charge amplifiers (type Kistler 5010 (Kistler Instrument Corporation, New York, NY, USA)) that generated output signals, which were transmitted to a data translation card (type DT 9836, Data Translation Inc., Marlborough, MA, USA) and then connected to a personal computer.

A Scanning Mobility Particle Sizer (SMPS, model #3080, TSI Inc., Shoreview, MN, USA) equipped with a nano DMA (Differential Mobility Analyzer) was used to measure ultrafine particles generated with sizes ranging from 7 nm to 100 nm during drilling. An Aerodynamic Particle Sizer (APS, model 3321, TSI Inc., Shoreview, MN, USA) was used for measuring of fine particles, with diameter ranging from 0.5 to 10 μm. For both pieces of equipment, the dust samples were sucked by a pump (1.5 L/min) through a suction tube, with the end of a tube placed near the machining area. The suction tube was connected to the dust measurement system, which consisted of APS and SMPS. The experimental scheme is illustrated in Figure 3.2.

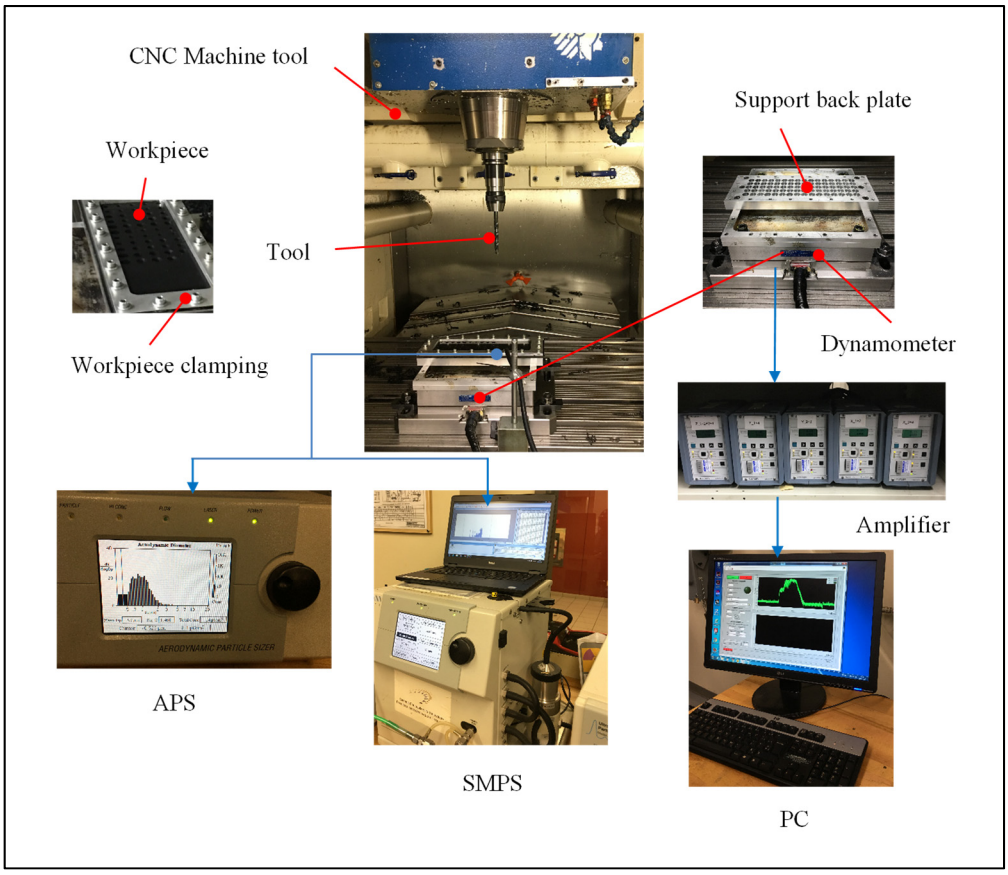

Figure 3.2 The experimental devices for machining and measurement system

The roughness profilometer (Mitutoyo, model SJ-410) (Mitutoyo America Corporation, Aurora, IL, USA) was used to measure the surface roughness. This equipment was connected to a computer with the help of the SURFPAK–SJ software for recording and analyzing the roughness data. The measurements of the surface roughness of a drilled hole were carried out in the feed direction, and were repeated three times for each tested condition.

The experiments were based on a full factorial design, with 3 input parameters at 3 levels. In order to obtain reliable and accurate results, each test was repeated three times, and the mean of the measured values was selected for analysis. Table 3.3 summarizes the factors investigated and their respective levels.

Table 3.3 The design of experiments

Factors	Level 1	Level 2	Level 3
f: Feed rate (mm/rev)	0.1	0.2	0.3
s: Spindle speed (rpm)	600	1500	2400
d: Drill bit diameter (mm)	6	8	10

3.3 Results and discussion

3.3.1 Thrust force

The thrust force was calculated as the average value from the thrust force signals when the main cutting edges and the chisel edge of the drill were in full contact with the workpiece. Table 3.4 presents the analysis of variance for the thrust force. The effect of the main factors and their interaction on the drilling process was analyzed by ANOVA. The main objective of ANOVA is to apply the statistical method to understand the effect of the individual factors. It is found that four factors have P-values smaller than 0.05, which are statistically significant at the 95% confidence interval. The feed rate (f) has the highest effect on the thrust force, followed by the spindle speed (s), the drill bit diameter (d) and the interaction sd. It is also shown that the interaction fs and the interaction fd are not statistically significant for the thrust force.

Table 3.4 ANOVA for thrust force

Source	Sum of Squares	D_f	Mean Square	F-Ratio	P-Value
f: Feed rate (mm/rev)	9121.5	1	9121.5	104.28	0.0000
s: Spindle speed (rpm)	3949.53	1	3949.53	45.15	0.0000
d: Drill bit diameter (mm)	2801.01	1	2801.01	32.02	0.0000
Interaction f.s (mm/min)	126.945	1	126.945	1.45	0.2424
Interaction f.d (mm^2/rev)	205.427	1	205.427	2.35	0.1411
Interaction s.d (rpm*mm)	1374.52	1	1374.52	15.71	0.0008
Total error	1749.41	20	87.4703		
Total (corr.)	19328.3	26			

The factors with statistically significant effects were selected to develop the experimental prediction model for the thrust force using regression analysis. The thrust force was related to the machining parameters as follows:

$$F_t = 42.82 + 225.11 \times f - 0.031 \times s - 2.68 \times d + 5.95 \times 10^{-3} \times s \times d \quad (3.1)$$

Where F_t is the thrust force (N), and f, s, and d denote the feed rate (mm/rev), the spindle speed (rpm), and the drill bit diameter (mm), respectively. The coefficient of correlation obtained from the ANOVA, R^2 was 89.23% and the R^2-adjusted was 87.27%. These coefficients indicate that the model is adequate for prediction of thrust force.

Figure 3.3 shows the main effects of the tested factors on thrust force. It can be seen that the feed rate has a larger effect on the thrust force than do the spindle speed and drill bit diameter. This is in agreement with other observations (Jayabal et al., 2011). Generally, the thrust force increased with the drill diameter, the feed rate, and the spindle speed.

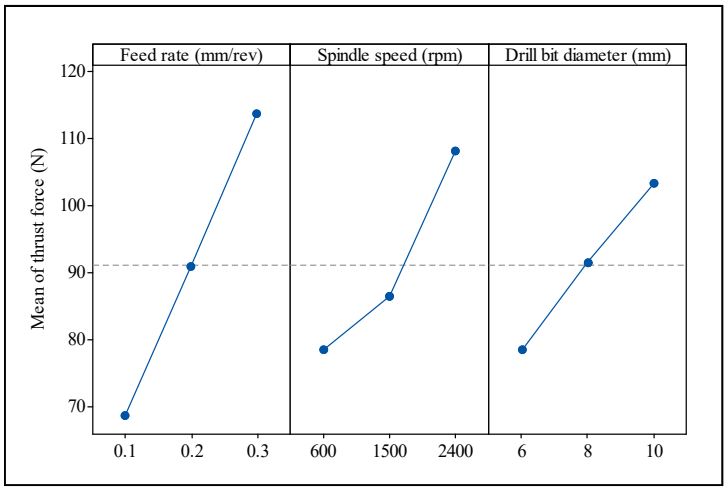

Figure 3.3 The main effects for thrust force

In Figure 3.4, it can be seen that the rise of thrust force follows an increase in feed rate. It can be interpreted that an increase in feed rate contributed to the larger of the cross-sectional area of the uncut chip. This led to an increase in the resistance to chip formation, and subsequently, to the higher thrust force value. This result is consistent with other studies (Debnath et al., 2017; Hadi Rezghi Maleki et al., 2019; Bajpai et al., 2017; Debnath et al., 2014; Palanikumar & Valarmathi, 2016; Basavarajappa et al., 2012; Latha et al., 2011). It also indicates that the thrust force increases rapidly with feed rate increase, especially at the highest spindle speed of 2400 rpm, with a drill of 10 mm (Figure 3.4c).

Figures 3.3 and 3.4c show that an increase of the thrust force results from the use of larger drill's diameter. This can be explained by the fact that an increase on drill bit diameter leads to an increase in the cross-sectional area of the uncut chip and the chisel edge width. Therefore, higher cutting forces are required. Furthermore, an increase in the drill's diameter makes the contact area between the workpiece material and drill bit larger, which results in increased friction, and thus thrust force increases (Vinayagamoorthy, 2017). This is in agreement with the results obtained from other studies (Vinayagamoorthy, 2017; Latha et al., 2011).

Figure 3.4 also depicts the interaction between the feed rate, the spindle speed, and the drill bit diameter on thrust force. It presents the thrust force in relation to the drill bit diameter with different feed rates and spindle speeds: 600 rpm (Figure 3.4a), 1500 rpm (Figure 3.4b), and 2400 rpm (Figure 3.4c). It is seen that the thrust force increases slightly with drill bit diameters ranging from 6 mm to 8 mm at different spindle speeds. Nevertheless, the thrust force has an unclear trend, with drill bit diameters ranging from 8 mm to 10 mm due to the interaction between the spindle speed and the drill bit diameter (Figure 3.4a–c). In general, the thrust force rose slowly with an increase in the drill bit diameter at spindle speeds ranging from 600 rpm to 1500 rpm. However, the thrust force increased significantly with drill's diameters at s = 2400 rpm.

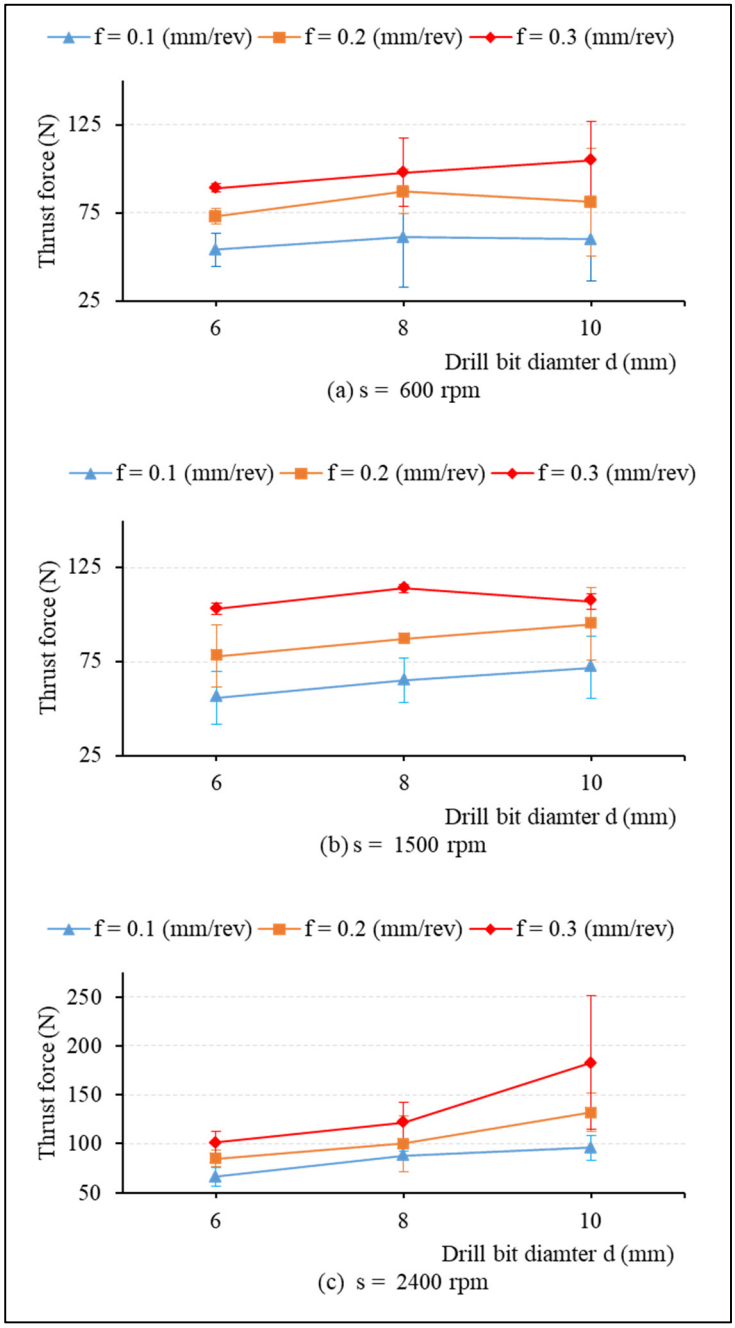

Figure 3.4 Thrust force related to drill bit diameter during drilling of hybrid biocomposite with different feed rates, at spindle speeds: (a) s = 600 rpm, (b) s = 1500 rpm, and (c) s = 2400 rpm

From Figures 3.3 and 3.4, it can be found that the thrust force increases with the spindle speed increase. Figure 3.5 indicates that the thrust force rises slowly with the spindle speed

(in the range of 600 rpm to 1500 rpm), and then increases significantly as the spindle speed rises up to 2400 rpm. This can be explained as follows:

The linear feed rate in mm/min, v_f, is expressed by $v_f = f * s$, where s is the spindle speed in revolution per minute (rev/min), and f is the feed rate in millimeter per revolution (mm/rev). It showed that the spindle speed increase leads to an increase in the linear feed rate v_f (mm/min) due to fact that the feed rate is an independent parameter. Consequently, the spindle speed increase results in an increase in the thrust force. This is similar to the results of other investigations, with an increase in the linear feed rate (mm/min) leading to an increase in thrust force (Palanikumar & Valarmathi, 2016; Basavarajappa et al., 2012; Latha et al., 2011). The maximum thrust force value was obtained at the highest value of input parameters (f = 0.3 mm/rev, s = 2400 rpm, and d = 10 mm).

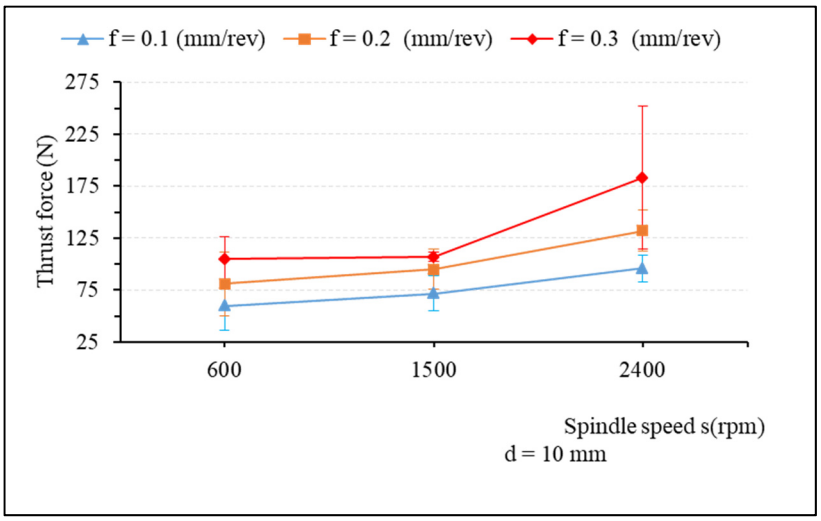

Figure 3.5 Thrust force versus the spindle speed when drilling hybrid biocomposite using drill bit diameter of 10 mm with various feed rates

3.3.2 Specific cutting energy for thrust force

The specific cutting energy (also called the specific cutting pressure) is defined as the cutting force per unit area of the uncut chip. During the drilling process with the standard twist drill bit, K_t denotes the specific cutting energy for the thrust force (N/mm^2), and is calculated as in the following equation (Sheikh-Ahmad, 2009):

$$K_t = (2 \times F_t)/(f \times d) \quad (3.2)$$

Where F_t, f, and d denote the thrust force (N), the feed rate (mm/rev), and the drill bit diameter (mm), respectively.

Table 3.5 presents the analysis of variance for specific cutting energy related to the thrust force. It shows that three tested factors have effects with P-values smaller than 0.05, which indicates that they are statistically significant at the 95% confidence level. The feed rate has the highest effect on the specific cutting energy for the thrust force. These factors were used to develop the empirical model for the prediction of the specific cutting energy for the thrust force. The result from the ANOVA shows that R^2 is 86.65% and the adjusted R^2 is 84.91%, which indicates that the model is suitable for prediction. The empirical model for specific cutting energy K_t (N/mm^2) was obtained as follow:

$$K_t = 237.31 - 393.57 \times f + 2.19 \times 10^{-2} \times s - 7.78 \times d \quad (3.3)$$

Where f (mm/rev) is the feed rate; s (rpm) is the spindle speed; and d (mm) is the drill diameter.

Table 3.5 ANOVA for specific cutting energy

Source	**Sum of Squares**	**D_f**	**Mean Square**	**F-Ratio**	**P-Value**
f: Feed rate (mm/rev)	27881.8	1	27881.8	137.47	0.0000
s: Spindle speed (rpm)	7015.2	1	7015.2	34.59	0.0000
d: Drill bit diameter (mm)	4361.16	1	4361.16	21.50	0.0002
Interaction f.s (mm/min)	768.16	1	768.16	3.79	0.0658
Interaction f.d (mm^2/rev)	388.855	1	388.855	1.92	0.1814
Interaction s.d (rpm*mm)	833.333	1	833.333	4.11	0.0562
Total error	4056.54	20	202.827		
Total (corr.)	45305.1	26			

Figures 3.6 and 3.7 showed that the specific cutting energy for the thrust force decreased with an increase in feed rate, but increased when the spindle speed increased. This result is in agreement with the literature (Faissal Chegdani & El Mansori, 2018). It is also observed that an increase in the drill's diameter contributes to a decrease of the specific cutting energy for the thrust force (Figure 3.6).

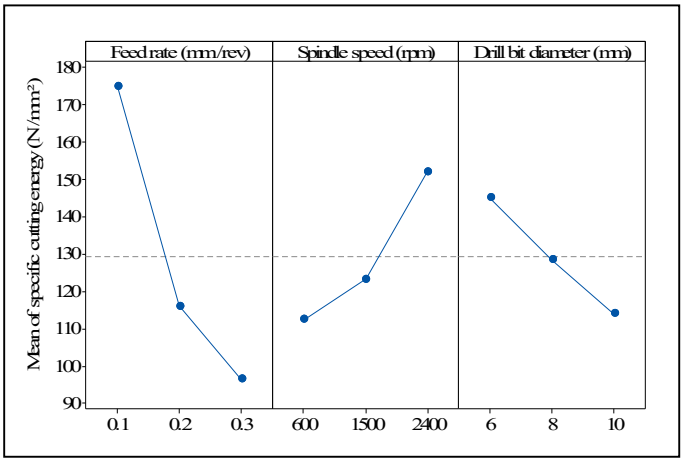

Figure 3.6 Main effects plot for specific cutting energy related to thrust force

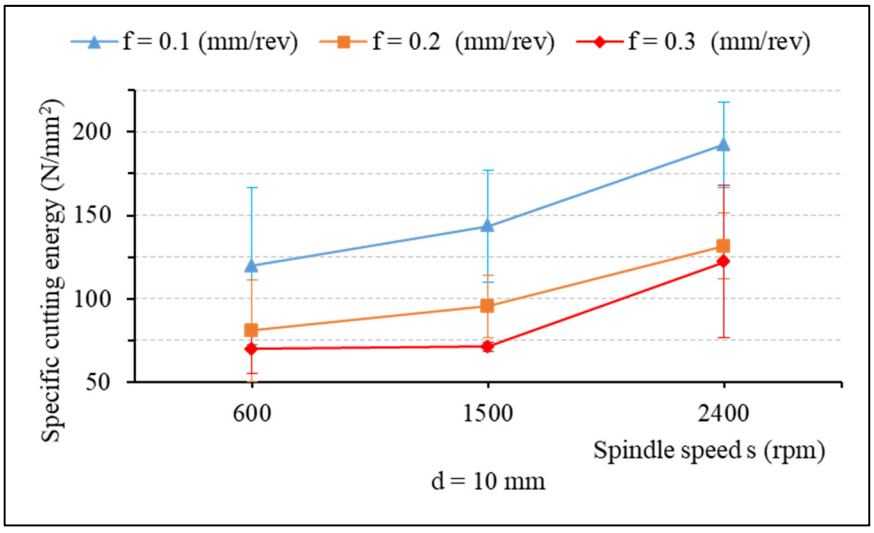

Figure 3.7 Specific cutting energy for thrust force as a function of spindle speed with different feed rates and drill bit diameter of 10 mm

3.3.3 Surface roughness

The surface roughness is one of the criteria for determining the machined surface quality. In the present research work, the surface roughness parameters were measured in the hole in a longitudinal direction. The roughness parameters were measured three times for each hole, with a cut-off length of 0.8 mm. The mean arithmetic average roughness (R_a) value and the maximum profile height (R_t) obtained from the measured results were used for evaluating the effect of cutting conditions on the machined surface. Figure 3.8 presents the measured profile of holes drilled in the longitudinal direction, at different cutting conditions. Figure 3.8a shows the drilled hole with the best surface finish at cutting condition (f = 0.2 mm/rev, s = 600 rpm, d = 6 mm). The highest surface roughness value was obtained at cutting condition (f = 0.3 mm/rev, s = 2400 rpm, d = 10 mm), illustrated in Figure 3.8b. The morphology of the surface before machining and the machined surface with the largest surface roughness value is presented in Figure 3.9. The machined surface indicates that neither uncut fibers nor delamination were found.

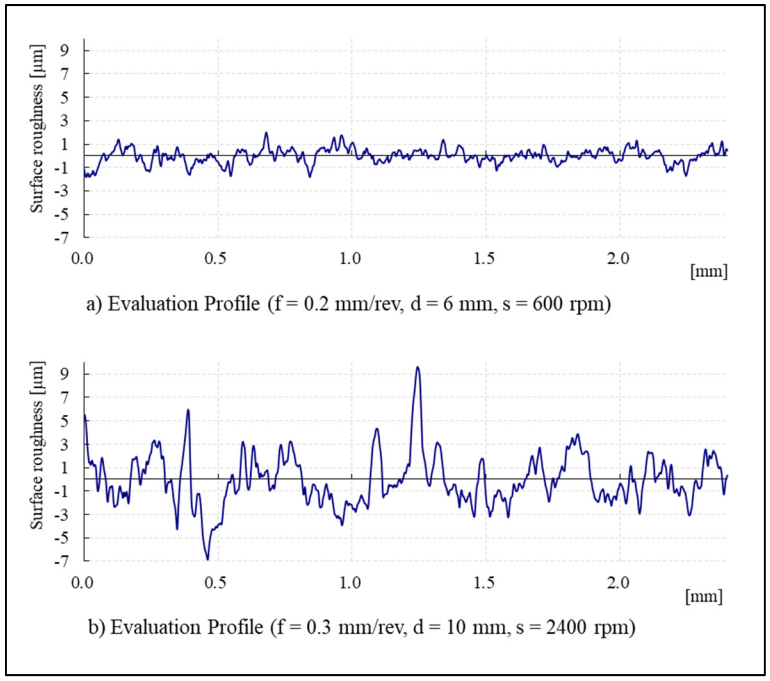

Figure 3.8 Surface roughness profile for drilled holes with different cutting conditions: (a) f = 0.2 mm/rev, d = 6 mm, s = 600 rpm; and (b) f = 0.3 mm/rev, d = 10 mm, s = 2400 rpm

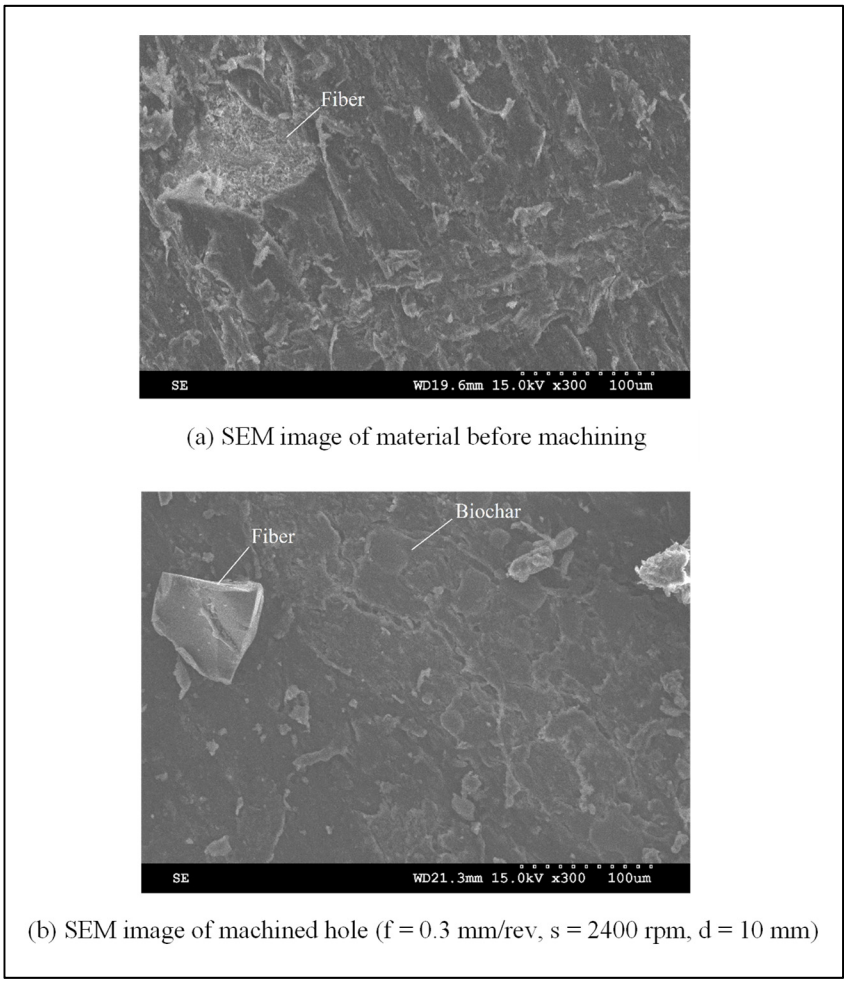

Figure 3.9 SEM images for hybrid biocomposite: (a) SEM image of surface before machining; (b) machined surface at f = 0.3 mm/rev, s = 2400 rpm, d = 10 mm

3.3.3.1 **The arithmetic average roughness (R_a)**

Table 3.6 indicates that three tested factors (Feed rate, spindle speed, and drill diameter) have P-values smaller than 0.05. These factors are statistically significant at the 95% confidence level. It is found that the drill bit diameter has the greatest influence on the surface roughness. The interaction of each factor with others (fd, fs, and sd) have no statistical significance. The coefficient of correlation was obtained R^2 is 85.46%, indicating the models as fitted explains 85.46% of the variability in surface roughness. The adjusted R^2 is 83.57%, which is more suitable for comparing models with different numbers of independent

variables. It showed that the model is adequate for prediction. The empirical model was obtained as follows:

$$R_a = -0.22 + 0.48 \times f + 16.33 \times 10^{-5} \times s + 0.1 \times d \quad (3.4)$$

Where f (mm/rev) is the feed rate; s (rpm) is the spindle speed; and d (mm) is the drill diameter.

Table 3.6 ANOVA for surface roughness R_a

Source	**Sum of Squares**	**D_f**	**Mean Square**	**F-Ratio**	**P-Value**
f: Feed rate (mm/rev)	0.0418569	1	0.0418569	4.50	0.0465
s: Spindle speed (rpm)	0.388962	1	0.388962	41.86	0.0000
d: Drill bit diameter (mm)	0.710829	1	0.710829	76.50	0.0000
Interaction f.s (mm/min)	0.00213333	1	0.00213333	0.23	0.6370
Interaction f.d (mm^2/rev)	0.006075	1	0.006075	0.65	0.4283
Interaction s.d (rpm*mm)	0.000133333	1	0.000133333	0.01	0.9058
Total error	0.185835	20	0.00929174		
Total (corr.)	1.33582	26			

Figure 3.10 presents the main effects on the arithmetic average roughness (R_a). Figure 3.11 illustrates the influence of cutting parameters on the surface roughness when drilling hybrid biocomposite with the smallest diameter drill bit (d = 6 mm). From Figures 3.10 and 3.11, it can be observed that the surface roughness increases with an increase in one of the three main factors of the drilling process in general. Figure 3.12 shows the influence of the drill bit diameter on surface roughness, with various cutting parameters. It is also observed that the use of the bigger drill bit diameter leads to a dramatic increase in the roughness, which is consistent with the result obtained from other investigations (Prakash et al., 2014).

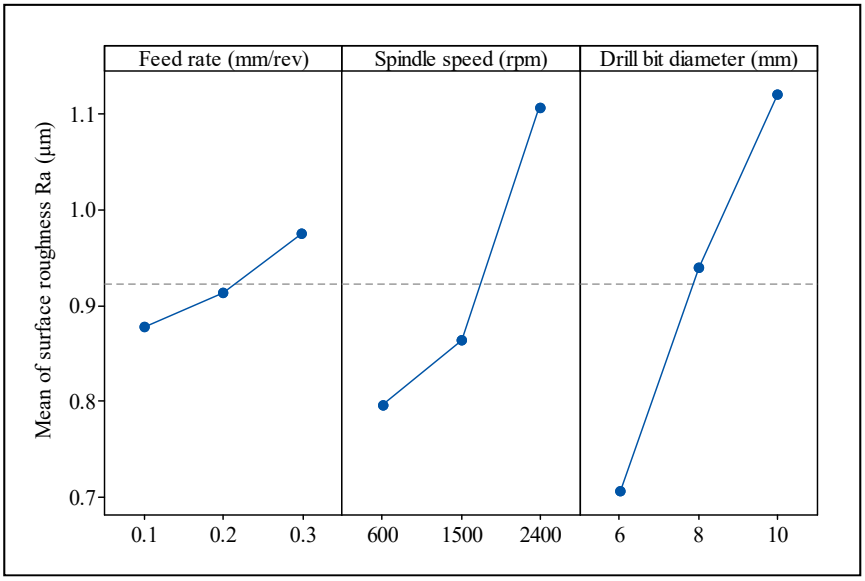

Figure 3.10 Main effects plot for the roughness (R_a)

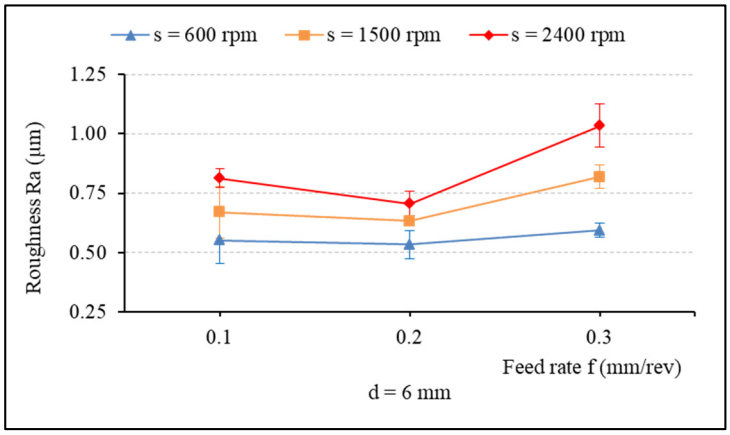

Figure 3.11 Surface roughness (R_a) versus the feed rate when drilling with different spindle speeds, d = 6 mm

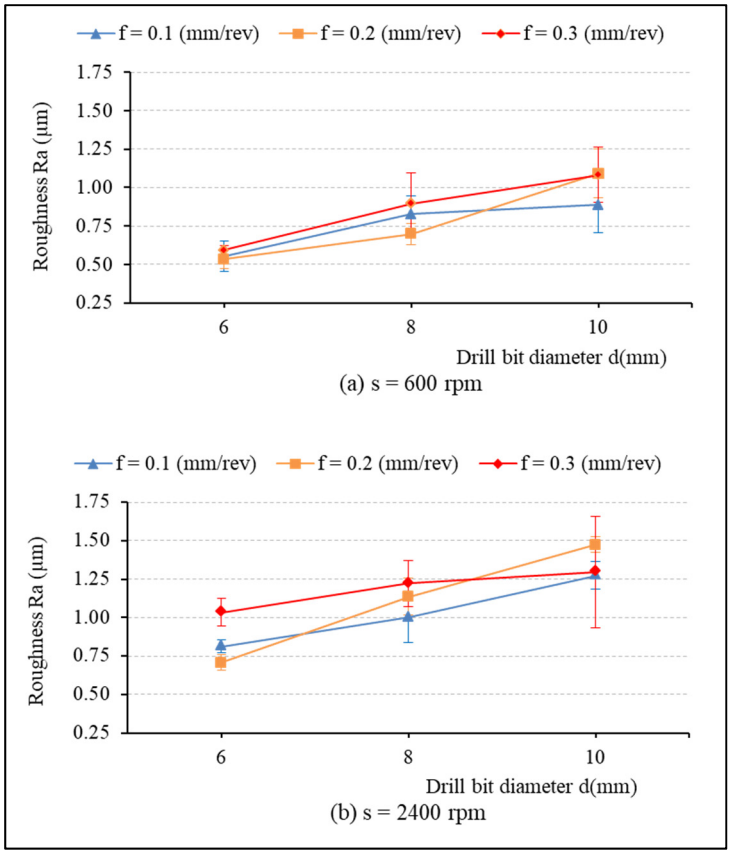

Figure 3.12 The roughness (R_a) versus drill's diameter with different feed rates and spindle speeds: (a) s = 600 rpm, (b) s = 2400 rpm

In Figure 3.11, it can be observed that R_a decreases slightly as the feed rate rises from 0.1 to 0.2 mm/rev, and then it experiences a dramatic increase with the rise of feed rate up to 0.3 mm/rev. It is observed that the surface roughness is more sensitive to variations of feed rate at the highest spindle speed (2400 rpm) than at the lowest spindle speed (600 rpm). It also shows the main influential trend that the surface roughness (R_a) increases slightly with an increase in feed rate (Figure 3.10), which is consistent with some studies (Prakash et al., 2014; Basavarajappa et al., 2012).

In Figure 3.10, it can be found that the spindle speed increase from 600 to 1500 rpm leads to a slight roughness increase; the roughness then increases sharply as the spindle speed rise up to 2400 rpm. This can be explained by the fact that the linear feed rate (mm/min) rises with the spindle speed increase, as mentioned above, and contributes to a reduced cutting time.

This in turn results in the reduction of contact time between the drill bit and the workpiece, a reduction of the polishing effect, and a simultaneous increase in thrust force. As a result, the surface roughness increases as the spindle speed increases.

3.3.3.2 **Maximum height of profile (R_t)**

The Pareto diagram (Figure 3.13) illustrates the effect of the machining parameters on the roughness R_t. It is seen that two factors (drill diameter and spindle speed) are statistically significant on the roughness R_t. From Figure 3.14, it can be observed that the main influential trend of cutting parameters on the maximum height of the profile (R_t) is similar to that of surface roughness R_a, discussed above. The R_t-values increase with an increase in the spindle speed (Figure 3.14a) and the drill bit diameter (Figure 3.14b)

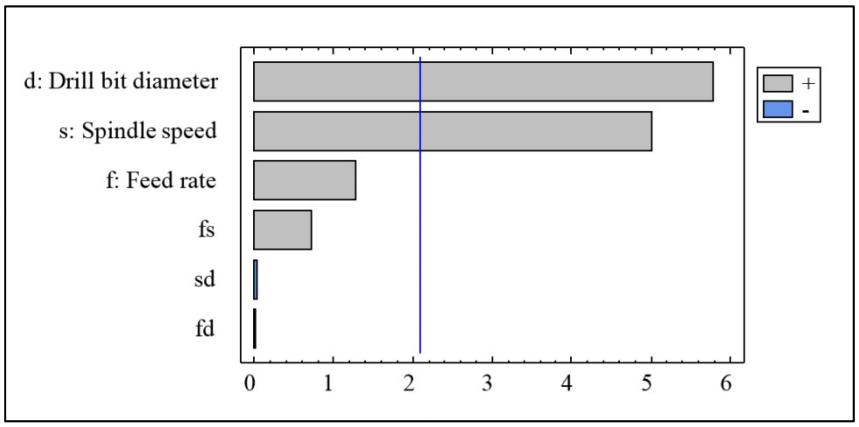

Figure 3.13 The chart of the effects for the surface roughness R_t

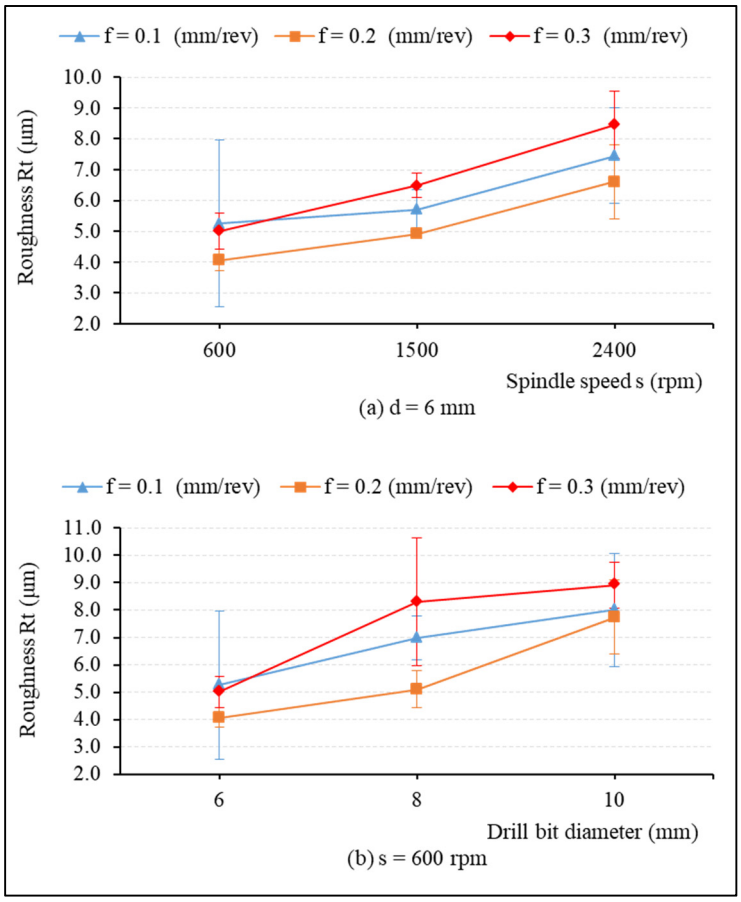

Figure 3.14 Roughness R_t versus the cutting conditions:
(a) d = 6 mm; and (b) s = 600 rpm

3.3.4 Dust emission during drill process

3.3.4.1 **Fine particle emission**

The rotation of the drill during machining creates an airflow movement around the drill tool, which results in the dispersion of dust generated at the cutting zone. The size and quantity of the dust depend on the cutting parameters, the workpiece, and the tool material (Kamguem et al., 2013; Riad Khettabi, Songmene, Zaghbani, et al., 2010). The aerodynamic particle sizer (APS) measures particles from 0.5 to 10 µm, and presents these results by parameters such as number concentration, mass concentration, and specific surface concentration, as a function of aerodynamic diameters. Particles with a size below 2.5 µm ($PM_{2.5}$) are very dangerous for

the machine operator and environment (Balout et al., 2007). In the present study, the fine particles (PM_{10}) were collected as output parameters for the investigation.

From the collected data, it is found that large quantities of fine particles with sizes smaller than 2.5 µm ($PM_{2.5}$) are generated during dry drilling of hybrid biocomposite (approximately 98% of total fine dust). Figure 3.15 presents the number of fine particles in relation to aerodynamic diameters when drilling hybrid biocomposite, with a drill of 6 mm and various spindle speeds. It is also seen that most particles generated are of a size ranging from 0.5 µm to 1.5 µm, with a peak occurring at 0.673 µm. The observation indicates that the number of fine particles decreased with the feed rate increase (Figure 3.15a,b).

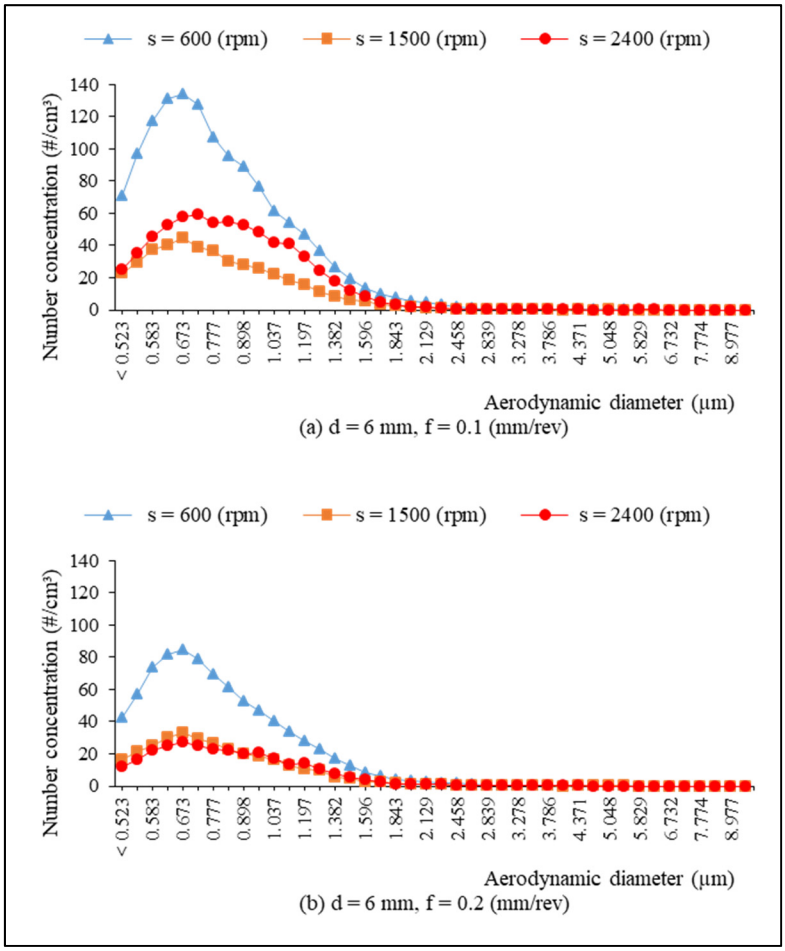

Figure 3.15 The number of fine particles versus aerodynamic diameters during drilling, with a drill of 6 mm: (a) f = 0.1 mm/rev; and (b) f = 0.2 mm/rev

Figure 3.16 presents the maximum value of number of fine particles obtained during the drilling of hybrid biocomposite with different cutting parameters, with a drill bit diameter of 6 mm. According to the collected data, most of the maximum number concentration values were obtained with a size of 0.673 µm, except for one case (f = 0.1 mm/rev, s = 2400 rpm), a particle size of 0.723 µm has a peak value of 59 (#/cm^3), followed by a size of 0.673 µm with 58 (#/cm^3). Therefore, it can be deduced that the fine particle with a size of 0.673 µm achieved the greatest number concentration versus other sizes in the same cutting condition.

From Figure 3.16, it can be seen that the spindle speed increase results in a decrease in the maximum fine particle number concentration value. It may be inferred that the rise of the spindle speed may cause particles generated to be dispersed away from the machining area, thereby reducing the number of measured particles near the cutting zone.

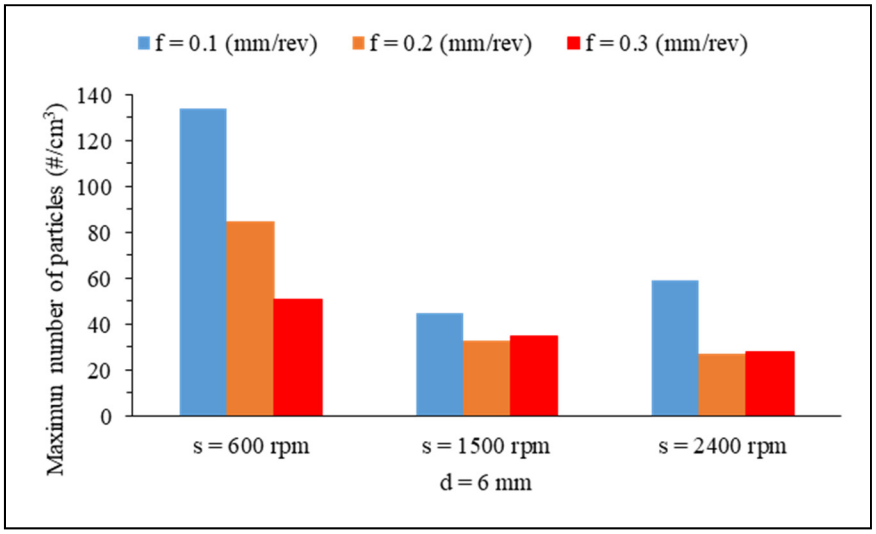

Figure 3.16 Peak value of number of fine particles related to particle size

The Pareto diagram (Figure 3.17) shows that the drill bit diameter (d) has the greatest effect on the fine particles (PM_{10}), followed by the feed rate (f) and the interaction between the speed and the drill diameter (sd). The spindle speed (s) and interactions fs and fd have no statistical significance for fine particles emission.

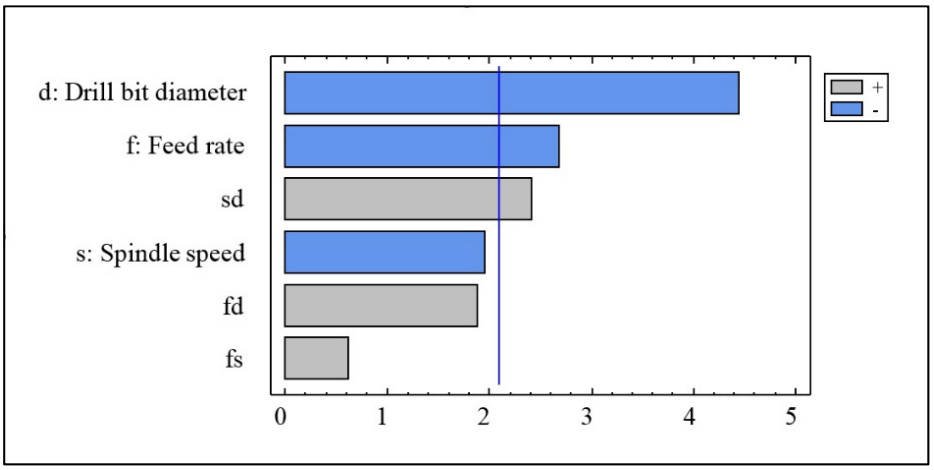

Figure 3.17 Pareto diagram for total number of fine particles (PM_{10})

Figure 3.18 indicates that an increase in feed rate and/or drill bit diameter contributes to a reduction in the total number of fine particles. Figure 3.19 presents the total number concentration of fine particles in relation to the feed rate when drilling hybrid composite at different spindle speeds, with a drill of 6 mm. It is observed that the rise in feed rate leads to a decrease in the total number of fine particles.

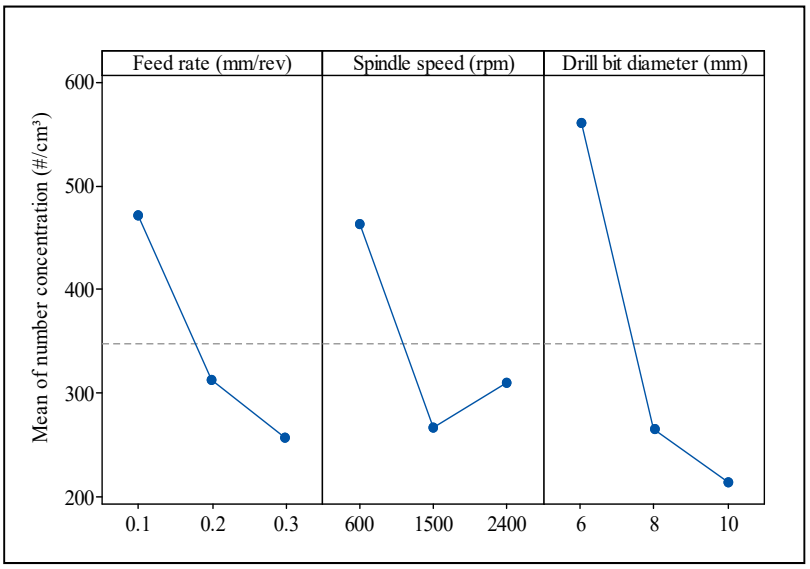

Figure 3.18 Main effect plot for fine particles emission

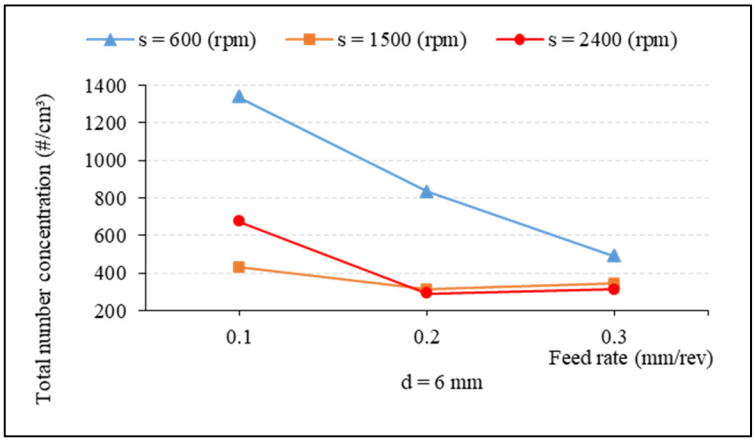

Figure 3.19 The number of fine particles versus the feed rate during drilling with different cutting parameters, d = 6 mm

In order to better understand the influence of the feed rate on the fine dust generated, additional experiments were conducted with s = 1500 rpm, d = 8 mm, and f = 0.05 - 0.3 mm/rev (Figure 3.20). It is observed that the main trend of the total number of fine particles points to a slight decrease as the feed rate increase. Figure 3.21 presents the total number concentration of fine particles as a function of drill bit diameter during drilling of biocomposite with different feed rates, s = 600 rpm. It was found that a larger drill bit diameter contributes to a decrease in the total number concentration of fine particles.

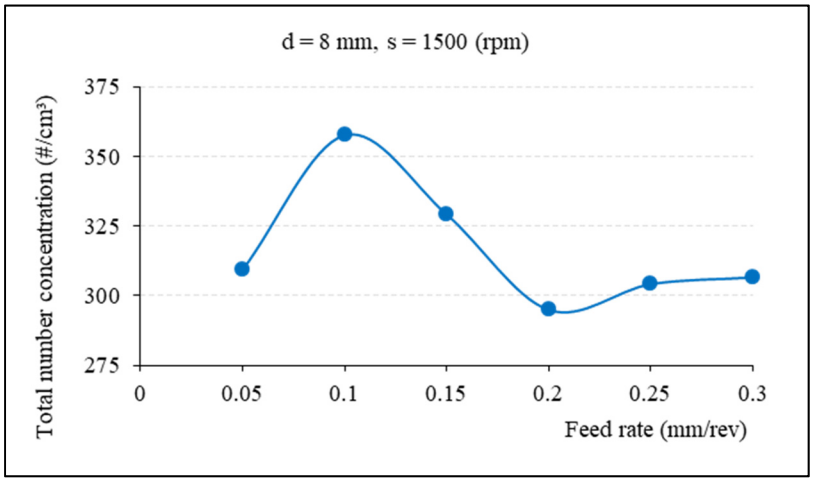

Figure 3.20 The fine particles related to the feed rate, with d = 8 mm, s = 1500 rpm

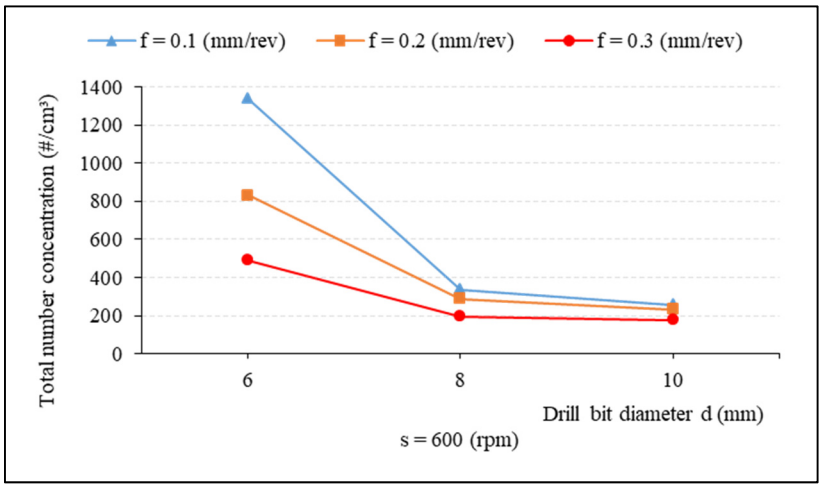

Figure 3.21 The number of fine particles related to drill bit diameter when drilling, with different feed rates, s = 600 rpm

3.3.4.2 **Ultrafine particle (UFP) emission**

Ultrafine particles with sizes ranging between 7 nm and 100 nm were used for the analysis presented in this sub-section. The Pareto diagram (Figure 3.22) indicates the influence of the tested factors and their interaction on the total number concentration of ultrafine particles during the drilling process. The tested factors and their interactions do not have statistically significant effects on ultrafine particles emitted at 95% confidence level. It was found that the spindle speed has a higher effect on ultrafine particles than do the feed rate and the drill's diameter.

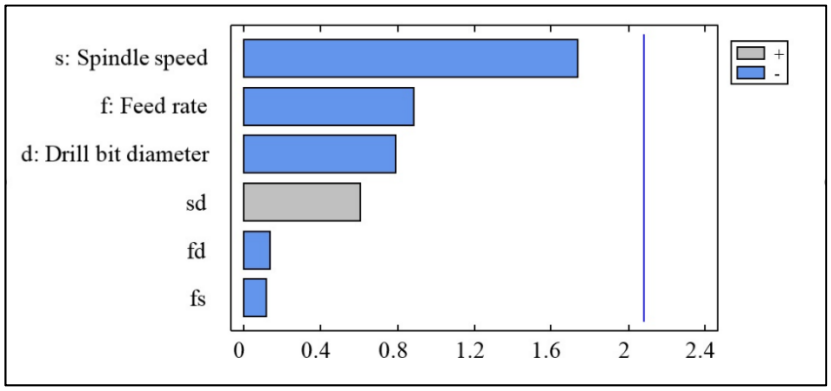

Figure 3.22 Pareto diagram for ultrafine particles emission

From Figure 3.23, it can be observed that the cutting conditions have an unclear influence on ultrafine particles emitted. Generally, the number concentration decreased with increasing spindle speed, drill bit diameter, and feed rate.

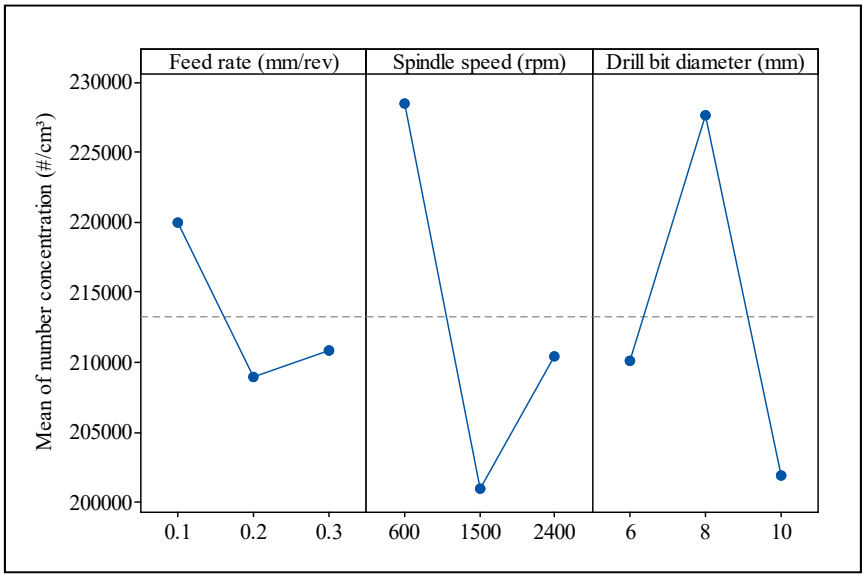

Figure 3.23 Main effect plot for total number concentration of ultrafine particles

Figure 3.24 presents the number concentration of ultrafine particles versus the aerodynamic diameter during drilling of hybrid biocomposite at different spindle speeds, with f = 0.1 (mm/rev), d = 10 mm (Figure 3.24a), and with f = 0.3 (mm/rev), d = 8 mm (Figure 3.24b). It is seen that most numbers of ultrafine particles have aerodynamic diameters ranging from 30 nm to 100 nm, with the greatest amount being around 50 nm.

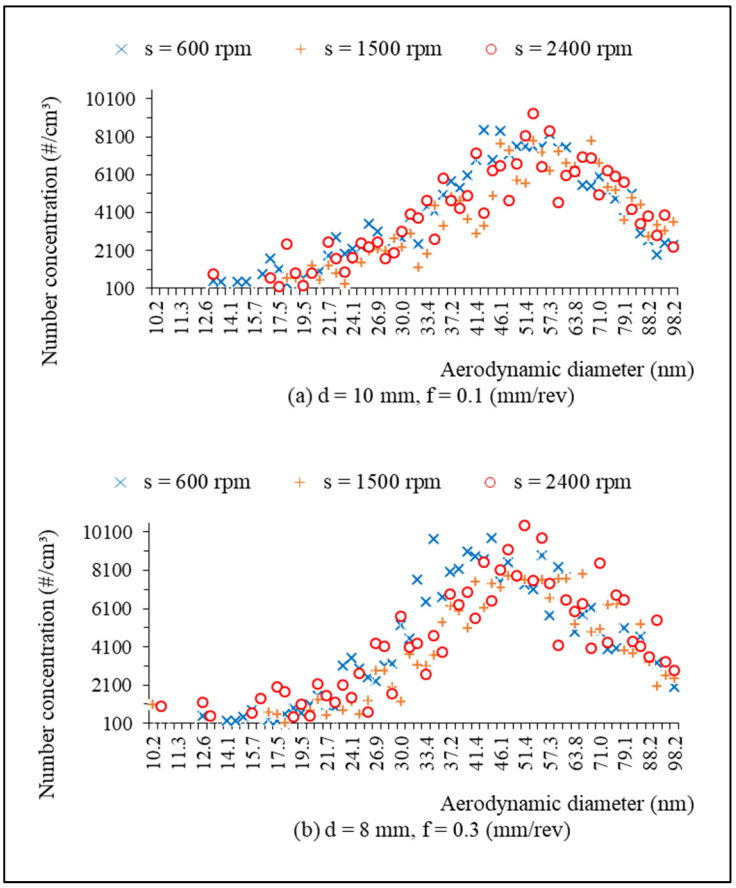

Figure 3.24 The number of ultrafine particles in relation to aerodynamic diameters when drilling with various machining parameters: (a) d = 10 mm, f = 0.1 mm/rev; (b) d = 8 mm, f = 0.3 mm/rev

Figure 3.25 shows the relationship between the peak value of number concentration of ultrafine particles and cutting parameters when drilling hybrid biocomposite with a drill of 6 mm. It was seen that the maximum value of the number concentration for ultrafine particles is not very sensitive to change in spindle speed and feed rate.

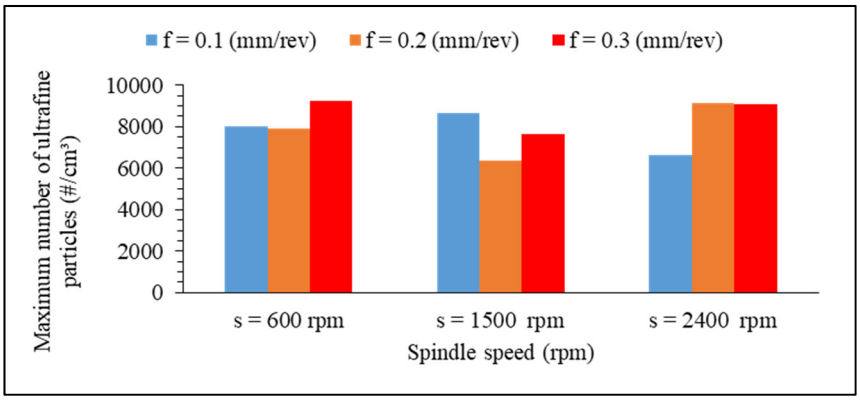

Figure 3.25 Relationship between maximum number concentration of ultrafine particles related to particle size and cutting parameters (drill: 6 mm)

3.4 Conclusions

In this investigation, the effects of cutting parameters and drill bit diameter on machinability in the dry drilling of a new hybrid biocomposite were studied. Based on the experimental data and statistical technique employed, the following conclusions are drawn:

The machining conditions significantly influence the thrust force. The feed rate was found to have a higher effect on the thrust force than did the spindle speed and drill bit diameter. An increase in thrust force results from an increase in cutting parameters and drill bit diameter.

The specific cutting energy for the thrust force considered as a material property was investigated. This energy increased with an increase in spindle speed and decreased with an increase in feed rate and/or drill bit diameter.

The drill bit diameter was observed to have a greater impact on the surface roughness than did the cutting parameters. The surface roughness decreased with a decrease in the drill's diameter, the spindle speed, and the feed rate.

During drilling of this new composite material, both fine particles (PM_{10}) and ultrafine particles (diameters ranging from 7–100 nm) were generated. The total number concentration

of fine particles reached 1300 #/cm^3, while the ultrafine particle generation reached 9000 #/cm^3 depending on machining conditions used and on the particle size studied. The drill bit diameter and the feed rate have significant effects on the fine dust generation, while the spindle speed is not statistically significant. The total number concentration of fine particles decreased with an increase in feed rate, spindle speed, and/or drill bit diameter. More fine particles emitted had aerodynamic diameters less than 2.5 μm. The cutting parameters and the drill bit diameter did not show significant statistical effects on ultrafine particle generation during drilling of the hybrid composite at the 95% confidence level. Ultrafine particle generation was therefore difficult to predict.

CHAPTER 4

EFFECTS OF REINFORCEMENTS AND CUTTING PARAMETERS ON MACHINABILITY OF POLYPROPYLENE-BASED BIOCOMPOSITE REINFORCED WITH BIOCARBON PARTICLES AND CHOPPED MISCANTHUS FIBERS

Dinh Son Tran[1, 2], Victor Songmene[1], Anh Dung Ngo[1], Jules Kouam[1]

[1] Department of Mechanical Engineering, École de Technologie Supérieure, ÉTS, Montreal, QC, H3C 1K3, Canada.
[2] Department of Mechanical Engineering, The University of Danang - University of Science and Technology, 54, Nguyen Luong Bang Street, Danang, Vietnam.

Article published in The International Journal of Advanced Manufacturing Technology, September 2020

Abstract

New biocomposites are increasingly being developed and applied in engineering and manufacturing. The reinforcement type used in biocomposite is one of the major factors that greatly affect machinability of biocomposite. This study investigated the drilling of two biocomposites (polypropylene-based biocomposite reinforced with biocarbon M1 (30wt% biocarbon + PP/POE/MAPP) and chopped miscanthus fibers M2 (30wt% miscanthus +PP/POE/MAPP)). A full factorial design was used for this study. The effects of drilling parameters and reinforcement types on surface roughness, thrust force, specific cutting energy, fine particles and ultrafine particle generation during were measured and analyzed. The results shows that thrust force and specific cutting energy during drilling of biocomposite M1 is bigger than that of biocomposite M2 under the same cutting conditions. However, the surface roughness and fine dust emitted when drilling biocomposite M1 are smaller than those from biocomposite M2, respectively. The reinforcement types of biocomposite, cutting parameters and drill diameter greatly affected fine particles emission. Meanwhile, the cutting conditions are not statistically significant for ultrafine particles generation during dry drilling of both biocomposites.

Keywords: biocomposite, surface roughness, machinability, thrust force, dust emission.

4.1 Introduction

In recent years, biocomposite materials have been applied and replaced synthetic fiber-reinforced composites for some applications like the automotive industry, construction, sports, due to their advantages such as low density, environmental friendliness, high specific stiffness and strength. Biocomposite has not been standardized because of the biodiversity and inconsistent characteristics of natural fibers (Peças et al., 2018). Therefore, it is necessary to understand its characteristics and machinability to apply biocomposite into each product appropriately. The machining process was applied for machining biocomposite depending on the requirement of the product assembly. Based on the literature, making holes by the conventional drilling on composite materials is quite common and inevitable for making a complete product (Vinayagamoorthy & Rajmohan, 2018).

The damage of the drilled hole such as peel-up and push-down delamination was directly affected by the thrust force developed during drilling of biocomposite, which was investigated by some studies (Vinayagamoorthy & Rajmohan, 2018). The thrust force is directly influenced by factors such as drill geometry and material, drill diameter, cutting parameters, reinforcement types (fibers, particles) and matrix of biocomposite (Vinayagamoorthy & Rajmohan, 2018). Maleki et al. (Hadi Rezghi Maleki et al., 2019) studied the machinability of drilling of jute/epoxy composite. They found that thrust force was greatly influenced by the feed rate, the increase in thrust force as a result of the increased feed rate for the types of drill bit used. HSS twist drill is considered to have smaller thrust force and delamination than carbide drill bits used (CoroDrill 854 and CoroDrill 856). Bajpai and Singh (2013) investigated the drilling behavior of sisal/PP biocomposite. They discovered that the drill point geometry is considered as a significant factor affecting cutting force, and the thrust force produced by a standard drill was higher than that of a trepanning drill. Debnath et al. (2017) studied the influence of tool geometry and machining parameters

on thrust forces when drilling woven nettle/PP biocomposite. The results show that drill geometry is considered to be an important factor influencing thrust forces, and the parabolic drill has thrust force is relatively smaller than step drill and four-facet drill. Yallew et al. (2016) studied the drilling of jute/PP biocomposite with various drill geometry. They observed that the drill geometry significantly influences the cutting forces generated. When drilling using a parabolic drill shows better in terms of lower thrust forces and smaller delamination than other types of drill bits (twist drill, Jo drill). Debnath et al. (2014) studied the machinability of biocomposites made from the same sisal fibers with different matrix (PP and epoxy) when drilling using three drill bits with different geometry. They concluded that the drilling behavior of biocomposites depends not only on drill geometry and machining parameters but also on the matrix of biocomposite. The drilling-induced damage was found is lower in sisal/PP compared to sisal/epoxy. When using a parabolic drill, the thrust force produced is smaller than other two drill bits (step drill and four-facet drill). In addition, an increase in thrust force as a consequence of an increase in feed rate for all drill bits used.

The quality of machined surface is quantified by surface roughness and delamination during drilling biocomposites, which was observed by several studies. Maleki et al. (H. Rezghi Maleki et al., 2019) conducted an investigation on the drilling of flax/epoxy biocomposite using three drill bits with different drill materials and geometry. The results showed that the type of drill bit used was the most significant effect on the damage of the machined surface. When drilling with an HSS drill bit, it is shown to be smaller in terms of the thrust force, delamination and roughness than that of carbide drill bits. They also concluded that HSS standard drill is suitable for machining of biocomposites because of its sharp cutting edge as compared to the carbide drill, meaning it is easy to cut biocomposite materials with soft and non-abrasive nature. This is also supplemented by the result from an investigation on drilling of jute/epoxy as mentioned above (Hadi Rezghi Maleki et al., 2019). The machinability of hemp/PCL biocomposite was investigated by Ismail et al. (Ismail, Dhakal, Dimla, et al., 2016). They noticed that the machined quality is influenced by feed rate in combination with the fiber aspect ratio of biocomposite. The increase in surface roughness as a result of an increase in the fiber aspect ratio of biocomposite and/or feed rate. However, the surface roughness decreases with the increased cutting speed. Roy Choudhury et al. (2018)

conducted an investigation on drilling of the woven fabric nettle fiber-reinforced epoxy composite with various drill bit geometry. They concluded that the increased surface roughness is a consequence of an increase in spindle speed and feed rate. The dagger drill and eight-facet drill are considered to provide lower in terms of surface roughness and thrust force compared to other drill geometries used (step, four-facet and parabolic drill). The spindle speed was found as a factor that has a great influence on machining heat generated, and the increased cutting temperature results from the increased spindle speed. Ismail et al. (Ismail, Dhakal, Popov, et al., 2016) investigated the machinability when drilling two composites (HFRP, and CFRP) with various cutting conditions. They showed that the surface roughness of CFRP is lower than that of HFRP, while CFRP presented a higher delamination drilling-induced damage. Tran et al. (2020) conducted an investigation on the dry drilling of new hybrid biocomposite, which consisted of biocarbon (15wt%), chopped miscanthus fibers (15wt%) and PP/POE/MAPP matrix. They found that the cutting parameters and drill diameters significantly affect the machinability of hybrid biocomposite in terms of surface roughness and cutting force. The increased thrust force and the increased machined surface roughness as a consequence of the increase in drill diameter and cutting parameters. Voss et al. (2017) showed that the tool geometry of the end mill has a significant effect on the machined surface quality during the slot milling of unidirectional CFRP laminate. They stated that the higher rake angle contributes to the increased surface quality of the milled edges. An increase in clearance angle leads to a reduction in cutting force and tool wear and also to an increase in milled surface quality. Chegdani et al. (2015) investigated the influence of fibers on the machinability when profile milling of different biocomposites (bamboo/PP, sisal/PP, and miscanthus/PP). The results showed that the machined surface of biocomposites is significantly affected by fiber stiffness and matrix-fiber interface quality. Chegdani and Mansori (Faissal Chegdani & El Mansori, 2019) analyzed the machinability of biocomposite according to the multiscale approach. They showed that the cutting behavior of natural fibers is independent of the polymer used in biocomposites. Cococcetta et al. (2020) have noticed that the lubrication has a good influence on surface part quality during the milling of 3D printed CFRP composite. The machining performance when milling CFRP composites under

the MQL (minimum quantity lubrication) conditions was better compared to dry milling: lower cutting forces, smaller tool wear, and a lower burr formation tendency.

The small size dust generated during machining poses a direct threat to the health of the machine operator. Therefore, it is necessary to examine the factors that influence the generation and dispersion of fine dust during machining of composite materials. However, the number of articles on this issue is very limited. To date, there have been a few studies on dust emission when machining composites. Haddad et al. (2014) conducted an investigation of the effect of cutting conditions on dust emission during trimming of CFRP composite. It is indicated that cutting parameters and tools have greatly affected fine particle emission. More dust generated is less than 2.5 μm in size, which is easily inhaled into the pulmonary alveoli and dangerous for the operator's health. The study is also shown that the proposed models for prediction of dust emission during machining of metal are not suitable for polymer composites. Marani et al. (2018) studied the influence of microstructure on dust emission when dry milling metal matrix composites. They indicated that the dust emission was directly affected by cutting conditions and microstructure of metal matrix composite. The ultrafine particles generated were lower for machining of composites with Ba and Bi modifiers as compared to base composite in the same cutting conditions. Dust particles emitted increase with the increased cutting speed in the range of 300 to 700 m/min and then decrease if the cutting speed continues to rise. Saidi et al. (2019) observed the dust particles emission when dry polishing granites with two types of abrasive grain size and various cutting parameters. They found that the fine dust decreases with increasing feed rate, and vice versa, the fine dust increases with increasing spindle speed for both types of granite. More fine particles are smaller than 2.5 μm were observed during the polishing of granites. Tran et al. (2020) studied dust generation related to cutting parameters and drill diameters when dry drilling of hybrid biocomposite. The results showed that fine dust was significantly affected by cutting conditions, and the majority of fine dust is less than 2.5 μm in size.

Based on the literature, the machinability of polymer-based composites depends strongly on their processing method, matrix, and reinforcement types (fibers, particles, etc. (Nassar et al., 2017; Sheikh-Ahmad, 2009)). It is expected that the machinability of biocomposite be

different to that of composite reinforced with synthetic fibers due to the difference in the mechanical properties of reinforcements used (nature and shape). For new biocomposites, studying their machinability is necessary to understand and apply them appropriately. Moreover, the investigation of fine dust emitted also needs to be taken care of simultaneously with other factors in the machining process. So far, the problem of dust generated during machining biocomposites has hardly been paid attention to by researchers.

In this study, the machinability of two biocomposites (M1 and M2) is observed by using the dry drilling process. The experimental design and the emperical data analysis are applied for investigating the effects of reinforcement types of biocomposite, cutting parameters and drill diameters on cutting force, specific cutting energy, roughness, and dust emission when drilling biocomposites. Moreover, the empirical data was taken from the results of another study (Tran et al., 2020), which aims to add more information to further understand the influence of the reinforcement type of biocomposites on machinability and dust generation during drilling biocomposites. The results obtained from this study contribute to understanding the effects of the drilling parameters and biocomposites' reinforcements on the machining performance indicators, and thereby could help manufacturers choosing the appropriate drilling parameters to achieve the desired surface quality. Furthermore, this study contributes to the selection of suitable cutting parameters to reduce the amount of fine dust emitted during the drilling of biocomposites.

4.2 Materials and method

4.2.1 Workpiece materials

The materials used for this investigation consists of two biocomposites, denoted M1 and M2. Both biocomposites M1 and M2 were made from the same matrix (PP/POE mixed with MAPP) randomly reinforced with biocarbon particles and chopped miscanthus fibers, respectively. The chemical composition of biocomposites M1, M2 and hybrid biocomposite (Tran et al., 2020) was presented in Table 4.1 (Dhaouadi, 2018). These include matrix (PP, POE, and MAPP), and reinforcement materials such as biocarbon particles, chopped

miscanthus fiber which are presented in the study (Tran et al., 2020). Chopped miscanthus fibers have an average length of 4 mm (Muthuraj et al., 2016). Biocarbon was made from the pyrolysis of chopped miscanthus fibers and then was ground in a hammer mill into a particle size of 0.4 mm, made by Competitive Green Technologies (Leamington, Ontario, Canada) (Wang et al., 2018). The mechanical properties of biocomposites (M1 and M2) and hybrid biocomposite are represented in Table 4.2 (Dhaouadi, 2018).

Table 4.1 Chemical composition of biocomposites (Dhaouadi, 2018)

Material	Components of material				
	PP (wt %)	POE (wt %)	MAPP (wt %)	biocarbon (wt %)	miscanthus (wt %)
M1	62	5	3	30	-
M2	62	5	3	-	30
Hybrid	62	5	3	15	15

Table 4.2 Mechanical properties of biocomposites (Dhaouadi, 2018)

Material	Young's modulus (MPa)	Tensile strength (MPa)	Flexural modulus (MPa)	Flexural strength (MPa)	Impact strength (J/m)
Biocomposite M1	2510	31	2146	52	294.5
Biocomposite M2	3872	37.3	3148	58.5	128.5
Hybrid	3175	34	2717	55	140

Biocomposites were supplied by the Bioproducts Discovery and Development Center at the University of Guelph. The equipment used and the steps to produce biocomposites are the same as those described in the study (Tran et al., 2020) for manufacturing hybrid biocomposite. The results obtained from the study (Dhaouadi, 2018) showed that biocomposite M1 was increased by 34%, 30% and 5% and that biocomposite M2 was increased by 107%, 92% and 30% in stiffness, flexural modulus and flexural strength as

compared to the matrix (PP/POE), respectively. Therefore, these new biocomposites can be considered as alternative materials to manufacture automotive parts. Figure 4.1 presents SEM images of biocomposites M1 and M2. It can be seen that the dispersion of biocarbon particles in the matrix of biocomposite M1 is relatively homogeneous. Figure 4.1a indicates the phenomenon of debonding between particles and the matrix was undetected. Figure 4.1b shows that the matrix-fiber debonding was observed on the SEM images. This is also a reason why the impact strength of M2 is greatly reduced as compared to the matrix (Dhaouadi, 2018).

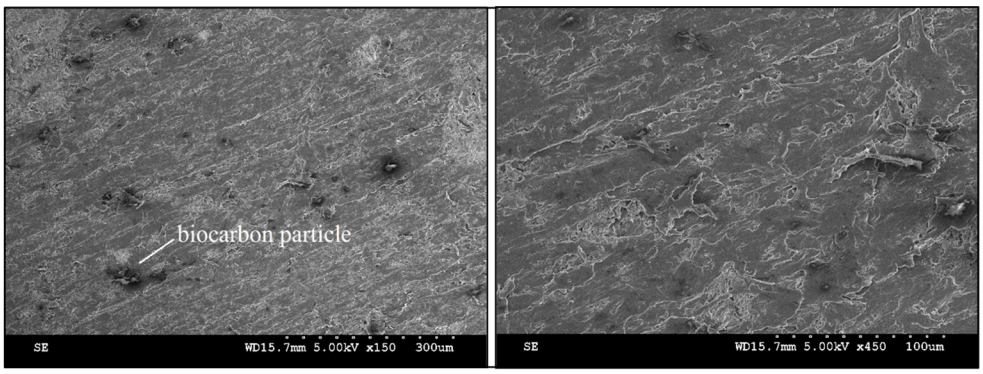

(a) SEM images for M1 (PP/POE/MAPP + biocarbon 30wt%)

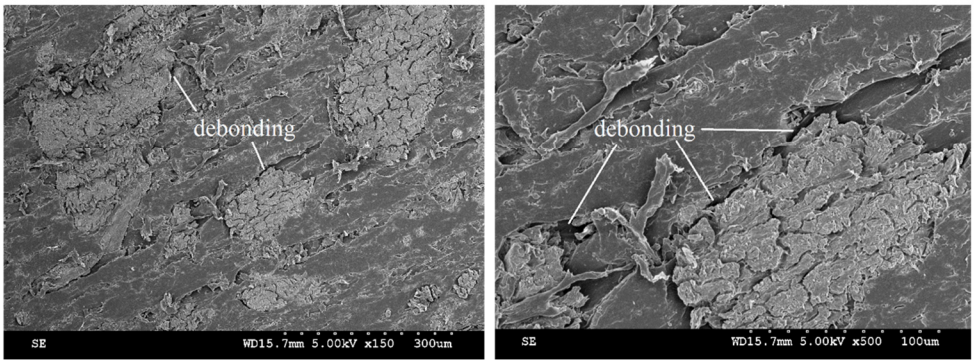

(b) SEM images for M2 (PP/POE/MAPP + miscanthus 30wt%)

Figure 4.1 SEM images of biocomposites: (a) SEM images for M1 (PP/POE/MAPP + biocarbon 30wt%); (b) SEM images for M2 (PP/POE/MAPP + miscanthus 30wt%)

4.2.2 Experimental procedure

The experiment was excuted on the CNC milling machine, HURON - K2X10 (Figure 4.2). Two biocomposites (M1 and M2) were drilled in the dry condition using backplate support. The workpiece sample has dimensions of 300 mm x 120 mm x 5 mm. The HSS twist drills are used for drilling biocomposites. Based on the literature and manufacture's catalog to select cutting parameters for the drilling process. Table 4.3 described the input factors and their levels used in the experimental design. A full factorial design is applied to the experimental design (Table 4.3). Table 4.4 presents the combination of the parameters obtained from the factorial design for the drilling of biocomposites M1 and M2. Each drilled hole was repeated 3 times under the same cutting condition, and a total of 162 drilled holes was machined (3^3 x 2 x 3).

Table 4.3 The experimental design

Factors	Level 1	Level 2	Level 3
f: feed rate (mm/rev)	0.1	0.2	0.3
s: spindle speed (rpm)	600	1500	2400
d: drill bit diameter (mm)	6	8	10
Biocomposite	M1 (PP/POE/MAPP + 30wt% biocarbon)	M2 (PP/POE/MAPP + 30wt% miscanthus)	

Table 4.4 The combination of factors used for the drilling of biocomposites M1 and M2

Testing number	Feed rate (mm/rev)	Spindle speed (rpm)	Drill diameter (mm)
1	0.1	600	6
2	0.2	600	6
3	0.3	600	6
4	0.1	1500	6
5	0.2	1500	6
6	0.3	1500	6
7	0.1	2400	6
8	0.2	2400	6
9	0.3	2400	6
10	0.1	600	8
11	0.2	600	8
12	0.3	600	8
13	0.1	1500	8
14	0.2	1500	8
15	0.3	1500	8
16	0.1	2400	8
17	0.2	2400	8
18	0.3	2400	8
19	0.1	600	10
20	0.2	600	10
21	0.3	600	10
22	0.1	1500	10
23	0.2	1500	10
24	0.3	1500	10
25	0.1	2400	10
26	0.2	2400	10
27	0.3	2400	10

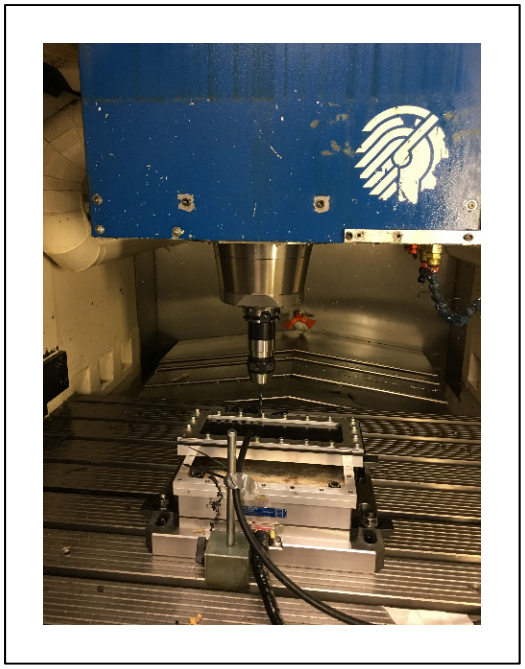

Figure 4.2 Image of workpiece sample mounted on table dynamometer and the Huron CNC milling machine tool

The dynamometer is placed and fixed on the machine table to directly measure the cutting forces (Kistler 9255B). The drilling force signals are directed to a charge amplifier (Kistler 5010), and then to a data translation card (DT 9836), which is connected with a personal computer. The cutting force signals are processed with the help of the Matlab-based signal-processing program installed on the personal computer. The backplate support (dimensions of 300 mm x 120 mm x 30 mm, and 80 drilled holes with a diameter of 12 mm) used for fixing workpiece sample, was directly clamped on the dynamometer table (Figure 4.3).

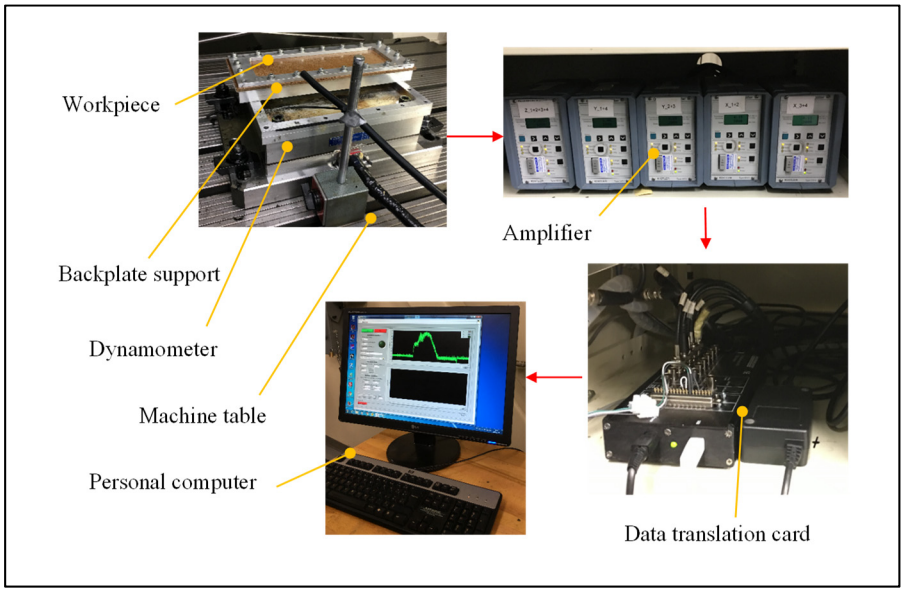

Figure 4.3 The devices used for measurement of cutting forces

Fine dust emitted during drilling biocomposites is measured by a system consisting of APS (Aerodynamic Particle Sizer) and SMPS (Scanning Mobility Particle Sizer). The fine particles with diameter in the range of 0.5 to 20 µm are measured by APS (Figure 4.4a). The ultrafine particles with sizes between 7 nm and 100 nm are measured by SMPS (Figure 4.4b).

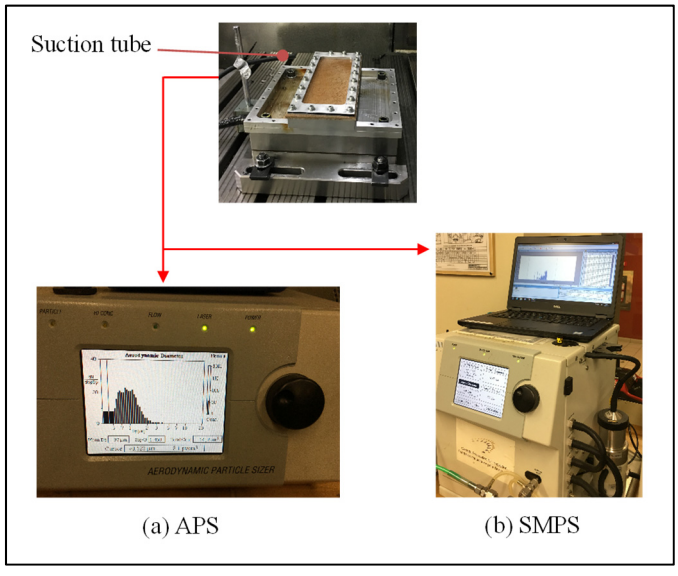

Figure 4.4 APS (model 3321, TSI, Inc.) and SMPS (model 3080, TSI, Inc.)

The surface roughness is measured by a profilometer (Mitutoyo, model SJ-410), which is directly connected to a personal computer. The measurement data is recorded and analyzed with the help of the SURFPAK-SJ software package installed on the computer. The roughness measurement is carried out in the feed direction and repeated 3 times for each drilled hole.

4.3 Results and discussion

4.3.1 Cutting force

Based on the literature, the thrust force is directly related to the damage of the machined surface during drilling biocomposite such as delamination, fiber pull-out, etc. Therefore, the thrust force is considered as one of factors used to evaluate the machinability of biocomposite. The value of thrust forces is determined in the stable phase of the drilling process, where all the cutting edges come in contact and feed into the workpiece material.

Table 4.5 presents the analysis of variance of thrust force for biocomposites M1 and M2. It can be seen that five effects are statistically significant on thrust force for biocomposite M1 (P-value less than 0.05), which include the tested factors (d, f, and s), and interactions sd and fd. It is also indicated that thrust force for biocomposite M1 is significantly affected by drill diameter (F = 83.1), followed by feed rate (F = 67.2), spindle speed (F = 60.55), interaction sd (F = 17.13), and interaction fd (F = 7.14). In Table 4.5, it is also found that only one factor (f) is statistically significant on thrust force at 95% confidence intervals for biocomposite M2 (P-value smaller than 0.05). Thus, it can be regconized that thrust force is significantly affected by feed rate for both biocomposites M1 and M2.

Table 4.5 Analysis of variance for thrust force (biocomposites M1 and M2)

Source	Sum of Squares	Df	Mean Square	F-Ratio	P-Value
Biocomposite M1					
f: feed rate (mm/rev)	*23980.5*	*1*	*23980.5*	*67.12*	*0.0000*
s: spindle speed (rpm)	*21632.0*	*1*	*21632.0*	*60.55*	*0.0000*
d: drill bit diameter (mm)	*29686.7*	*1*	*29686.7*	*83.10*	*0.0000*
f (mm/rev) x s (rpm)	1452.0	1	1452.0	4.06	0.0574
f (mm/rev) x d (mm)	*2552.08*	*1*	*2552.08*	*7.14*	*0.0146*
s (rpm) x d (mm)	*6120.08*	*1*	*6120.08*	*17.13*	*0.0005*
Total error	7145.13	20	357.256		
Total (corr.)	92568.5	26			
Biocomposite M2					
f: feed rate (mm/rev)	*4170.89*	*1*	*4170.89*	*203.68*	*0.0000*
s: spindle speed (rpm)	0.0555556	1	0.0555556	0.00	0.9590
d: drill bit diameter (mm)	26.8889	1	26.8889	1.31	0.2654
f (mm/rev) x s (rpm)	10.0833	1	10.0833	0.49	0.4909
f (mm/rev) x d (mm)	24.0833	1	24.0833	1.18	0.2911
s (rpm) x d (mm)	52.0833	1	52.0833	2.54	0.1264
Total error	409.546	20	20.4773		
Total (corr.)	4693.63	26			

The italic values show statistically significant effects

Figure 4.5 presents the surface plot of the thrust force for biocomposite M1. It is found that the thrust force has increased as a result of increased drilling parameters (d, f and s). Figure 4.6 illustrates the surface plot of the thrust force for biocomposite M2. It is shown that the thrust force increases significantly with increasing feed rate, however, the influence of drill diameter and spindle speed is not clear on the thrust force for biocomposite M2. Generally, a slight increase in thrust force could be seen when increasing drill diameter for biocomposite M2. It can be concluded that the rise of feed rate leads to the increased thrust force for both

biocomposites (M1 and M2). This is in agreement with other studies (Hadi Rezghi Maleki et al., 2019; Debnath et al., 2017; Debnath et al., 2014). Therefore, it is necessary to consider the selection of feed rate when drilling biocomposites.

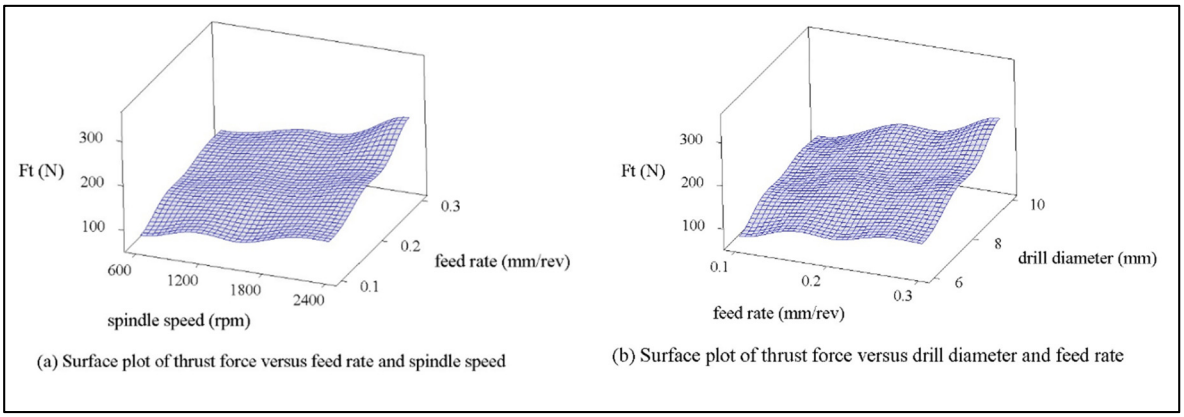

Figure 4.5 The surface plot of thrust force for biocomposite M1

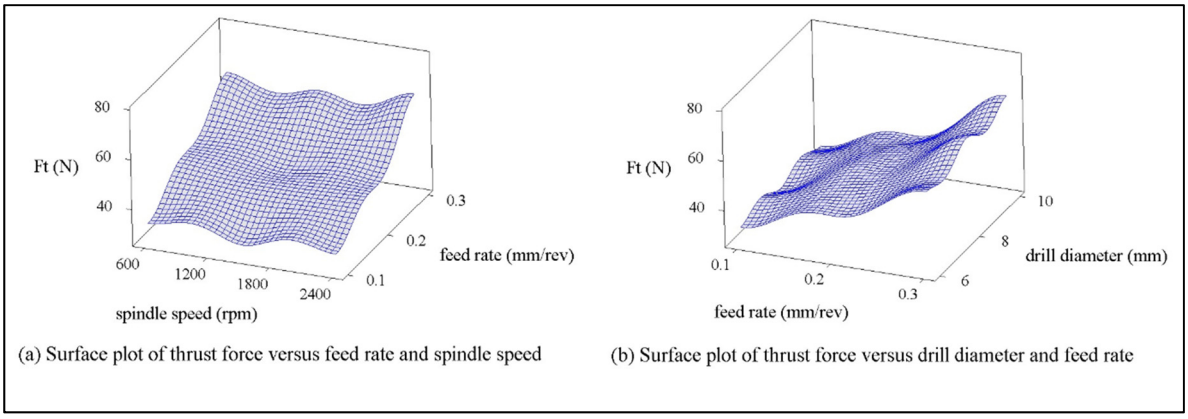

Figure 4.6 The surface plot of thrust force for biocomposite M2

Figure 4.7 shows the relationship between the thrust force with cutting parameters when drilling biocomposites using a drill diameter of 10 mm. It is indicated that an increase in feed rate and/or spindle speed will result in a significant increase in thrust force for biocomposite M1. However, the spindle speed has a negligible impact on thrust force, and the thrust force increases slightly as a consequence of the increased feed rate for biocomposite M2.

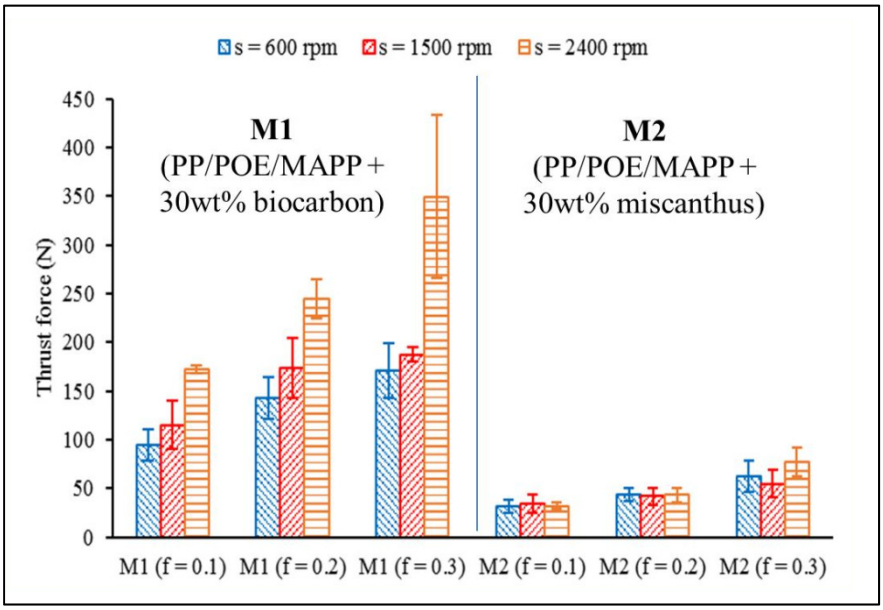

Figure 4.7 The measured thrust force when drilling biocomposites M1 and M2 (d :10 mm) as a function of spindle speeds and feed rates

Figure 4.8 compares the thrust forces developed during the drilling of two biocomposites (M1 and M2) under the same drilling conditions (cutting parameters and drill bit diameter). The horizontal axis presents testing numbers ranging from 1 to 27, where each testing number was executed in the same drilling conditions for biocomposites. The vertical axis shows the mean value of the thrust force for three iterations. It is observed that the thrust force created when drilling biocomposite M1 is much higher than that of biocomposite M2 in the same cutting condition. This could be explained due to the fact that the impact strength of M1 is 129.18% larger than that of M2 (Table 4.2), leading to M1 having a higher toughness compared to M2. Consequently, it needs a higher cutting force for removing material. Moreover, M2 has higher stiffness and brittle than M1, so biocomposite M2 is easier to cut out during machining.

The experimental result showed that the rise of drill diameter and spindle speed does not seem to change the thrust force for biocomposite M2. Meanwhile, thrust force increases significantly with spindle speed and drill bit diameter for biocomposite M1. Consequently, the bigger the spindle speed and drill diameter, the larger the difference in thrust force when

drilling both biocomposites M1 and M2 (Figure 4.8). It also indicates that the smallest difference in thrust force between M1 and M2 obtained at testing number 2 (d = 6 mm, s = 600 rpm, and f = 0.2 mm/rev), and the thrust force of M1 is 72.94% bigger than that of M2. The highest difference in thrust force obtained at testing number 26 (d =10 mm, s = 2400 rpm, and f = 0.2 mm/rev), and thrust force of M1 is 446.5% higher than that of M2.

In Figure 4.8, it can be seen that biocomposite M1 (30wt% biocarbon) has a greater thrust force than biocomposite M2 (30wt% miscanthus) with the same machining conditions. To better understand the influence of reinforcement type used in biocomposites on thrust force, Figure 4.8 is added to a line chart of thrust force (dashed green line) for hybrid biocomposite, which is drawn from the experimental data of another study (Tran et al., 2020). It is indicated that under the same drilling conditions, thrust force generated by drilling of hybrid biocomposite is in the range from thrust force of biocomposite M2 (lower limit) to thrust force of biocomposite M1 (upper limit). Therefore, it can be deduced that thrust force generated during drilling is directly proportional to the weight ratio of biocarbon particles used in biocomposite, whereas the thrust force is inversely proportional to the weight ratio of chopped miscanthus fibers used in biocomposite.

It can be recognized that the reinforcement type used in biocomposites greatly affects the machinability of biocomposites. The thrust force is not only affected by the reinforcement of biocomposite (biocarbon, miscanthus), but also by the adhesion between the reinforcement and matrix. Consequently, there is a difference in machinability of one biocomposite compared to another one, and it is impossible to take the results obtained from the machining of one biocomposite to apply to others.

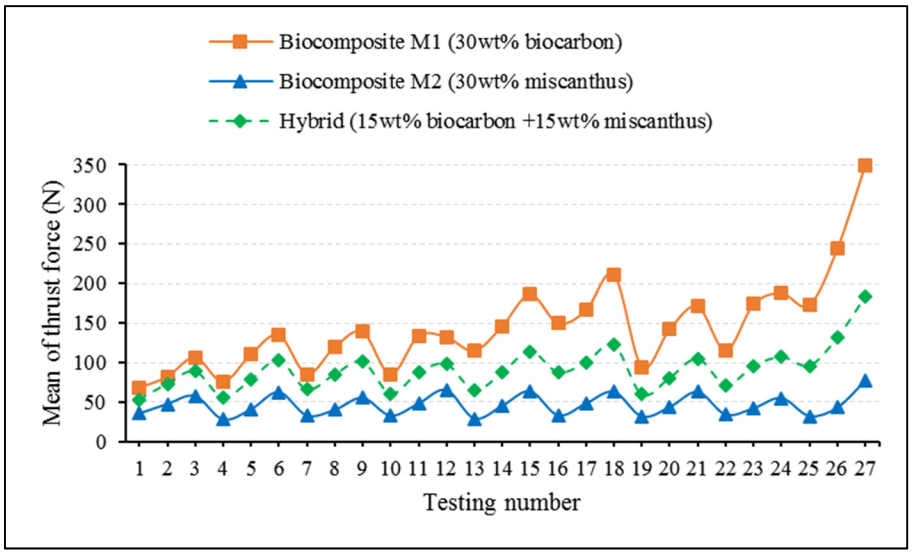

Figure 4.8 The thrust force related to the testing numbers under the same cutting condition for biocomposites

4.3.2 Specific cutting energy

The specific cutting energy is one of parameters that identify the machinability of material, it is also considered as a material property. The specific cutting energy is defined as the energy consumed to remove a unit volume of workpiece material. In this study, the specific cutting energy related to thrust force is experimentally determined by thrust force and material removal rate. The standard twist drill is used to perform the experiment, and the specific cutting energy for thrust force is calculated by the following equation (Sheikh-Ahmad, 2009).

$$K_t = (2 \times F_t)/(f \times d) \quad (4.1)$$

Where d (mm) is the drill bit diameter, f (mm/rev) is the feed rate, F_t (N) is the thrust force, and K_t (N/mm^2) is the specific cutting energy related to thrust force.

Figure 4.9a presents the Pareto diagram of the specific cutting energy for thrust force of biocomposite M1. It is shown that three effects are statistically significant on the specific

cutting energy for thrust force of biocomposite M1: the feed rate (f), the spindle speed (s) and the interaction sd. However, the drill bit diameter (d) is not statistically significant.

Figure 4.9b shows the Pareto diagram of the specific cutting energy for thrust force of biocomposite M2. It can be seen that three effects have the statistical significance on the specific cutting energy for thrust force of biocomposite M2: the drill diameters (d), the feed rate (f), and the interaction fd. Meanwhile, the spindle speed (s) is not statistically significant at 95% confidence level.

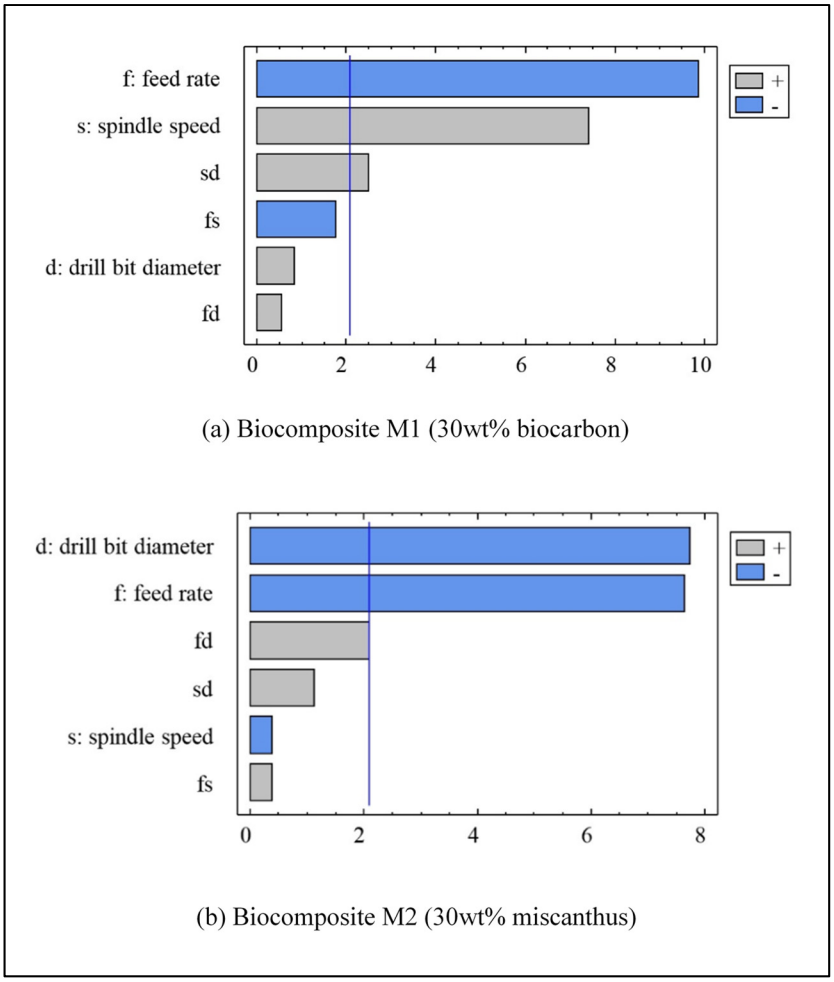

Figure 4.9 The standardized Pareto chart of the specific cutting energy for thrust force: (a) biocomposite M1, and (b) biocomposite M2

Figure 4.10 shows the relationship between specific cutting energy and drilling parameters for biocomposite M1. It is shown that an increase in specific cutting energy for thrust force as a result of increasing spindle speed (s) and/or decreasing feed rate (f). Figure 4.11 indicates that a decrease in specific cutting energy for biocomposite M2 as a consequence of an increase in drilling parameters (d, f, and s).

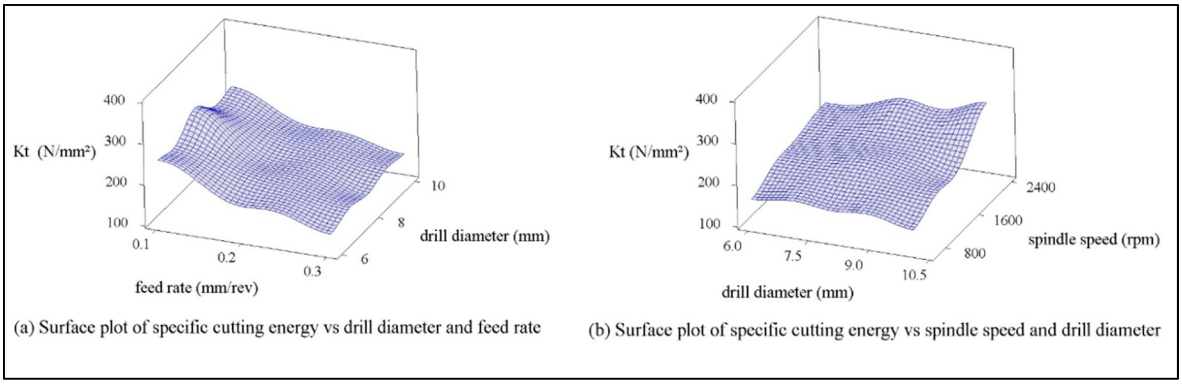

Figure 4.10 The surface plot of specific cutting energy for thrust force of biocomposite M1

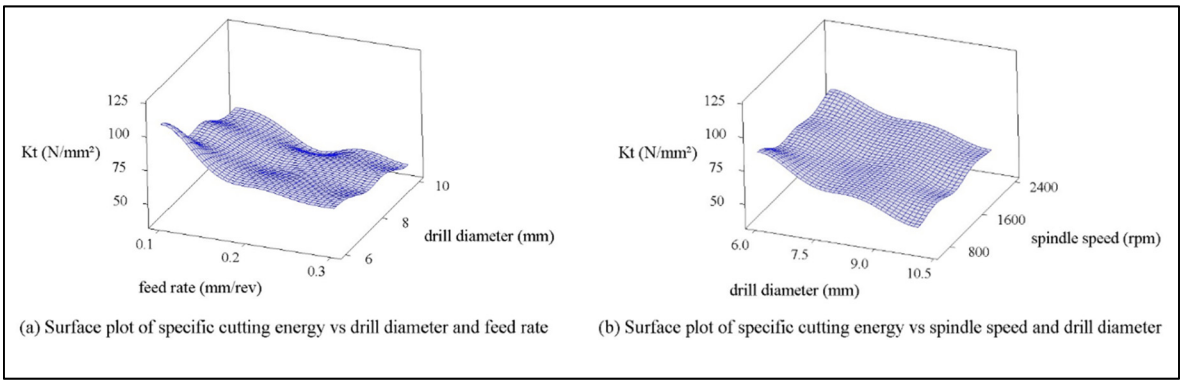

Figure 4.11 The surface plot of specific cutting energy for thrust force of biocomposite M2

Figure 4.12 compares the specific cutting energy for biocomposites when drilling with the same cutting condition. The vertical axis shows the mean value of the specific cutting energy associated with 27 tests (see Table 4.4 for machining conditions) presented in the horizontal axis. For each biocomposite, the same machining conditions were used for drilling. The

experimental data from the drilling of hybrid biocomposite in the study (Tran et al., 2020) was also included and presented on the line chart (green dashed line, Figure 4.12).

From the line charts, it is easy to see that the specific cutting energy of biocomposite M1 is much larger than that of biocomposite M2 under the same cutting conditions. Furthermore, the magnitude of specific cutting energy of hybrid biocomposite is in the range from the specific cutting energy of biocomposite M2 (lower limit) to that of biocomposite M1 (upper limit) in the same drilling parameters. Therefore, it can be realized that the specific cutting energy is directly proportional to the weight ratio of biocarbon particles and inversely proportional to the weight ratio of miscanthus fibers used in biocomposite.

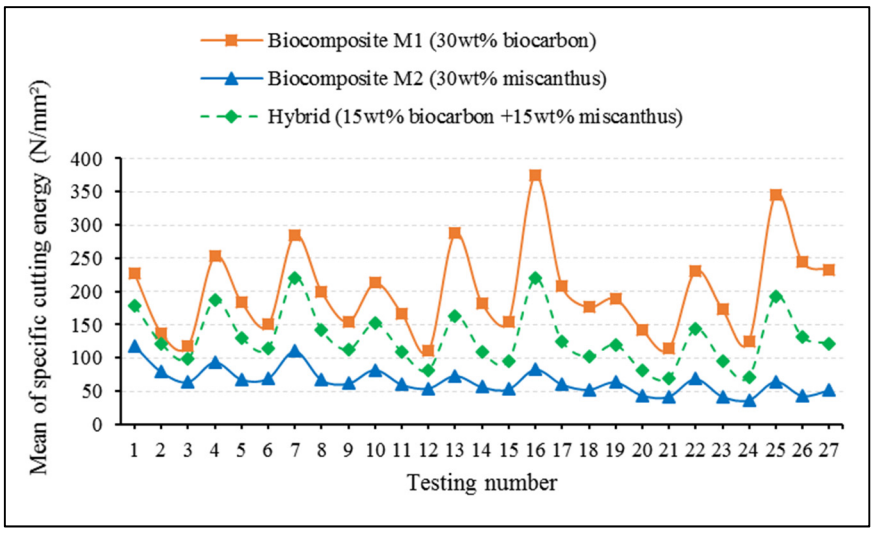

Figure 4.12 The specific cutting energy related to testing numbers for biocomposites

4.3.3 Surface roughness

The quality of the drilled surface for polymer-based composite materials is generally evaluated by the surface roughness and delamination factor such as peel-up, push-down. In this study, the drilled-hole quality was assessed through the roughness R_t and R_a. Where R_t is determined by the maximum peak-to-valley heigh of the profile, and R_a is defined as the arithmetic mean value of the profile. The roughness was measured in the feed direction. Each

drilled hole was measured three times in different positions and the mean value was selected for analysis.

4.3.3.1 **The roughness R_a**

Table 4.6 presents the analysis of variance for the roughness R_a when drilling biocomposites M1 and M2. It can be seen that three effects (s, d and interaction sd) have the statistical significance on the roughness R_a at 95% confidence level for biocomposite M1. It also showed that the spindle speed is the highest significant effect (F = 100.22), followed by drill diameter (F = 91.65), and interaction sd (F = 41.8). However, the feed rate is statistically insignificant on the roughness R_a for biocomposite M1. In Table 4.6, it is also observed that four effects (d, s, f and interaction sd) have the statistical significance on the roughness R_a at 95% confidence level for biocomposite M2. In which, the drill bit diameter is the highest effect (F = 30.78), followed by spindle speed (F = 15.28), interaction sd (F = 14.9), and feed rate (F = 7.96).

Table 4.6 Analysis of variation for roughness R_a (biocomposites M1 and M2)

Source	Sum of Squares	Df	Mean Square	F-Ratio	P-Value
Biocomposite M1					
f: feed rate (mm/rev)	0.000355556	1	0.000355556	0.05	0.8290
s: spindle speed (rpm)	*0.7442*	*1*	*0.7442*	*100.22*	*0.0000*
d: drill bit diameter (mm)	*0.680556*	*1*	*0.680556*	*91.65*	*0.0000*
f (mm/rev) x s (rpm)	0.0	1	0.0	0.00	1.0000
f (mm/rev) x d (mm)	0.000533333	1	0.000533333	0.07	0.7914
s (rpm) x d (mm)	*0.310408*	*1*	*0.310408*	*41.80*	*0.0000*
Total error	0.14851	20	0.00742551		
Total (corr.)	1.88456	26			
Biocomposite M2					
f: feed rate (mm/rev)	*0.178006*	*1*	*0.178006*	*7.96*	*0.0106*
s: spindle speed (rpm)	*0.341689*	*1*	*0.341689*	*15.28*	*0.0009*
d: drill bit diameter (mm)	*0.688356*	*1*	*0.688356*	*30.78*	*0.0000*
f (mm/rev) x s (rpm)	0.0481333	1	0.0481333	2.15	0.1579
f (mm/rev) x d (mm)	0.0420083	1	0.0420083	1.88	0.1857
s (rpm) x d (mm)	*0.333333*	*1*	*0.333333*	*14.90*	*0.0010*
Total error	0.447327	20	0.0223663		
Total (corr.)	2.07885	26			

The italic values show statistically significant effects

Figures 4.13 and 4.14 show that the increase of the roughness R_a as a result of an increase in drill diameter and/or spindle speed for both biocomposites M1 and M2. The roughness R_a increases as feed rate increases for biocomposite M2, but the influence of feed rate is negligible for surface roughness of biocomposite M1.

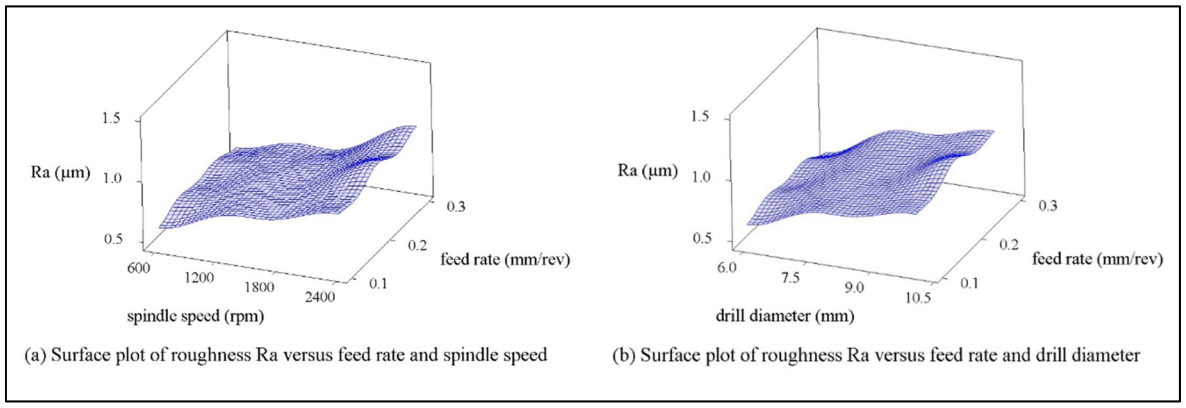

Figure 4.13 The surface plot of the roughness R_a for biocomposite M1

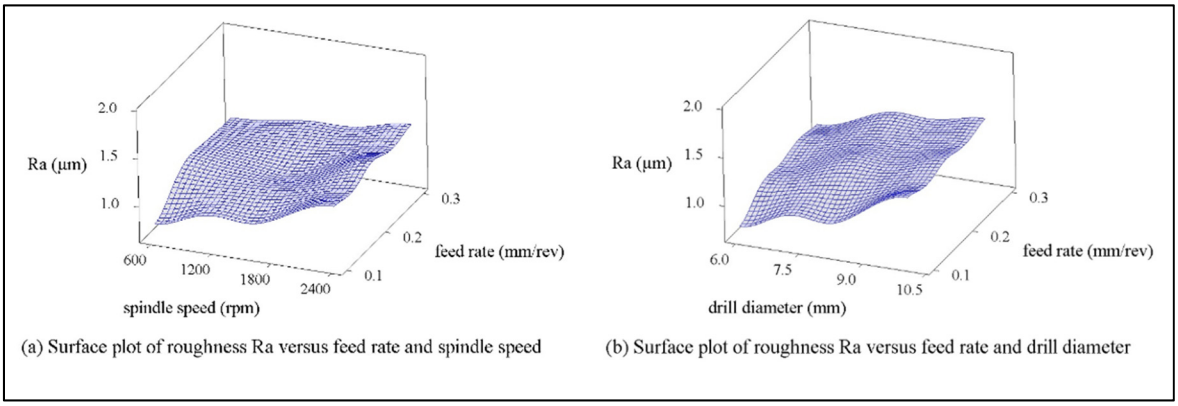

Figure 4.14 The surface plot of the roughness R_a for biocomposite M2

Figure 4.15 compares the surface roughness R_a of two biocomposites (M1 and M2) during drilling under the same cutting conditions. The horizontal axis indicates the testing number ranging from 1 to 27, where each testing number was performed in the same drilling parameters for both biocomposites. The vertical axis presents the mean value of the roughness R_a. It is found that under the same drilling conditions, the R_a value of biocomposite M2 is greater than that of biocomposite M1, except for the test numbers 13 and 23, which could be explained by the heterogeneity of biocomposite. The empirical result showed that the highest difference in the roughness R_a of two biocomposites obtained at

testing number 6 (d = 6 mm, f = 0.3 mm/rev and s = 1500 rpm), and the R_a value of biocomposite M2 is 101.82% bigger than that of biocomposite M1.

Figure 4.15 has been added to a line chart (green dashed line) showing the values of roughness R_a related to testing numbers for hybrid biocomposite. In which, experimental data are taken from the study (Tran et al., 2020). It is realized that the roughness R_a of hybrid biocomposite is mostly in the range from the roughness R_a of biocomposite M1 (lower limit) to the roughness R_a of biocomposite M2 (upper limit). So the reinforcement type of biocomposite significantly affects the roughness of the drilled hole surface. It can be inferred that the increase of the weight ratio of miscanthus used in biocomposite causes an increase in roughness. In contrast, the surface roughness decreased as a result of the increased weight ratio of biocarbon used in biocomposites.

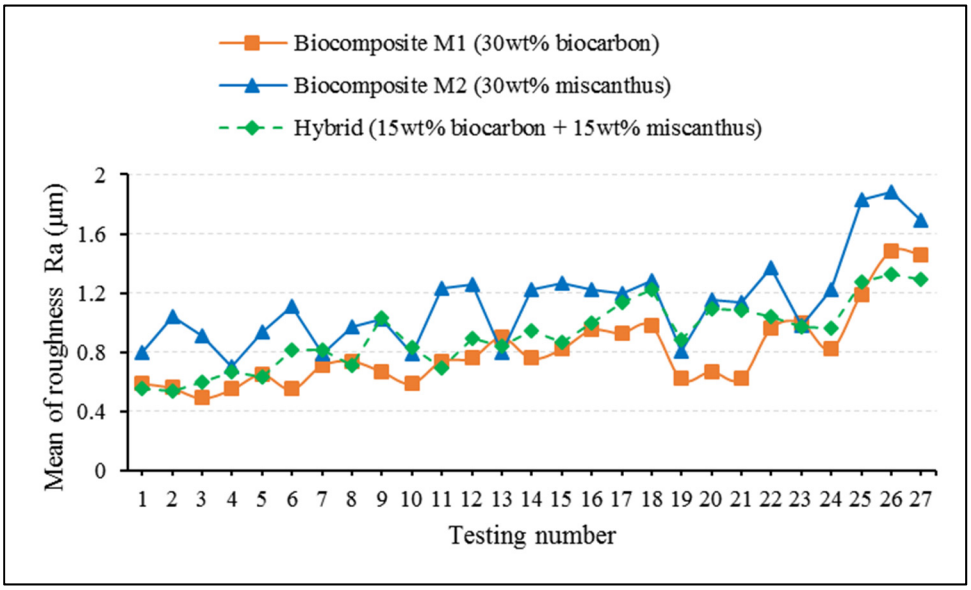

Figure 4.15 The surface roughness R_a related to the testing numbers for biocomposites

Figure 4.16a, b shows the profile evaluation of drilled hole surface in the measurement length for biocomposites M1 and M2, respectively. The drilled holes with the same cutting condition were chosen for measurement (test number 6), where the highest difference in roughness R_a was found for two biocomposites. It can be seen that biocomposite M1 has a

slight change in roughness, whereas biocomposite M2 shows a large variation in roughness in the measurement length.

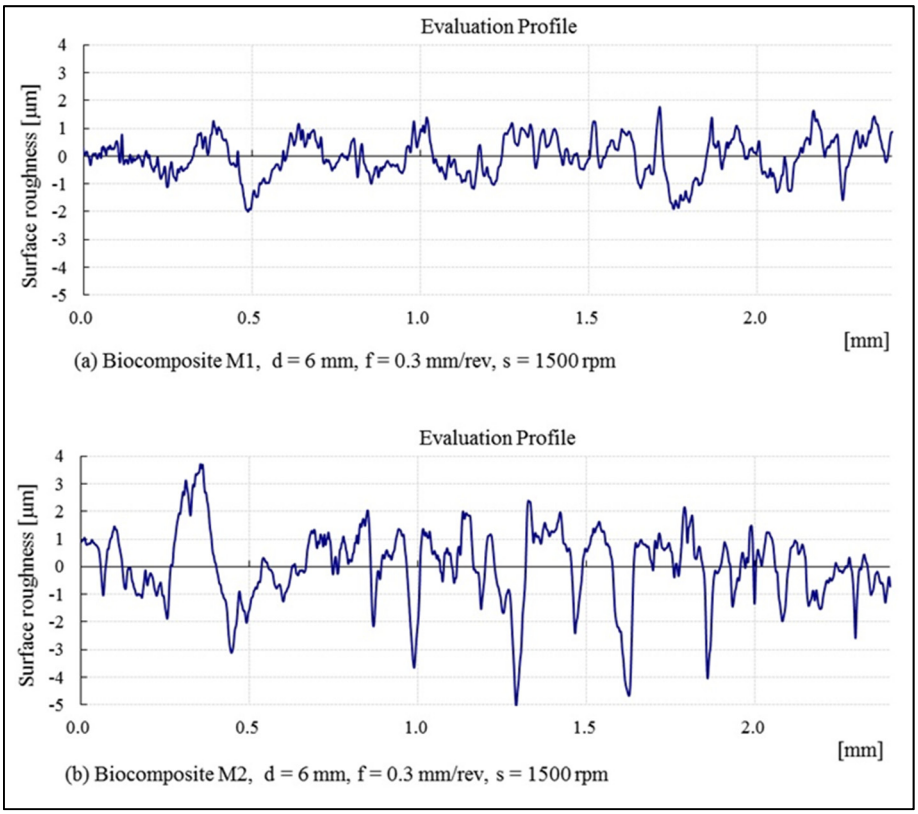

Figure 4.16 The evaluation profile of the drilled hole for biocomposites: (a) biocomposite M1, and (b) biocomposite M2

Figure 4.17a shows the SEM images of the drilled hole surface of biocomposite M1. It is indicated that some biocarbon particles have been separated from the drilled hole surface and the debonding phenomenon of matrix and biocarbon particles has occurred. Figure 4.17b presents some damages of the drilled hole surface of biocomposite M2 have been observed, such as fibers pull out and the matrix-fibers debonding. There are pores on the drilled hole surface due to the fibers have been pulled out from the machined surface, which is the cause for poor surface quality.

It can be recognized that the reinforcement type of biocomposite has a great influence on the drilling surface. Figure 4.17a presents the damage of drilling surface that is less visible for biocomposite M1, while more damage has been found on the drilling surface for biocomposite M2 (Figure 4.17b).

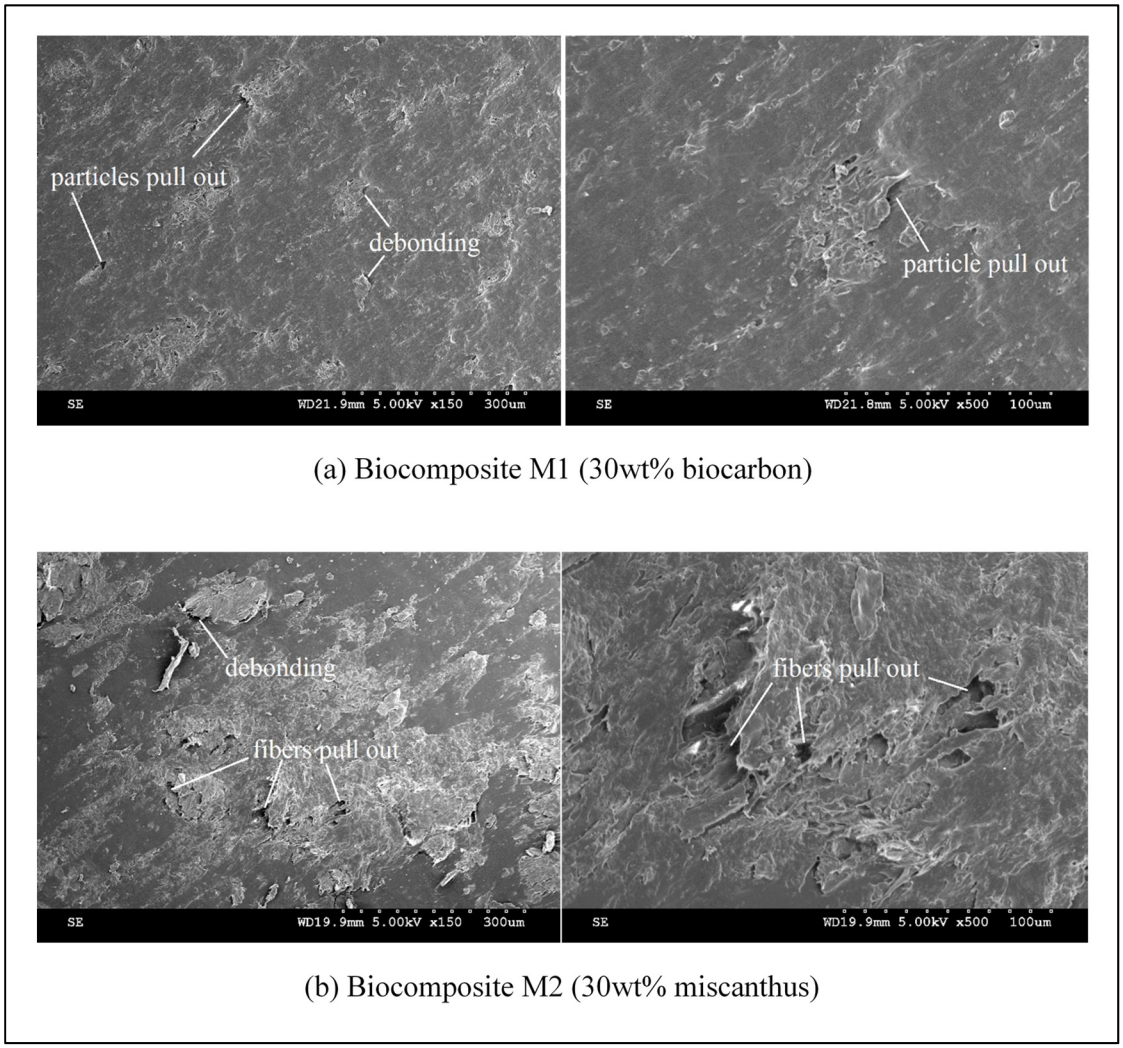

Figure 4.17 SEM images of the drilled-hole surfaces, with d = 10 mm, s = 2400 rpm, f = 0.3 mm/rev: (a) biocomposite M1, and (b) biocomposite M2

Table 4.7 presents the empirical models of the surface roughness R_a, specific cutting energy and thrust force for both biocomposites M1 and M2. The effects are not statistically significant for the target factors were eliminated to establish the empirical model. It can be

observed that R^2 value of all models close to 1, and thereby the empirical models are suitable for prediction.

The parameters in Table 4.7 included F_t, K_t, R_a, f, s and d. Where R_a (µm) is the arithmetic mean roughness, K_t (N/mm^2) is the specific cutting energy-related to thust force, F_t (N) is the thrust force, d (mm) is the drill bit diameter, s (rpm) is the spindle speed, and f (mm/rev) is the feed rate.

Table 4.7 Empirical models for biocomposites M1 and M2

Material	**Empirical model**	**R^2 (%)**
M1	$F_t = 118.407 - 218.333 \times f - 6.186 \times 10^{-2} \times s - 13.097 \times d + 72.917 \times f \times d + 12.546 \times 10^{-3} \times s \times d$	90.7
	$K_t = 345.201 - 592.683 \times f - 31.929 \times 10^{-3} \times s - 12.731 \times d + 10.188 \times 10^{-3} \times s \times d$	87.2
	$R_a = 0.769 - 48.889 \times 10^{-5} \times s - 36.806 \times 10^{-3} \times d + 8.935 \times 10^{-5} \times s \times d$	92.1
M2	$F_t = 15.852 + 152.222 \times f$	88.8
	$K_t = 197.372 - 354.311 \times f - 12.731 \times d + 25.363 \times f \times d$	85.0
	$R_a = 1.024 + 99.444 \times 10^{-2} \times f - 58.765 \times 10^{-5} \times s - 41.111 \times 10^{-3} \times d + 9.259 \times 10^{-5} \times s \times d$	74.1

4.3.3.2 **The roughness R_t**

Figure 4.18a, b shows Pareto diagrams of the roughness R_t for two biocomposites M1 and M2, respectively. Figure 4.18a indicates that three effects (s, d, and interaction sd) are statistically significant at 95% confidence intervals to the surface roughness R_t for biocomposite M1. In which, the spindle speed (s) is the highest significant effect on the

roughness R_t, followed by the drill bit diameter (d) and interaction sd. Figure 4.18b presents three effects (s, d, sd), which are also statistically significant for biocomposite M2. However, the interaction sd is the largest effect on the roughness R_t, followed by drill bit diameter (d) and spindle speed (s).

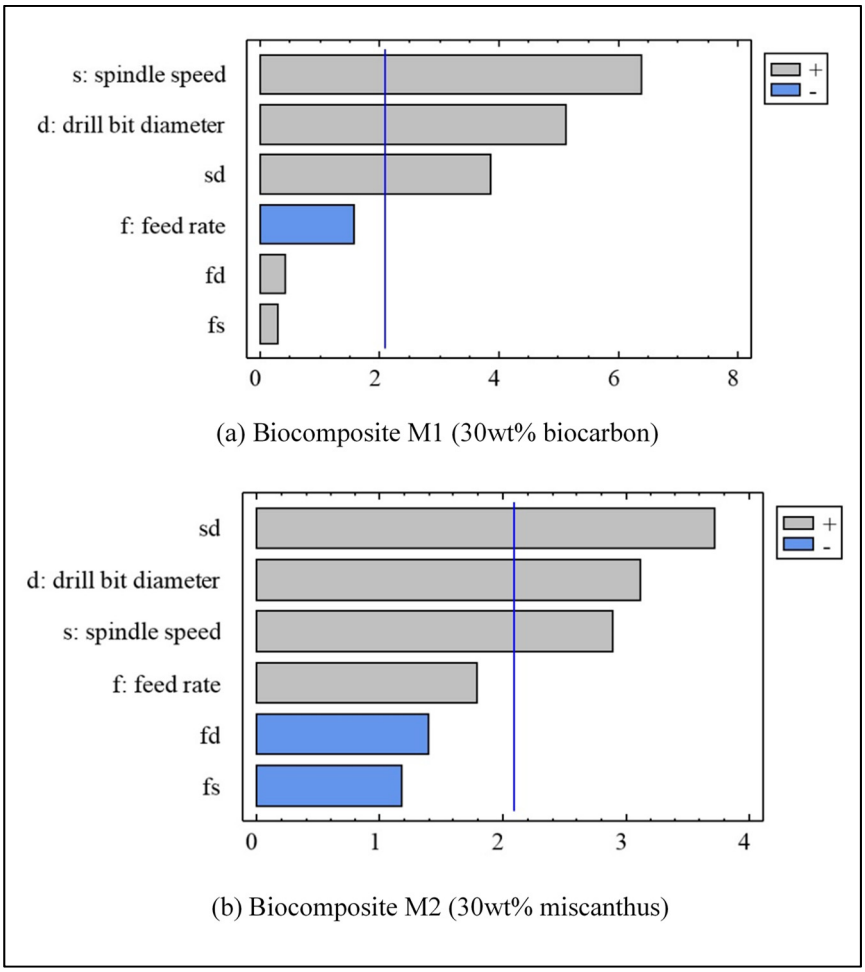

Figure 4.18 The standardized Pareto chart for surface roughness (R_t): (a) biocomposite M1, and (b) biocomposite M2

Figures 4.19 and 4.20 show the surface plot of the roughness R_t for two biocomposites M1 and M2, respectively. It is easy to see that the roughness R_t increases significantly with increasing drill diameter and/or spindle speed for both biocomposites. This influential trend is similar to that for the roughness R_a as mentioned above. Figure 4.21 compares the surface roughness R_t of two biocomposites M1 and M2 under the same cutting conditions. It is

shown that the surface roughness R_t of biocomposite M2 is much larger than that of biocomposite M1, except for the testing numbers 7 and 13.

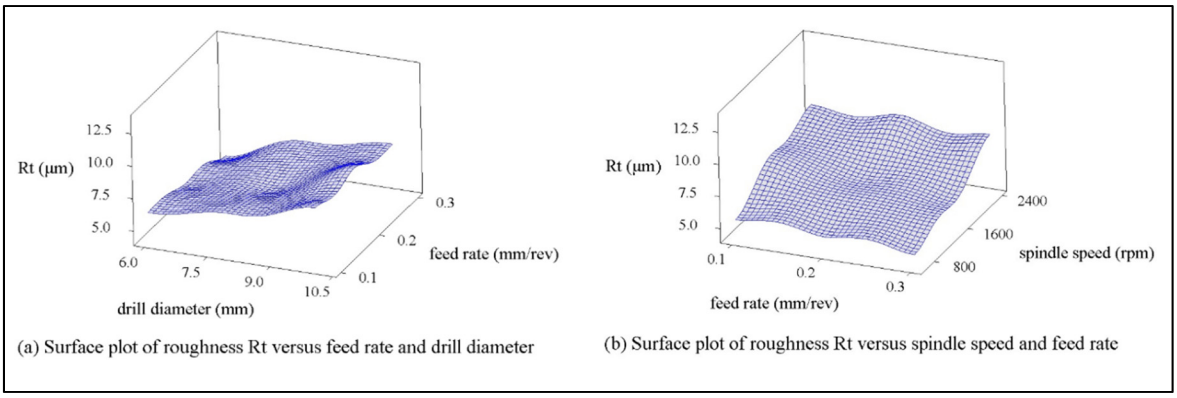

Figure 4.19 The surface plot of the roughness R_t for biocomposite M1

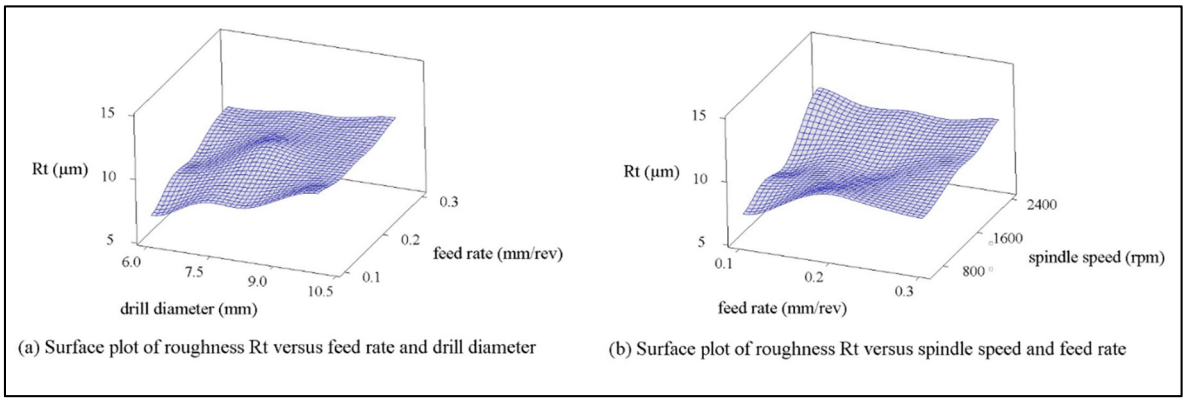

Figure 4.20 The surface plot of the roughness R_t for biocomposite M2

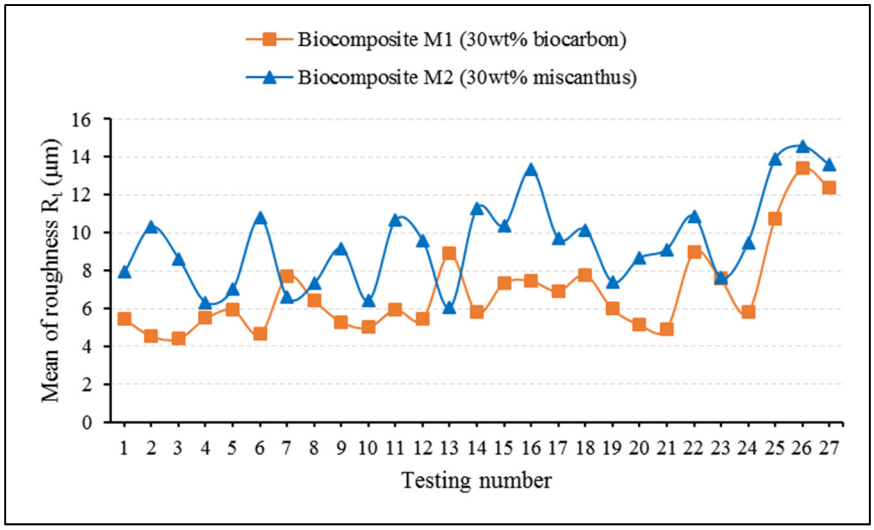

Figure 4.21 The relationship between the roughness R_t and testing number for both biocomposites M1 and M2

4.3.4 The dust generated during machining

4.3.4.1 **Fine particle emission**

Fine dust generated during drilling hybrid biocomposite is greatly influenced by cutting parameters and drill diameter (Tran et al., 2020). In this investigation, the effect of reinforcement type and drilling parameters on the fine particle emission was observed. The particle sizes ranging from 0.5 to 10 µm were selected for analysis. Figure 4.22 presents the Pareto chart of fine particle emission (PM10) for both biocomposites M1 and M2. It is noticed that three effects (s, d, and sd) are statistically significant on fine particle emission for both biocomposites at 95% confidence level. The interaction sd is the highest significant effect on fine particles generated for both materials. The feed rate (f) has the statistical significance on the number concentration of fine particles for biocomposite M2 (Figure 4.22b). However, the feed rate has no statistical significance on fine particle emission for biocomposite M1 (Figure 4.22a).

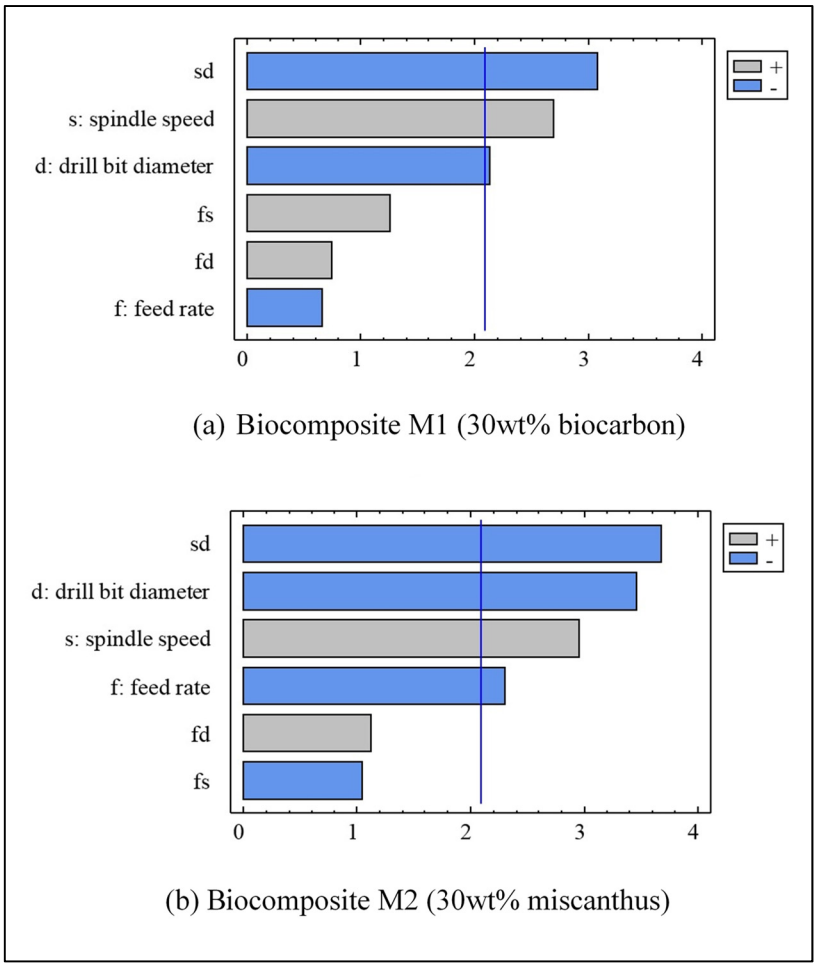

Figure 4.22 The standardized Pareto chart for fine particle emission (PM10): (a) biocomposite M1, and (b) biocomposite M2

Figures 4.23 and 4.24 illustrate the surface plot of the number of fine particles emission for biocomposite M1 and M2, respectively. It is shown that the emission of fine particles increases as the spindle speed increases and decrease with increasing feed rate and drill diameter for both biocomposites. This influential trend is similar to the results obtained from other studies (Saidi et al., 2019; Saidi et al., 2015) during the polishing of granite.

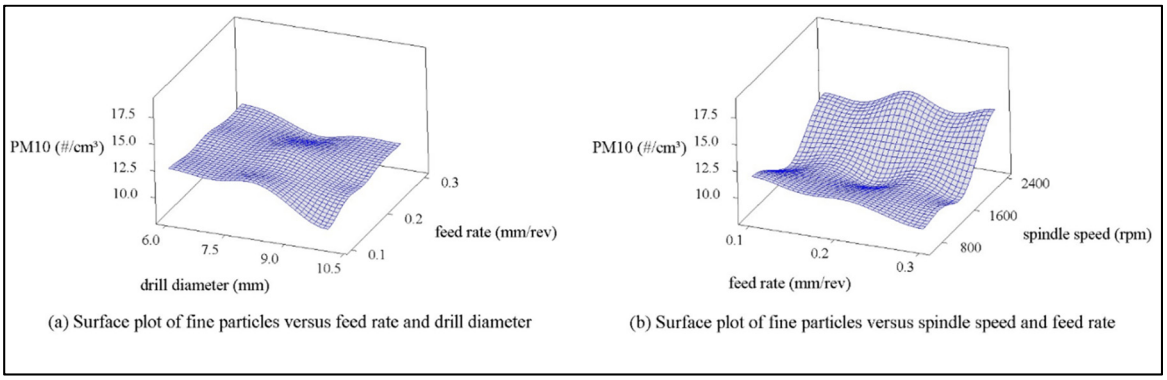

Figure 4.23 The surface plot of the number concentration of fine particle emission (PM10) for biocomposite M1

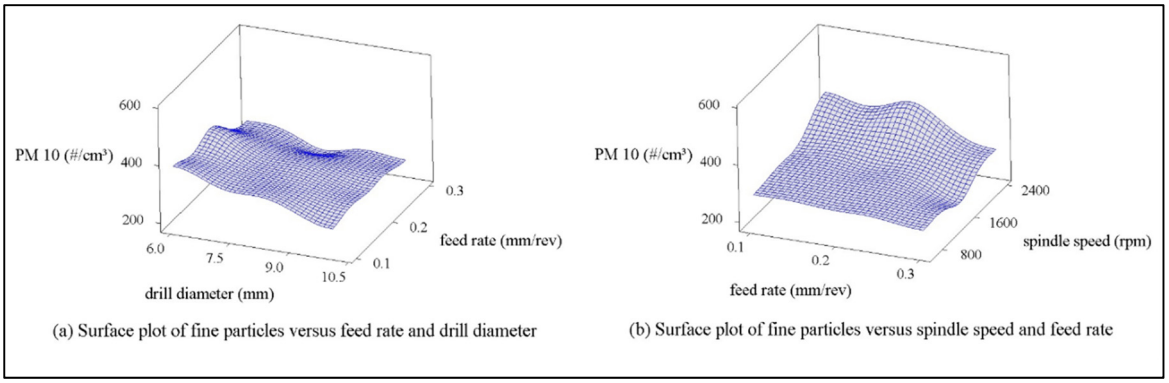

Figure 4.24 The surface plot of the number concentration of fine particle emission (PM10) for biocomposite M2

Figure 4.25 shows the relationship between the number of fine particles emitted (PM10) and the aerodynamic diameter for both biocomposites M1 and M2, with drilling parameters: d = 6mm, f = 0.2 mm/rev, and s = 600, 1500, 2400 rpm. It is shown that the number of fine particles increases with increasing spindle speed for both biocomposites. The majority of particles are smaller than 2 µm in size, and a peak value obtained at 0.673 µm, except for a particular case of biocomposite M1, which obtained a peak value at 0.723 µm with s = 2400 rpm (Figure 4.25a). According to the empirical data, fine particles with sizes smaller than 2.5µm (PM2.5) accounted for approximately 94% and 97% of the total fine particles created (PM10), respectively for biocomposites M1 and M2. Figure 4.25 also shows that the amount

of fine dust generated from biocomposite M2 is much larger (about 20 times) than that of biocomposite M1 with the same cutting parameters.

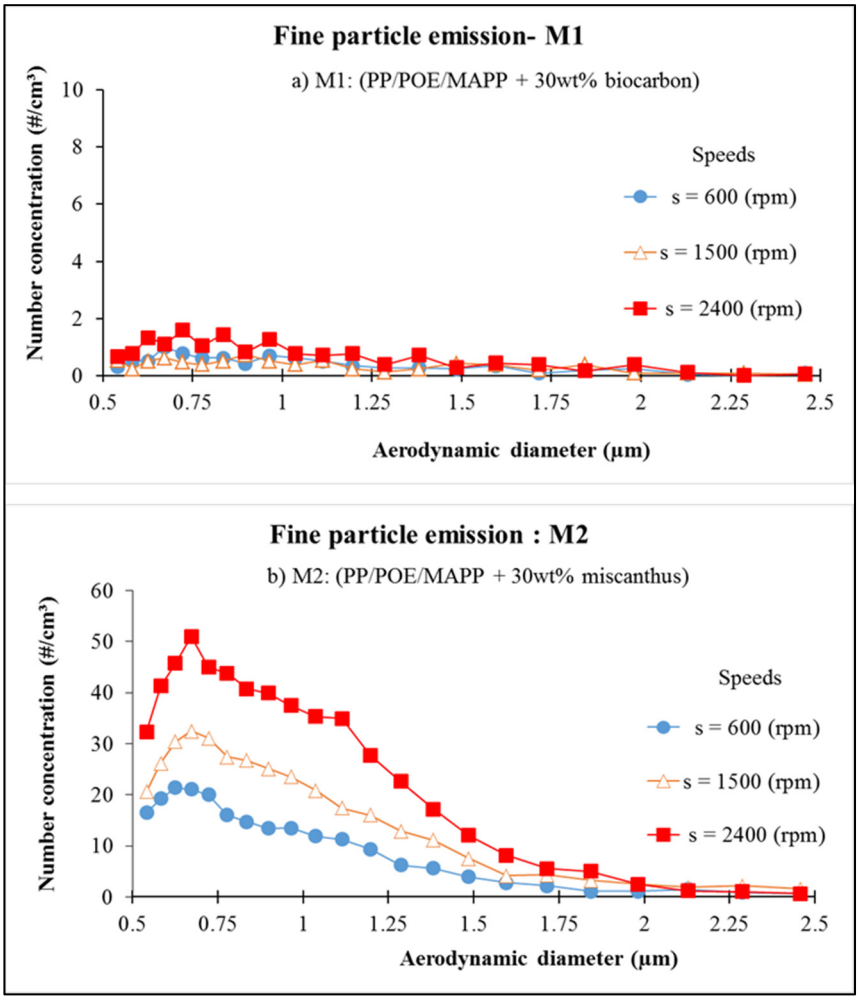

Figure 4.25 The number of fine particles related to aerodynamic diameters:
(a) biocomposite M1, and (b) biocomposite M2; d = 6mm, f = 0.2 mm/rev

Figure 4.26 compares the total number of fine particles (PM10) generated from different biocomposites when drilling using the same cutting parameters. The horizontal axis presents the test numbers from 1 to 27, where each testing number has the same cutting parameters for various biocomposites. The vertical axis shows the total number of fine particles emitted during drilling biocomposites. Figure 4.26 shows that the total number of fine particles generated from drilling biocomposite M1 is almost unchanged, whereas the total number of

fine dust generated from biocomposite M2 varies greatly with cutting conditions. The total number concentration of fine particles generated from biocomposite M2 is much bigger than that from biocomposite M1 in all cases.

The difference in fine particle emission when drilling two types of biocomposites (M1 and M2) could be explained as follows. The results from the study (Wang et al., 2018) indicated that biocarbon with a small size to improve the impact strength of biocomposite. Muthuraj et al. (2016) concluded that biocomposite reinforced with the shorter length of miscanthus fibers has a higher impact strength than the longer one because of the difference in fiber pull-out mechanism during testing. Biocomposite showed lower impact and tensile strength compared to matrix (PBS/PBAT) because of the lack of interfacial interaction between matrix and miscanthus fibers (Muthuraj et al., 2017). From SEM images (Figure 4.1), it is shown that the matrix-biocarbon bonding of biocomposite M1 is better than the adhesion of miscanthus fibers and matrix of biocomposite M2. Additionally, SEM images (Figure 4.17b) are also indicated that miscanthus fibers have been pulled out and the pores have occurred on the drilled hole surface of biocomposite M2. Moreover, the impact strength of biocomposite M1 is greater than that of biocomposite M2, so it requires higher energy to remove biocarbon particles from the biocomposite as compared to miscanthus fibers (Dhaouadi, 2018). This means that miscanthus fibers are more easily separated from biocomposite than biocarbon particles. Consequently, more fine dust generated from drilling biocomposite M2 than biocomposite M1.

Figure 4.26 has been added to a line chart (green dashed line) showing the total number of fine particles emitted corresponding to the testing numbers when drilling hybrid biocomposite. The line chart for hybrid biocomposite was drawn based on the empirical data from the study (Tran et al., 2020). It is recognized that the amount of fine dust generated is greatly influenced by the reinforcement type of biocomposite. The increase of fine dust emission as a result of drilling biocomposite reinforced with the increased weight ratio of miscanthus fibers or the decreased weight ratio of biocarbon.

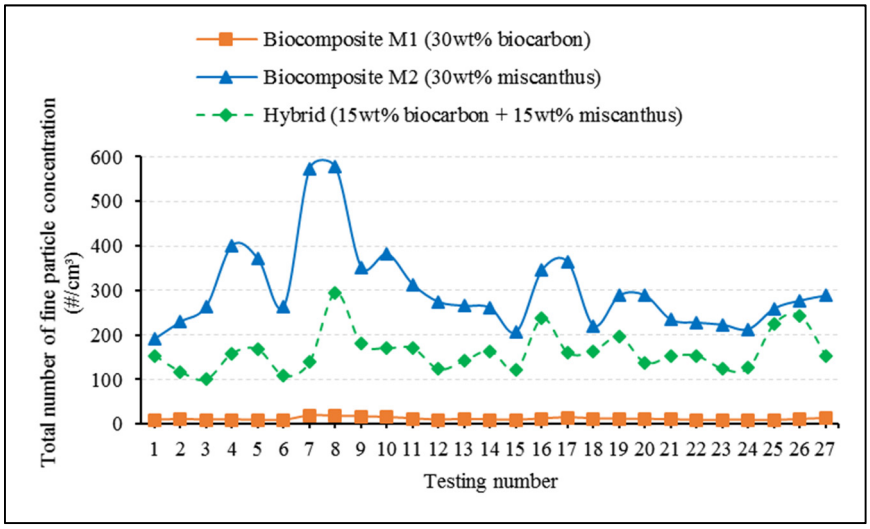

Figure 4.26 The total number concentration of fine particle related to testing numbers for both biocomposites (M1 and M2)

4.3.4.2 **Ultrafine particles (UFP)**

The ultrafine dust particles with aerodynamic diameters in the range of 7 to 100 nm were selected for analysis in this subsection, which was taken from SMPS. Figures 4.27a and 4.27b show the Pareto diagram for the total number of UFP corresponding to biocomposites M1 and M2. It is found that no effect is statistically significant on the total number of UFP for both biocomposites at 95% confidence intervals. Therefore, it can be noticed that the ultrafine particles generated during the drilling of biocomposites are unpredictable.

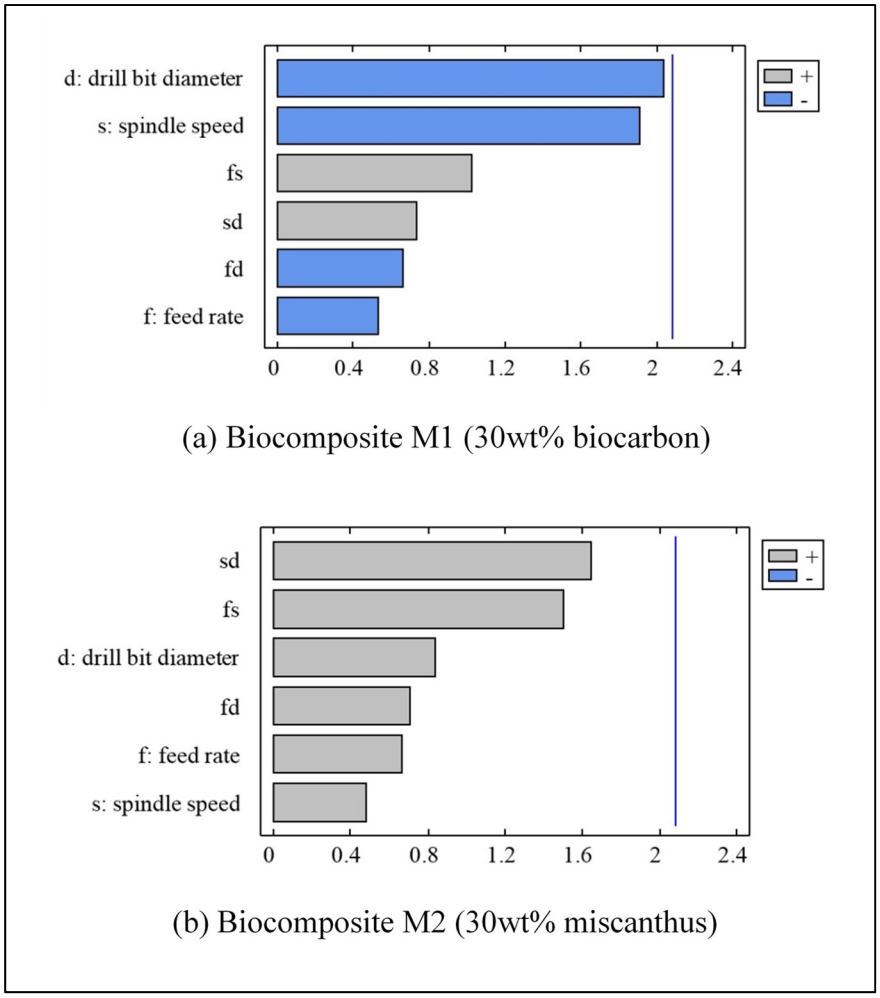

Figure 4.27 The standardized Pareto chart for the total number of UFP: (a) biocomposite M1, and (b) biocomposite M2

Figures 4.28 and 4.29 show the relationship between the total number of ulttrafine particles and the cutting parameters for biocomposites M1 and M2, respectively. The number of UFP is not affected by the cutting conditions as mentioned above, but it can be seen that each reinforcement type of biocomposite (biocarbon, miscanthus fiber) has a different effect on UFP emission.

Figure 4.28 shows a decrease in the total number of UFP as a result of an increase in one of the tested factor (f, s, d) for biocomposite M1. In contrast, the total number of UFP increases slightly with increasing f, s, and d for biocomposite M2 (Figure 4.29).

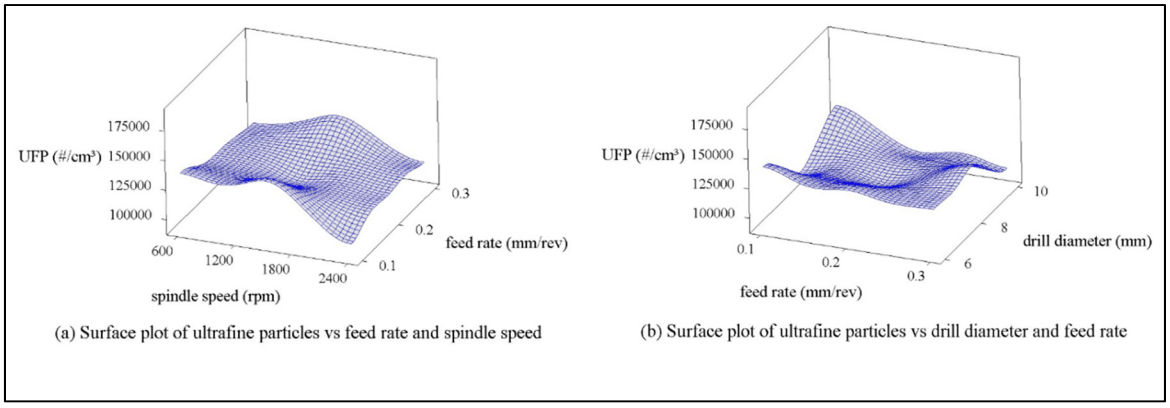

Figure 4.28 The surface plot of the total number of UFP for biocomposite M1

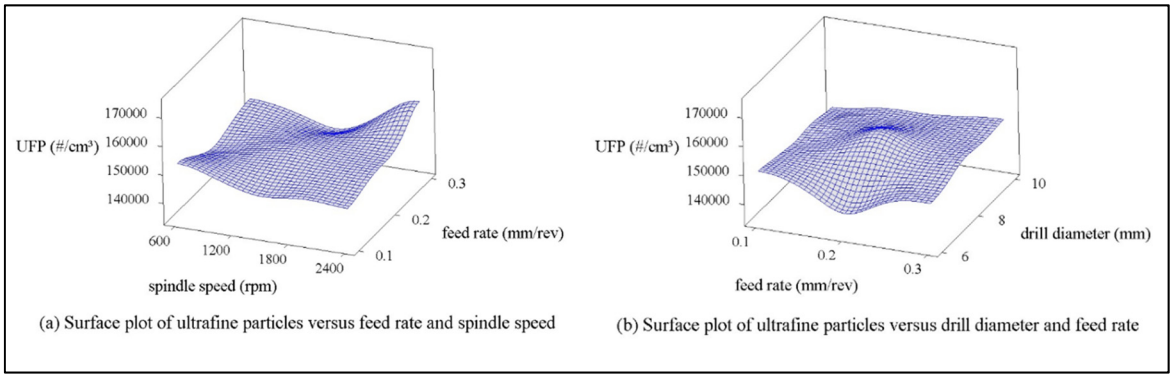

Figure 4.29 The surface plot of the total number of UFP for biocomposite M2

Figure 4.30 compares the total number of UFP emitted during the drilling of biocomposites M1 and M2. The horizontal axis presents the testing numbers from 1 to 27, where each testing number was conducted with the same drilling parameters for both biocomposites. The vertical axis shows the total number of UFP emission. It is indicated that more ultrafine particles generated from biocomposite M2 than biocomposite M1, except for some tests such as 1, 2, 15, 22 (Figure 4.30). The total number of UFP for biocomposite M2 fluctuated slightly around the average value of 149,700 (#/cm³) when changing the drilling conditions

(the total number concentration ranging from 135,000 to 174,000 #/cm³). Meanwhile, the total number of UFP for biocomposite M1 decreases with increasing tested factors (d, s and f). The highest difference in total number of UFP between both biocomposites is 61,300 #/cm³, obtained at the test number of 27.

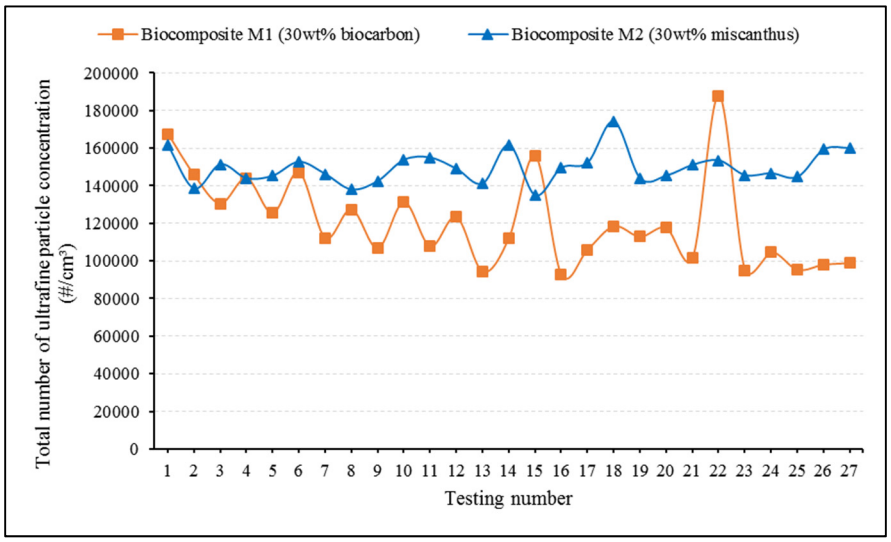

Figure 4.30 The total number of UFP related to testing number for biocomposites (M1 and M2)

4.4 Conclusions

This study investigated the influence of machining conditions and the reinforcement type of biocomposite on machinability during the dry drilling of biocomposites. Based on the statistical technique and empirical data analysis, some conclusions are drawn as follows.

The reinforcement type of biocomposite (biocarbon particle, miscanthus fiber) significantly affects the machinability of biocomposites. The increase of weight ratio of miscanthus fibers used in biocomposite leads to an increase in surface roughness (R_a, R_t) and fine particles emitted (PM10), and results in a decrease in thrust force and specific cutting energy. In contrast, an increase in terms of thrust forces and specific cutting energy, and a decrease in

terms of surface roughness and fine particles generated as a result of the increased weight ratio of biocarbon particles used in biocomposite.

The effect of drilling parameters on machinability of biocomposites M1 and M2 are different, which could be due to the interaction between cutting conditions and biocomposite materials. Two tested factors (s and d) are statistically significant for thrust force when drilling biocomposite M1, however, they are not statistically significant for thrust force for biocomposite M2. The increase of thrust force for both biocomposites are a result of the increased feed rate. The thrust force created of biocomposite M1 is much larger than that of biocomposite M2 under the same drilling condition. An increase in drill diameter and/or spindle speed leads to a significant difference in thrust force generated between two biocomposites.

The specific cutting energy is significantly influenced by feed rate and decreased with the increased feed rate for both biocomposites M1 and M2. The specific cutting energy of biocomposite M1 is higher than biocomposite M2 under the same drilling parameters.

The surface roughness (R_a, R_t) and fine dust emission (PM10) are greatly influenced by two tested factors (s and d) for both biocomposites M1 and M2. The surface roughness increase is the result of an increase in drill diameter and spindle speed. The surface roughness and fine dust emission during drilling of biocomposite M2 are much greater than that of biocomposite M1, respectively.

More fine particles are generated with the size smaller than 2.5 μm during dry drilling of both biocomposites M1 and M2. The fine particles emission increase with the increased spindle speed. In contrast, the increase of drill diameter and feed rate result in the decrease of fine particles for both biocomposites. Nevertheless, the ultrafine particle emission is not affected by drilling parameters for both biocomposites. Therefore, it is impossible to predict the ultrafine particles generated when drilling biocomposites.

CHAPTER 5

REGRESSION AND ANFIS-BASED MODELS FOR PREDICTING OF SURFACE ROUGHNESS AND THRUST FORCE DURING DRILLING OF BIOCOMPOSITES

Dinh Son Tran[1, 2], Victor Songmene[1], Anh Dung Ngo[1]

[1] Department of Mechanical Engineering, École de Technologie Supérieure, ÉTS, Montreal, QC, H3C 1K3, Canada.
[2] Department of Mechanical Engineering, The University of Danang - University of Science and Technology, 54, Nguyen Luong Bang Street, Danang, Vietnam.

Article submitted for publication in Neural Computing and Applications, August 2020.

Abstract

Surface roughness and thrust force are known to be important machinability indicators when drilling biocomposites. It is very essential to develop models for predicting the effect of cutting parameters on these machining process performance indicators. In this study, a full factorial design is used to investigate the effects of machining parameters (feed rate, drill diameter, and spindle speed) on drilling of three types of biocomposites: Polypropylene/Polyolefin elastomers reinforced with biocarbon and/or miscanthus. Two predictive models, including regression and ANFIS-based model, are established to predict thrust force (F_t) and surface roughness (R_a) based on empirical data. The proposed regression models showed good accuracy for the tested biocomposites. These models are then used as the objective functions for by genetic algorithms (GA) optimization to find the optimal drilling parameters leading to minimal values of thrust force and surface roughness. The results show that ANFIS-based models have better predictive accuracy for thrust force and surface roughness than the regression-based models. The influence of drilling parameters on machinability is shown to be dependent on the type of reinforcement.

Keywords: machinability, regression, ANFIS, GA, biocomposite, natural reinforcements.

5.1 Introduction

Biocomposites are expected to replace other materials to manufacture automotive parts because of their advantages such as light weight, environmental friendliness, reasonable price, and diverse natural resources (Koronis et al., 2013). These materials have been developed by researchers and manufacturers to diversify biocomposite materials to meet the need to reduce product weight and fuel efficiency of cars (Peças et al., 2018). Making holes with conventional drilling process for biocomposites is widely used in order to assemble the product easily (Nassar et al., 2017). When drilling these composites, surface roughness and thrust force are the key parameters of machinability, and they are significantly influenced by cutting parameters such as drill diameter, spindle speed, and tool feed rate (Tran et al., 2020). Due to the heterogeneous and anisotropic properties of composite materials, predictive models are usually established mainly based on experimental machining data. The empirical regression-based model is commonly used to establish relationships between output responses such as surface roughness, cutting force, cutting temperature, tool wear, etc. and cutting parameters (tool diameter, feed rate, cutting speed, depth of cut). Jayabal et al. (2011) have established models for predicting thrust force, torque, and tool wear during drilling of glass/coir/polyester hybrid composite. These developed regression models show relatively good predictive results. Bajpai and Singh (2013) used the regression model for the prediction of thrust force and torque when drilling sisal/PP biocomposite. Mata et al. (2010) demonstrated that the predictive results of cutting forces obtained by regression analysis are comparable to the experimental data obtained during the turning of Carbon/PEEK composite.

Some researchers have used regression models in combination with GA to select the optimal parameters for machining processes: Zain et al. (2010) for milling process; Kumar and Hynes (2019) for thermal drilling of galvanized sheet metal, and Krishnaraj et al. (2012) for drilling of composite (CFRP). Subramanian et al. (2013) combined GA with Response Surface Methodology to find the optimal parameters for cutting forces during milling of Al7075-T6. Other researchers have used ANFIS (Adaptive Neuro-Fuzzy Inference System), which is a combination of the properties of artificial neural network and fuzzy logic. It improves the disadvantages of artificial neural network, so to allow its use in solving many

practical problems (Karaboga & Kaya, 2019). In recent years, ANFIS-based models have been applied to predict output responses such as cutting force, surface roughness, tool life, and cutting temperature during machining of materials. They are also used to determine the effect of input factors such as feed rate, cutting speed, tool diameter, tool geometries, and workpiece materials on the output responses in machining processes. Marani et al. (2019) used ANFIS models to predict the surface roughness and the cutting force when machining Al-20 Mg2Si-2Cu metal matrix composite and obtained results in good agreement with experimental data. Kumar and Hynes (2019) used the same techniques and also obtained good prediction for the thermal drilling of galvanized steel. ANFIS models were also used successfully to predict the cutting temperature during the turning of hard steel (Savkovic et al., 2019) and for predicting the material removal rate and surface roughness when turning stainless steel 202 (Shivakoti et al., 2019). Abbas et al. (2017) have shown that the ANFIS model has better prediction accuracy for surface roughness than that of the regression model during the turning of high-strength steel.

The rapid development of new biocomposites requires manufacturers to quickly understand their machinability to meet production needs. The use of limited empirical data to build predictive models to predict the factors affecting the machining process can help to quickly assess the machining performance of these new biocomposites. In this study, the experiments were conducted based on a full factorial design with three levels. Three types of biocomposites were drilled dry using different diameters of HSS twist drills (6, 8, and 10 mm) with various spindle speed and feed rate. Regression and ANFIS-based models for predicting the thrust force and the arithmetic average surface roughness (R_a) were established for the tested biocomposites. The comparison of the predicted accuracy of these two models is assessed using MAPE (Mean Absolute Percentage Error), RMSE (Root Mean Square Error), and R^2 (correlation coefficient). Moreover, the optimal drilling parameters minimizing the Ra-values and thrust force were determined using GA optimization.

5.2 Experimental setup

5.2.1 Workpiece materials

The tested biocomposites have the same matrix PP/POE (Polypropylene/Polyolefin elastomer) randomly reinforced with chopped miscanthus fibers and biocarbon particles. MAPP (Maleic Anhydride grafted Polypropylene), a compatibilizer, was added to improve the adhesion between matrix and reinforcement material (Behazin et al., 2017b). The finely chopped miscanthus fibers have an average length of 4 mm, while biocarbon particles were made from the pyrolysis of miscanthus fibers. The tested biocomposites are made from the press molding process, the sources of materials and the biocomposites fabrication process are described in (Tran et al., 2020). The three types of biocomposite used for this study, are symbolized as M1, M2, and M3 (hybrid). Their mechanical properties and chemical compositions are given in Table 5.1 (Dhaouadi, 2018).

Table 5.1 Mechanical properties and chemical composition of tested biocomposites

Materials	**Chemical composition**				
	PP (wt %)	POE (wt %)	MAPP (wt %)	Biocarbon (wt %)	miscanthus (wt %)
M1	62	5	3	30	-
M2	62	5	3	-	30
M3 (hybrid)	62	5	3	15	15
Mechanical properties					
	Young's modulus (MPa)	Tensile strength (MPa)	Flexural modulus (MPa)	Flexural strength (MPa)	Impact strength (J/m)
M1	2510	31	2146	52	294.5
M2	3872	37.3	3148	58.5	128.5
M3 (hybrid)	3175	34	2717	55	140

5.2.2 Experimental procedure

Figure 5.1 presents the equipment used to conduct the experiment. Biocomposite samples with dimensions of 300 x 120 x 5 mm^3 were placed and clamped on the machine table of CNC machine tool. HSS twist drill bits with diameters of 6, 8, and 10 mm were used for dry drilling. The drilling parameters were selected from the tool manufacturer's catalogue and the literature. A full factorial design was applied to conduct the experiments. The tested factors and their levels are described as Table 5.2. Each experiment was repeated three times. For each biocomposite, a total of 81 (3^3x3) experiments were performed, and for the entire test plan, a total of 243 holes (81x3) were drilled.

Cutting forces were measured directly during the drilling process using a table-dynamometer (Kistler 9255B). The cutting force signals in X, Y, and Z-axis were transmitted to and recorded on a personal computer and analyzed with the help of Matlab software. The surface roughness of the drilled hole was measured along the longitudinal axis of the hole, using a roughness profilometer (Mitutoyo, model SJ-410). The data were recorded directly on a personal computer supported by SURPAK-SJ software.

Table 5.2 Factors and their levels used for experimental design

Factors	**Low**	**Medium**	**High**
d: drill diameter (mm)	6	8	10
s: spindle speed (rpm)	600	1500	2400
f: feed rate (mm/rev)	0.1	0.2	0.3
Biocomposite	M1 (PP/POE/MAPP +30wt% biocarbon)	M2 (PP/POE/MAPP +30wt% miscanthus)	M3 (hybrid) (PP/POE/MAPP + 15wt% biocarbon + 15wt% miscanthus)

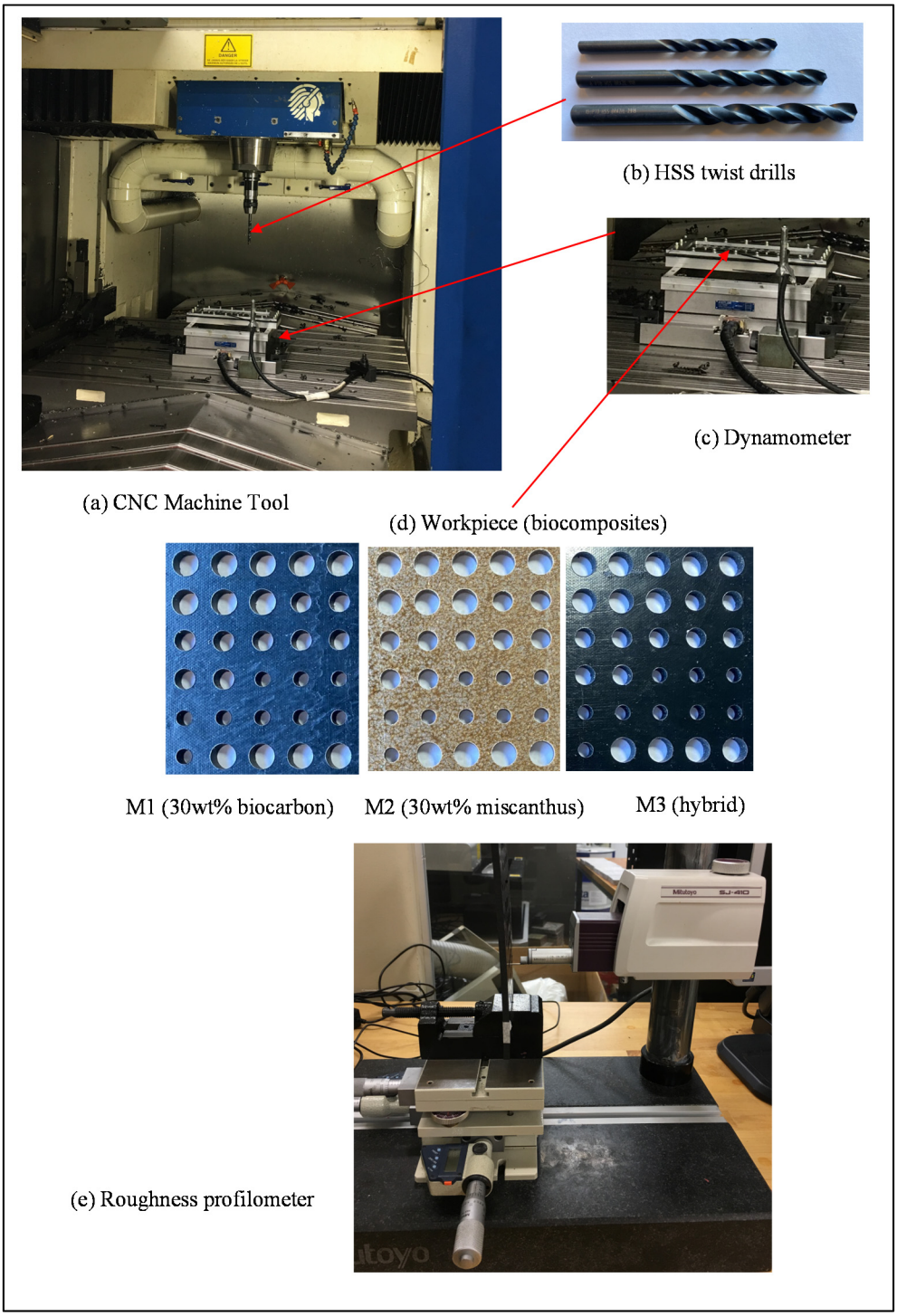

Figure 5.1 The experimental devices

5.2.3 Experimental data collecting and analyzing procedure

5.2.3.1 **Cutting forces measurement**

Figure 5.2 presents a typical thrust force signal recorded during drilling a hole of the biocomposite M1. The drilling process can be divided into three main stages: Phase 1 begins at the time of the drill chisel edge penetrates into the workpiece until the whole cutting edges come into contact with the workpiece. At this stage, the thrust force increases rapidly in a short time because of the increased cross-section area of uncut chip. Phase 2 takes place when the whole drill cutting edges and chisel edge come into contact with the workpiece. Thrust force fluctuates slightly with a relatively stable value in this phase due to the unchanged cross-section area of uncut chip, known as a stable drilling phase. The final phase starts at the time the chisel edge exit the workpiece until the entire main cutting edges are no longer in contact with the workpiece. The thrust force gradually decreases until it reaches approximately zero.

The thrust force created during drilling is taken from the average value of the Z-axis cutting force signals in the stable drilling phase (phase 2). As mentioned above, each drilled hole having the same drilling parameters and biocomposite was carried out three times. Therefore, the thrust force (F_t) used for analysis is calculated by mean value of thrust forces as equation (5.1).

$$F_t = \frac{1}{3}.\sum_{i=1}^{3} F_{ti} \tag{5.1}$$

Where F_{ti} is the thrust force of the i^{th}-drilled hole.

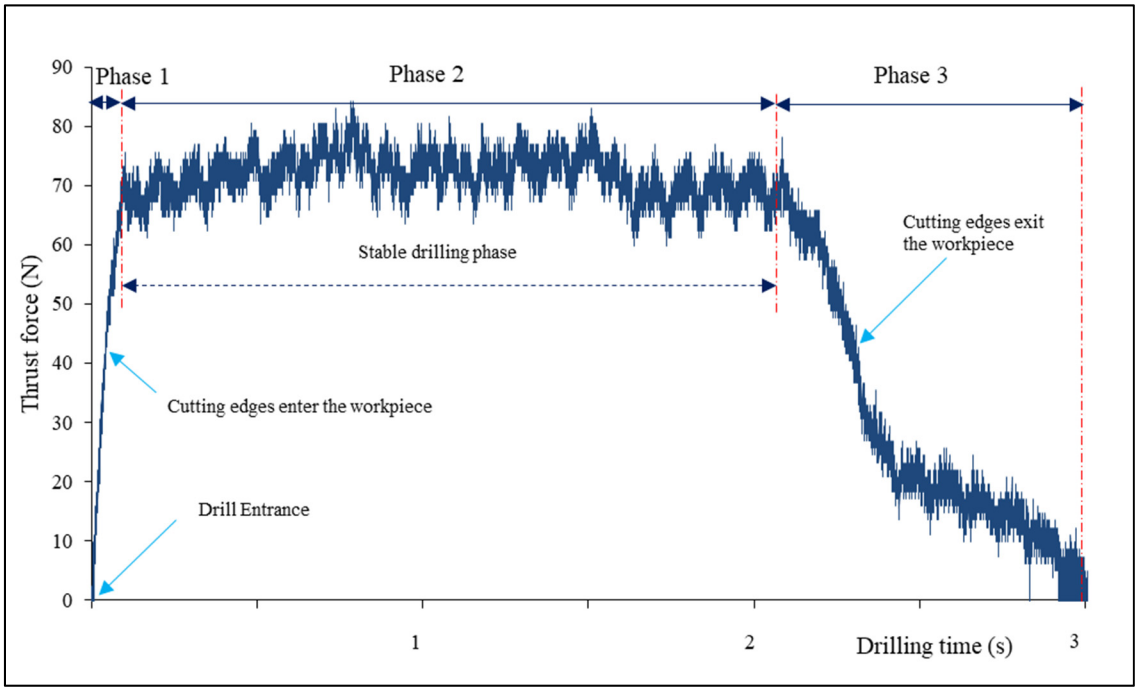

Figure 5.2 The thrust force signal during the drilling of bicomposite M1 (d = 6mm, f = 0.2 mm/rev, s = 600 rpm)

5.2.3.2 **Surface roughness measurement**

Figure 5.3 presents an example of the recorded surface profile measured longitudinally on the surface of a drilled hole. The cut-off measurement length of 0.8 mm is repeated three times, so the total measured length of 2.4 mm. Table 5.3 summarizes the values of the recorded roughness parameters for a drilled hole surface. According to literature, the roughness R_a is one of the important parameters that was usually chosen to evaluate the quality of the machined surface. In this study, the arithmetic average roughness (R_a) was selected to analyze and establish the predictive models for surface roughness.

In this investigation, each drilled hole was measured at least twice in distinct positions. The mean value of the roughness R_a was selected for analysis and calculated by equation (5.2) as follows.

$$R_a = \frac{1}{6}.\sum_{i=1}^{6} R_{ai} \tag{5.2}$$

Where R_{ai} is the roughess (R_a) of the i^{th} measurement

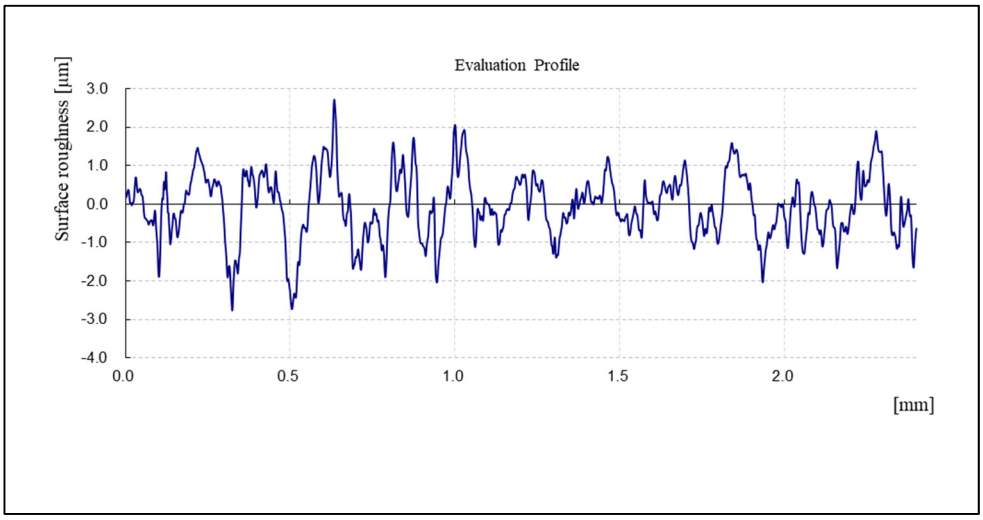

Figure 5.3 The profile of a drilled-hole surface: M1 (d = 6 mm, f = 0.2 mm/rev, s = 600 rpm)

Table 5.3 The roughness parameters of biocomposite M1
(d = 6mm, f = 0.2 mm/rev, s = 600 rpm)

Standard	ISO 1997	N	3
Profile	R	Cut-Off	0.8mm
λs	2.5µm	Filter	GAUSS
Ra	0.674 µm	Rmr(c)1	0.333 %
Rq	0.843 µm	Rmr(c)2	0.771 %
Rz	4.505 µm	Rdc	0.480 µm
Rp	2.225 µm	Rt	5.486 µm
Rv	2.279 µm	Rz1max	5.486 µm
Rsk	-0.159	Rk	2.170 µm
Rkµ	2.903	Rpk	0.804 µm
Rc	2.949 µm	Rvk	1.052 µm
RPc	60.09 /cm	Mr1	8.875 %
RSm	166.4 µm	Mr2	90.063 %
RDq	0.090	A1	3.57
Rmr	0.125 %	A2	5.23

5.2.3.3 **Experimental data results**

Table 5.4 shows the values of thrust force and surface roughness (R_a) obtained from the experimental data and calculated using equations (5.1) and (5.2), respectively. The output responses (thrust force and surface roughness R_a) are presented corresponding to the drilling parameters (f, s, and d) and respectively for each biocomposite. These data are used to establish the predictive models for thrust force and surface roughness based on multiple regression analysis and ANFIS (Adaptive Neuro-Fuzzy Inference System).

Table 5.4 The mean values of thrust force and roughness R_a of biocomposites

Test run	**Feed rate**	**Spindle speed**	**Drill diameter**	**Thrust force, F_t (N)**			**Roughness R_a (µm)**		
	(mm/rev)	(rpm)	(mm)	**M1**	**M2**	**M3**	**M1**	**M2**	**M3**
1	0.1	600	6	67.94	35.48	53.68	0.59	0.80	0.55
2	0.2	600	6	81.99	47.41	72.95	0.56	1.04	0.53
3	0.3	600	6	106.45	57.65	89.01	0.49	0.91	0.59
4	0.1	1500	6	75.83	28.16	56.08	0.55	0.70	0.67
5	0.2	1500	6	110.20	40.63	78.43	0.65	0.94	0.63
6	0.3	1500	6	135.04	62.58	103.16	0.55	1.11	0.82
7	0.1	2400	6	85.47	33.14	66.23	0.71	0.79	0.81
8	0.2	2400	6	119.59	40.10	85.08	0.74	0.97	0.71
9	0.3	2400	6	138.87	55.33	101.22	0.67	1.02	1.04
10	0.1	600	8	84.97	32.88	60.78	0.59	0.79	0.83
11	0.2	600	8	133.60	48.04	87.23	0.74	1.23	0.70
12	0.3	600	8	132.33	65.23	97.87	0.76	1.26	0.90
13	0.1	1500	8	114.88	29.27	65.08	0.90	0.80	0.84
14	0.2	1500	8	146.13	45.12	87.34	0.76	1.22	0.97
15	0.3	1500	8	186.06	63.63	114.17	0.82	1.27	0.86
16	0.1	2400	8	149.76	33.12	87.79	0.95	1.22	1.00
17	0.2	2400	8	166.14	48.22	100.15	0.93	1.20	1.14
18	0.3	2400	8	211.66	62.95	122.36	0.98	1.28	1.22
19	0.1	600	10	94.62	31.78	59.80	0.62	0.81	0.89
20	0.2	600	10	142.47	43.70	80.90	0.67	1.15	1.09
21	0.3	600	10	171.14	62.82	104.76	0.62	1.14	1.08
22	0.1	1500	10	115.23	34.22	71.76	0.96	1.37	1.04
23	0.2	1500	10	173.93	42.16	95.38	1.00	0.98	0.97
24	0.3	1500	10	187.59	55.11	107.00	0.82	1.22	0.96
25	0.1	2400	10	172.78	32.31	96.21	1.19	1.83	1.28
26	0.2	2400	10	244.29	43.12	131.51	1.48	1.88	1.48
27	0.3	2400	10	349.68	76.99	183.06	1.46	1.69	1.30

5.3 Multiple Regression based Models

5.3.1 Regression Models

In this investigation, two regression models were introduced to establish the predictive models for thrust force (F_t) and surface roughness (R_a). The first one is based on the second-order nonlinear mathematical model described in equation (5.3). The second model is described as equation (5.4) and was established from equation (5.3) by eliminating the second-order parameters.

$$Y = a_0 + a_1.X_1 + a_2.X_2 + a_3.X_3 + a_4.X_1^2 + a_5.X_2^2 + a_6.X_3^2 + a_7.X_1.X_2 + a_8.X_1.X_3 + a_9.X_2.X_3 \quad (5.3)$$

$$Y = a_0 + a_1.X_1 + a_2.X_2 + a_3.X_3 + a_4.X_1.X_2 + a_5.X_1.X_3 + a_6.X_2.X_3 \quad (5.4)$$

Where Y is the predictive value, a_i is regression coefficients, and X_1, X_2 and X_3 are the drilling parameters (f, s, and d).

After obtaining the regression models based on equations (5.3) and (5.4), the next step is to compare and select the best predictive models for thrust force and surface roughness. A better predictive model based on equations (5.3) or (5.4) will be selected by comparing MAPE (Mean Absolute Percentage Error) and RMSE (Root Mean Square Error). MAPE and RMSE are calculated by equations (5.5) and (5.6), respectively.

$$MAPE = \frac{100\%}{n}\sum_{i=1}^{n}\left|\frac{E_i - Y_i}{E_i}\right| \quad (5.5)$$

$$RMSE = \sqrt{\frac{1}{n}\sum_{i=1}^{n}(E_i - Y_i)^2} \quad (5.6)$$

Where n is the number of data samples, E_i are the experimental values, Y_i are the predicted values were calculated from prediction models.

Table 5.5 presents the values of MAPE and RMSE values calculated from the regression models of thrust force and surface roughness (R_a) based on equations (5.3) and (5.4) for each type of biocomposite, respectively. From Table 5.5, it can be seen that the values of MAPE and RMSE values obtained from the empirical modelling of thrust force based on equation (5.3) are smaller than that based on equation (5.4), respectively for each biocomposite. Except for only MAPE (7.96%) calculated by equation (5.3)-based model, which is slightly larger than MAPE (7.83%) obtained from equation (5.4)-based model for biocomposite M1. It can be inferred that the predictive models for thrust force based on equation (5.3) have better predictive accuracy than that based on equation (5.4) for all biocomposites. Consequently, the predictive models for thrust force based on equation (5.3) were selected. The regression models for thrust force of biocomposites M1, M2 and M3 were presented by equations (5.7), (5.8) and (5.9), respectively, in Table 5.6.

Table 5.5 The comparison of the mathematical models based on equations (5.3) and (5.4)

Material	Mathematical Models	MAPE	RMSE
Thrust force (N)			
M1 (30wt% biocarbon)	Equation (5.3)-based model	7.96 %	15.51
	Equation (5.4)-based model	7.83%	16.27
M2 (30wt% miscanthus)	Equation (5.3)-based model	5.33%	3.44
	Equation (5.4)-based model	6.65%	3.87
M3 (hybrid)	Equation (5.3)-based model	5.31%	7.49
	Equation (5.4)-based model	6.12%	8.05
Surface roughness R_a (μm)			
M1 (30wt% biocarbon)	Equation (5.3)-based model	17.49%	0.19
	Equation (5.4)-based model	7.41%	0.08
M2 (30wt% miscanthus)	Equation (5.3)-based model	32.04%	0.46
	Equation (5.4)-based model	9.57%	0.14
M3 (hybrid)	Equation (5.3)-based model	31.7%	0.39
	Equation (5.4)-based model	8.48%	0.09

From Table 5.5, it can be seen that values of MAPE and RMSE of the predictive models for surface roughness R_a based on equation (5.3) are significantly higher than that based on equation (5.4) corresponding to each biocomposite. Therefore, the regression models based on the equation (5.4) are chosen to establish the predictive models for surface roughness R_a. The empirical models for surface roughness R_a of biocomposites M1, M2 and M3 were illustrated in Table 5.6, respectively for equations (5.10), (5.11) and (5.12).

Table 5.6 The empirical models for thrust force and surface roughness R_a

Biocomposites	**Thrust force (N)**	
M1	$F_t = 97 - 272 * f - 0.1197 * s + 4.2 * d - 313 * f^2 + 0.000011 * s^2 - 1.08 * d^2 + 0.1202 * f * s + 72.8 * f * d + 0.01255 * s * d$	(5.7)
M2	$F_t = 27.6 - 47.6 * f - 0.02169 * s + 4.91 * d + 309 * f^2 + 0.000003 * s^2 - 0.475 * d^2 + 0.0103 * f * s + 7.43 * f * d + 0.001208 * s * d$	(5.8)
M3	$F_t = 93.7 + f - 0.0638 * s - 4.7 * d + 12 * f^2 + 0.000008 * s^2 - 0.129 * d^2 + 0.0361 * f * s + 20.7 * f * d + 0.00595 * s * d$	(5.9)
	Surface roughness R_a (µm)	
M1	$R_a = 0.939 - 1.13 * f - 0.000463 * s - 0.0515 * d + 0.000174 * f * s + 0.115 * f * d + 0.00008 * s * d$	(5.10)
M2	$R_a = 0.428 + 4.39 * f - 0.000538 * s + 0.0059 * d - 0.000687 * f * s - 0.295 * f * d + 0.000105 * s * d$	(5.11)
M3	$R_a = -0.336 + 1.16 * f + 0.000103 * s + 0.1184 * d + 0.000148 * f * s - 0.112 * f * d + 0.000005 * s * d$	(5.12)
F_t : thrust forces; R_a : surface roughness ; d (mm): drill diameter; f (mm/rev): feed rate; s (rpm): spindle speed		

5.3.2 Graphical comparison of the predictive models

Figure 5.4 presents the predicted values of thrust forces obtained from the regression models and the experimental values for all the tested biocomposites. It can be seen that the predicted values of thrust force obtained from the equation (5.3)-based model are closer to the experimental values than those obtained from the equation (5.4)-based model. Therefore, it is appropriate to choose the predictive models for thrust forces based on equation (5.3).

Figure 5.5 presents the predicted values of surface roughness R_a obtained from the regression model and experimental values. It is noticeable that the predicted values of the equation (5.3)-based models show large deviations compared to the experimental values. Meanwhile, the predicted values of the equation (5.4)-based models are very close to the experimental values. Therefore, regression models based on equation (5.4) are suitable for the prediction of surface roughness R_a for the tested biocomposites.

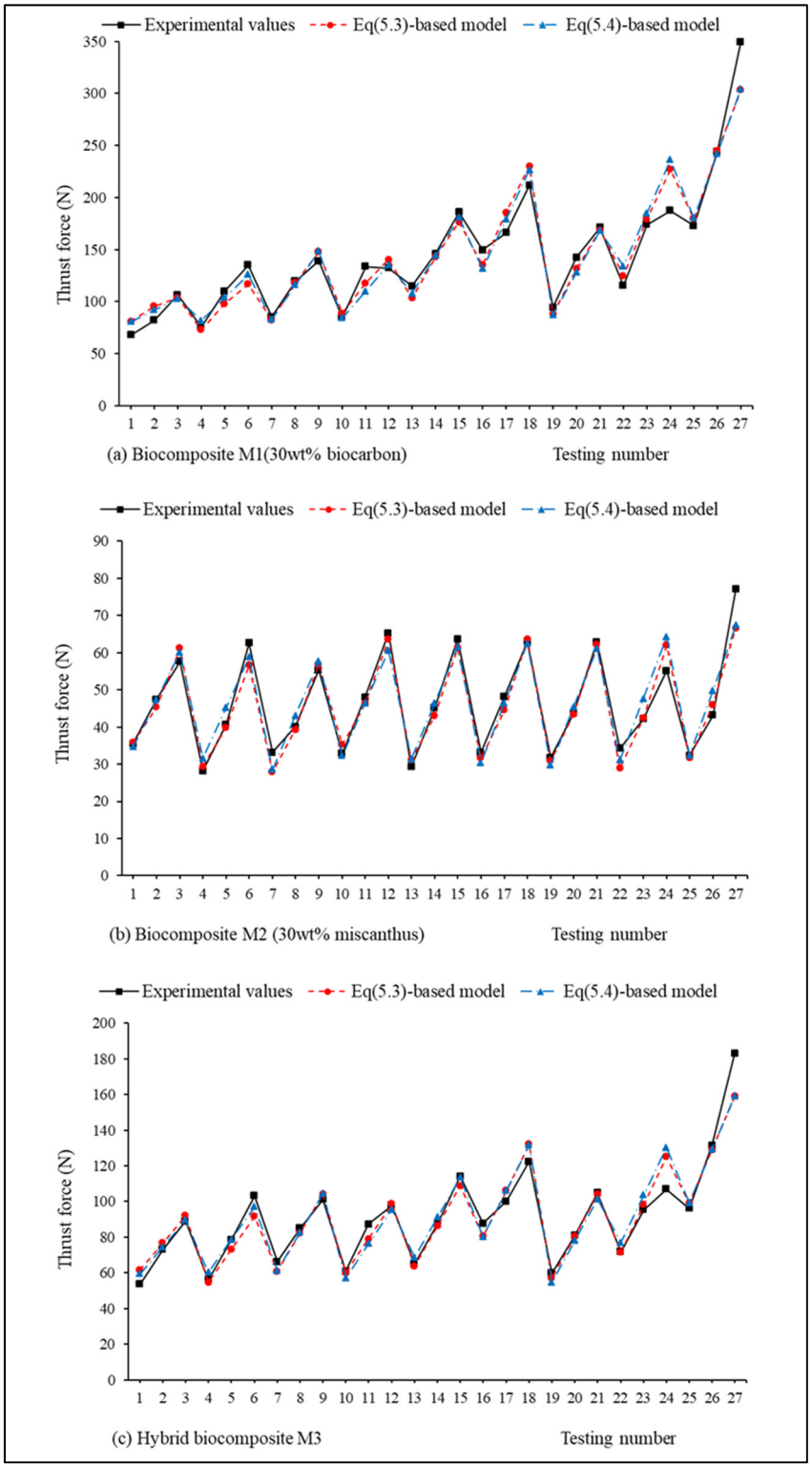

Figure 5.4 The comparison of the predictive and experimental results of thrust force for the three tested biocomposites

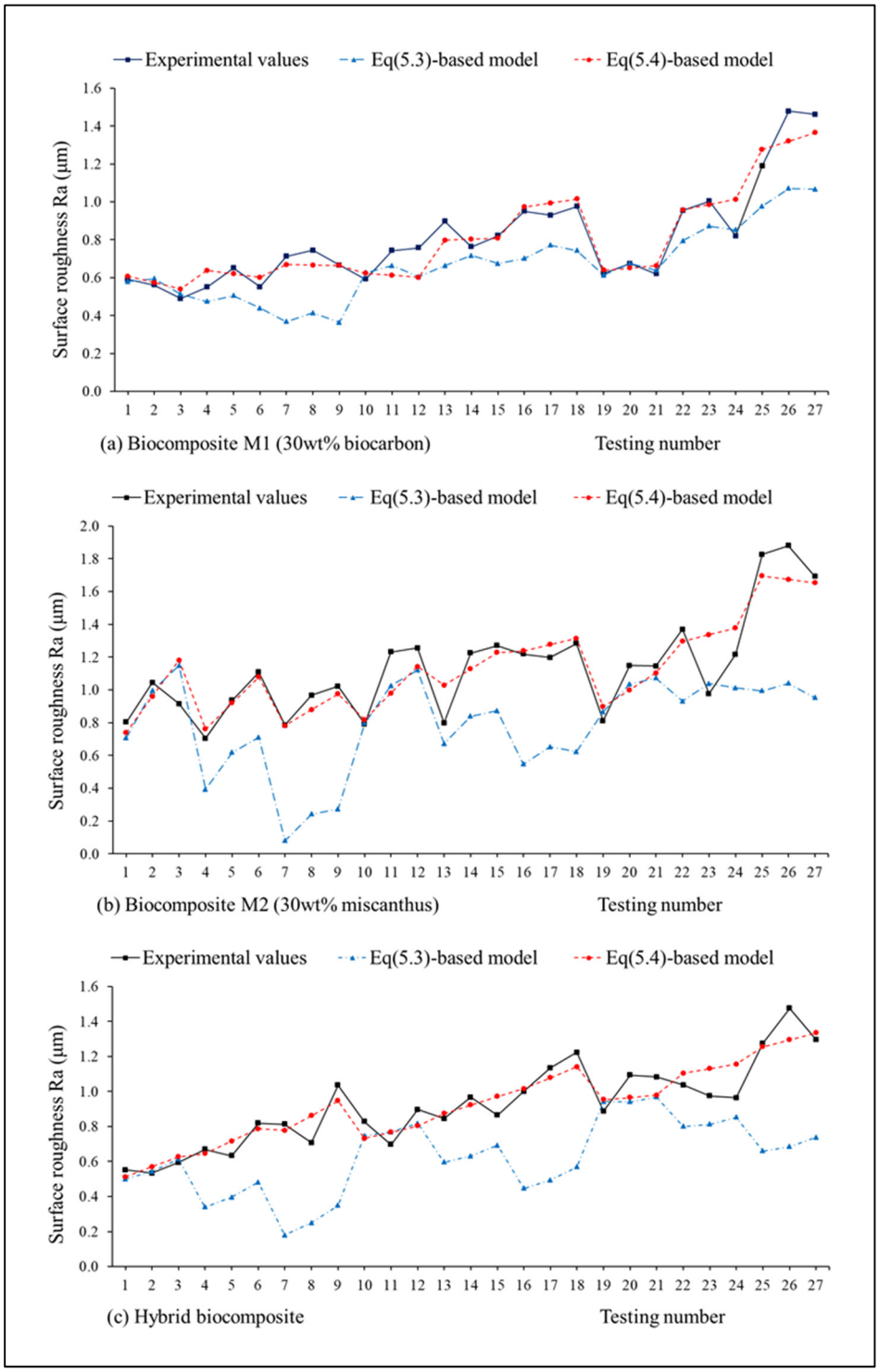

Figure 5.5 The comparison of the predictive and experimental results of surface roughness R_a for the tested biocomposites

5.3.3 Optimization of thrust forces and surface roughness using Genetic Algorithm

Genetic Algorithm (GA) is one of the most attractive techniques useful to optimize problems in applied engineering. This is a recognized technique to optimize an objective function according to predefined boundary conditions (linear or nonlinear) (Kumar & Hynes, 2019). GA has been applied in some machining studies to determine optimal parameters. Savas and Ozay (2008) have found the optimal cutting parameters to achieve the smallest surface roughness using GA in the tangential turn-milling process. Imani et al. (2020) combined ANN and GA to optimize cutting forces and surface roughness in milling process.

The goal of this subsection is to determine the optimal cutting parameters (d, s, f) to achieve the minimum values of thrust force and surface roughness R_a when drilling the tested biocomposites. The Matlab toolbox was used to find the minimum value from the objective function. The fitness function is taken from the regression models of the thrust force and surface roughness R_a for biocomposites (eq (5.7) to (5.12)) and expressed by the following equations (eq (5.13) to (5.18)).

$$y(1) = 97 - 272 * x(1) - 0.1197 * x(2) + 4.2.x(3) - 313 * \left(x(1)\right)^2 + 0.00001 * \left(x(2)\right)^2 - 1.08 * \left(x(3)\right)^2 + 0.1202 * x(1) * x(2) + 72.8 * x(1) * x(3) + 0.01255 * x(2) * x(3) \quad (5.13)$$

$$y(2) = 27.6 - 47.6 * x(1) - 0.02169 * x(2) + 4.91 * x(3) + 309 * \left(x(1)\right)^2 + 0.000003 * \left(x(2)\right)^2 - 0.475 * \left(x(3)\right)^2 + 0.0103 * x(1) * x(2) + 7.43 * x(1) * x(3) + 0.001208 * x(2) * x(3) \quad (5.14)$$

$$y(3) = 93.7 + x(1) - 0.0638 * x(2) - 4.7 * x(3) + 12 * \left(x(1)\right)^2 + 0.000008 * \left(x(2)\right)^2 - 0.129 * \left(x(3)\right)^2 + 0.0361 * x(1) * x(2) + 20.7 * x(1) * x(3) + 0.00595 * x(2) * x(3) \quad (5.15)$$

$$y(4) = 0.939 - 1.13 * x(1) - 0.000463 * x(2) - 0.0515 * x(3) + 0.000174 * x(1) * x(2) + 0.115 * x(1) * x(3) + 0.000080 * x(2) * x(3) \quad (5.16)$$

$$y(5) = 0.428 + 4.39 * x(1) - 0.000538 * x(2) + 0.0059 * x(3) - 0.000687 * x(1) * x(2) - 0.295 * x(1) * x(3) + 0.000105 * x(2) * x(3) \quad (5.17)$$

$$y(6) = -0.336 + 1.16 * x(1) + 0.000103 * x(2) + 0.1184 * x(3) + 0.000148 * x(1) * x(2) - 0.112 * x(1) * x(3) + 0.000005 * x(2) * x(3) \quad (5.18)$$

Where y(i) is the fitness function; x(1), x(2) and x(3) represent the parameters f, s and d, respectively. The limitation of parameters: $0.1 \leq x(1) \leq 0.3$; $600 \leq x(2) \leq 2400$; $6 \leq x(3) \leq 10$.

Table 5.7 shows the key parameters used in the GA toolbox. Table 5.8 presents the minimum values of thrust force and surface roughness R_a obtained from the optimal drilling parameters (f, s, and d), respectively for each biocomposite.

Table 5.7 GA parameters

Parameters	**Values**
Number of variables	3
Bounds	Lower [0.1 600 6]; Upper [0.3 2400 10]
Population size	100
Selection function	Stochastic uniform
Crossover fraction	0.8
Crossover function	Scattered
Number of generation	300
Stall generation	50

Table 5.8 The minimum values of thrust force and roughness R_a

Material	**Thrust force – $(F_t)_{min}$ (N)**	f (mm/rev)	s (rpm)	d (mm)
M1	72.84	0.1	1460	6
M2	27.77	0.1	2160	6
M3 (hybrid)	54.75	0.1	1520	6
Roughness – $(R_a)_{min}$ (µm)				
M1	0.54	0.3	600	6
M2	0.74	0.1	600	6
M3 (hybrid)	0.51	0.1	600	6

5.4 ANFIS based models

5.4.1 Structure of the proposed ANFIS model

ANFIS is a system that combines properties of fuzzy logic and neural networks. This is a hybrid system consisting of five layers with different functions, as described in Figure 5.6. The proposed structure has four inputs, namely feed rate (f), spindle speed (s), drill diameter (d), and the weight ratio of miscanthus fiber used in biocomposite (wt%), which are used to predict one output response such as thrust force (F_t) or surface roughness (R_a). Five layers of ANFIS structure included fuzzification layer (1), rule layer (2), normalization layer (3), defuzzification layer (4), and summation layer (5) (Karaboga & Kaya, 2019). The applied equations of each layer of the proposed ANFIS model presented from (5.19) to (5.24) in Table 5.9.

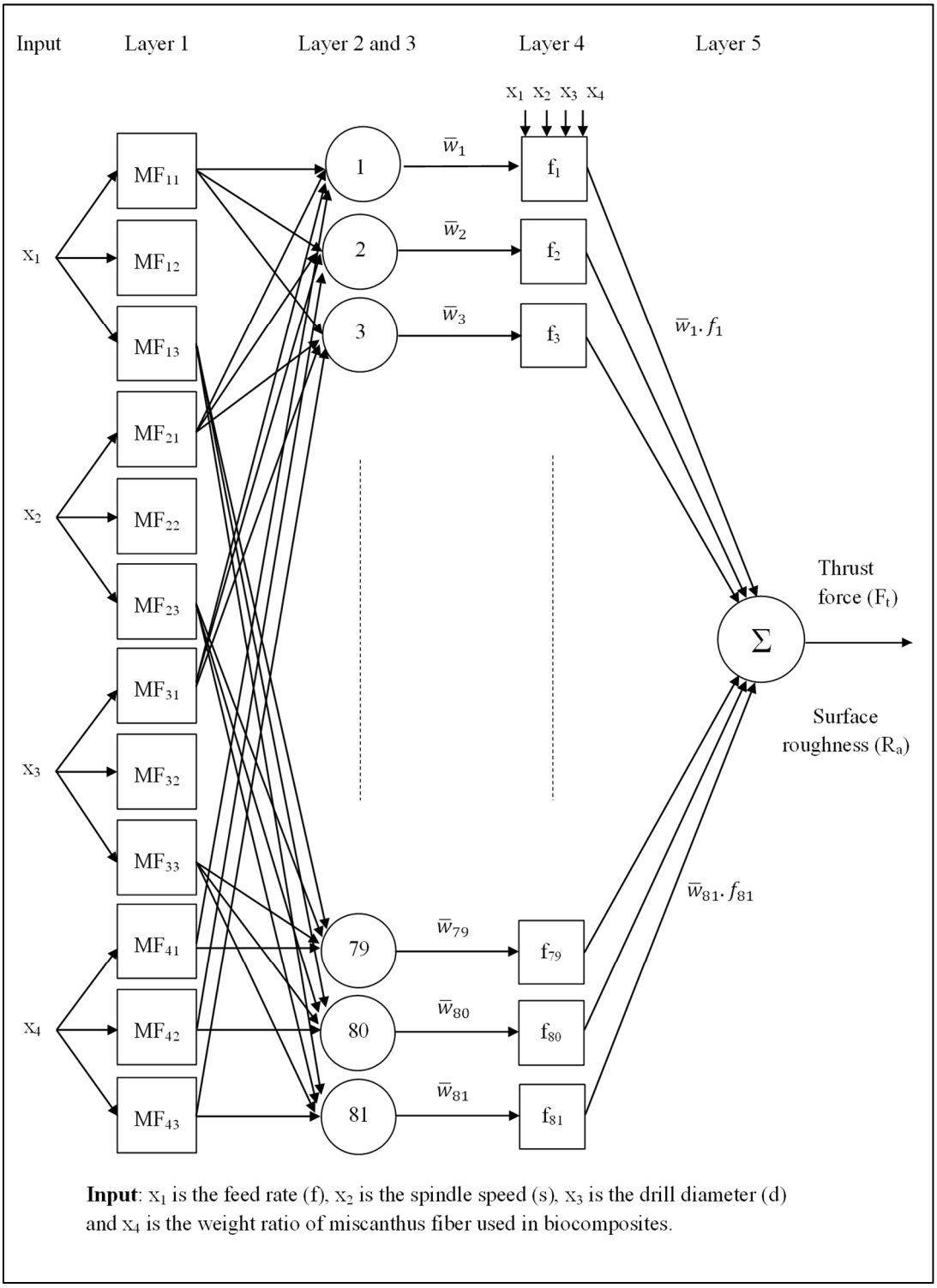

Figure 5.6 The structure of the proposed ANFIS model for thrust force and surface roughness R_a

Table 5.9 The equations for each layer of proposed ANFIS

Layer number	Equation	
1	$\mu_{Ai}(x) = gauss2mf(x;\sigma,c) = \begin{cases} e^{\frac{-(x-c_1)^2}{2.\sigma_1^2}} & x \le c_1 \\ 1 & c_1 \le x \le c_2 \\ e^{\frac{-(x-c_2)^2}{2.\sigma_2^2}} & x \ge c_2 \end{cases}$	(5.19)
	where c,σ are the MF parameters	
	$O_{1i}^1 = \mu_{1i}(x_1);\ O_{2j}^1 = \mu_{2j}(x_2);\ O_{3k}^1 = \mu_{3k}(x_3),$ $O_{4l}^1 = \mu_{4l}(x_4);$ (for i, j, k and l = 1,2,3)	(5.20)
	x_1, x_2, x_3, x_4 are input nodes; 1i, 2j, 3k, 4l are the labels associated with input nodes	
2	$O_r^2 = w_r = \mu_{1i}(x_1).\mu_{2j}(x_2).\mu_{3k}(x_3).\mu_{4l}(x_4);$ $r \in \{1 \div 81\}$	(5.21)
	w_r is the rule weight	
3	$O_r^3 = \overline{w}_r = \frac{w_r}{\sum_{r=1}^{81} w_r}$; $\overline{w}_r$ is the relative rule weight	(5.22)
4	$O_r^4 = \overline{w}_r.f_r = \overline{w}_r(p_r x_1 + q_r x_2 + r_r x_3 + s_r x_4 + t_r)$	(5.23)
	f_r is linear function of the inputs; p_r, q_r, r_r, s_r and t_r are the coefficients	
5	$O^5 = \sum_{r=1}^{81} \overline{w}_r.f_r$; (O^5 is thrust force F_t or surface roughness R_a)	(5.24)

It is important to choose the type of membership function (MFs) and the number of MFs used in ANFIS because they relate to the predictive accuracy between the input and output parameters of ANFIS-based model (Marani et al., 2019). By comparing the value of RMSE to choose the best model with type and number of MFs determined. RMSE (Root Mean Square Errors) is calculated by equation (5.6).

In order to achieve a good predictive model for thrust force and surface roughness, a total of 256 ANFIS structures were established, and RMSE tested for each output response. The

ANFIS structure having a smaller value of RMSE will be selected. Tables 5.10 shows RMSE-values of different ANFIS structures for thrust force. It can be seen that the minimum value of RMSE is $8.53x10^{-5}$, corresponding to an ANFIS structure that has 4 input parameters, 3 MFs for each input (3 3 3 3), and type of membership function is gauss2mf. This ANFIS model was selected for the prediction of thrust force and surface roughness.

Table 5.12 presents RMSE-values of the different ANFIS structures for surface roughness R_a. It can be seen that the value of RMSE ($9.81x10^{-7}$) of ANFIS structure selected, as mentioned above, is relatively small compared to other structures. This ANFIS model will be reasonable for the prediction of surface roughness R_a.

The ANFIS structure for thrust force and surface roughness R_a is generally described in Figure 5.6, 3 MFs was applied for each input (3 3 3 3), and gaus2mf is used for all membership functions. Consequently, the predictive model has 81 rules. Table 5.9 presents the mathematical equations describing the relationship between layers in the proposed ANFIS structure.

5.4.2 ANFIS-based model for thrust force

Table 5.11 shows the values of MAPE, RMSE, and R^2 obtained from the predictive models of thrust force for all biocomposites. MAPE and RMSE were calculated by equations (5.5) and (5.6), respectively. The R^2-value was calculated by equation (5.25), as follows.

$$R = \frac{\sum_{i=1}^{n}\left(\left(E_i - M_{Y_i}\right)\left(Y_i - M_{E_i}\right)\right)}{\sqrt{\left(\sum_{i=1}^{n}\left(E_i - M_{E_i}\right)^2\right)\left(\sum_{i=1}^{n}\left(Y_i - M_{Y_i}\right)^2\right)}} \tag{5.25}$$

Where R is correlation coefficient, E_i is the experimental value, Y_i is the predicted value, M_{Ei} is mean value of E_i, M_{Yi} is mean value of Y_i, n is the number of data samples, and i = 1 ÷ n.

From Table 5.11, it can be seen that values of MAPE and RMSE obtained from regression model for each biocomposite are much larger than those of ANFIS model, respectively. Meanwhile, R^2-value of ANFIS model is larger than that of regression model, respectively

for each biocomposite. Consequently, the proposed ANFIS model predicts thrust force more accurately than the regression model for all biocomposites.

Table 5.10 The RMSE-values of various ANFIS structures for thrust force

Number of MF for input				**Membership functions**							
x_1	x_2	x_3	x_4	**Trimf**	**Trapmf**	**gbellmf**	**gaussmf**	**gauss2mf**	**pimf**	**dsigmf**	**psigmf**
2	2	2	2	10.42	10.45	10.41	10.43	10.74	10.43	10.71	10.71
2	2	2	3	10.02	10.03	10.03	10.03	10.03	10.03	10.03	10.03
2	2	3	2	9.60	9.63	9.59	9.62	9.96	9.61	9.92	9.92
2	2	3	3	9.14	9.14	9.14	9.14	9.14	9.14	9.14	9.14
2	3	2	2	7.34	7.39	7.34	7.37	7.94	7.37	7.75	7.75
2	3	2	3	6.77	6.79	6.79	6.79	6.79	6.79	6.79	6.79
2	3	3	2	5.20	5.25	5.19	5.23	6.02	5.23	5.75	5.75
2	3	3	3	4.27	4.30	4.30	4.30	4.30	4.30	4.30	4.30
3	2	2	2	9.96	10.00	9.96	9.98	10.30	9.98	10.27	10.27
3	2	2	3	9.51	9.51	7.22	9.51	9.51	9.51	7.80	7.80
3	2	3	2	8.90	8.94	8.89	8.92	9.28	8.92	9.24	9.24
3	2	3	3	8.01	7.16	5.44	7.21	5.38	6.25	7.17	7.17
3	3	2	2	6.49	6.54	6.48	6.52	7.00	6.52	6.95	6.95
3	3	2	3	5.57	5.57	5.57	5.57	5.57	5.57	5.57	5.57
3	3	3	2	3.03	3.14	3.01	3.09	4.30	3.08	3.92	3.92
3	3	3	3	$9.2\text{x}10^{-5}$	$1.1\text{x}10^{-4}$	$9.5\text{x}10^{-5}$	$9.4\text{x}10^{-5}$	$8.5\text{x}10^{-5}$	$1.1\text{x}10^{-4}$	$1.1\text{x}10^{-4}$	$1.1\text{x}10^{-4}$

Table 5.11 The comparison of predictive models for thrust force

Material	**Regression-based model**			**ANFIS-based model**		
	MAPE (%)	RMSE	R^2 (%)	MAPE (%)	RMSE	R^2 (%)
M1 (30wt% biocarbon)	7.96	15.51	92.96	0.0022	0.00305	99.99
M2 (30wt% miscanthus)	5.33	3.44	92.61	0.0064	0.00306	99.97
M3 (hybrid)	5.31	7.49	92.08	0.0001	0.00024	99.99

Figure 5.7 presents the surface plot of predicted thrust force based on ANFIS model in relation to drilling parameters for three types of biocomposite. It is observed that the thrust force increases with the increased feed rate for all biocomposites. There are differences in the influence of spindle speed and drill diameter on thrust forces for types of biocomposites. The thrust force was found to decrease with the decreased spindle speed and drill diameter for biocomposites M1 and M3, while the influence of drill diameter and spindle speed on thrust force is negligible for biocomposite M2. The thrust force of biocomposite M1 generated is much greater than did other two biocomposites (M2 and M3) when drilling with various cutting parameters.

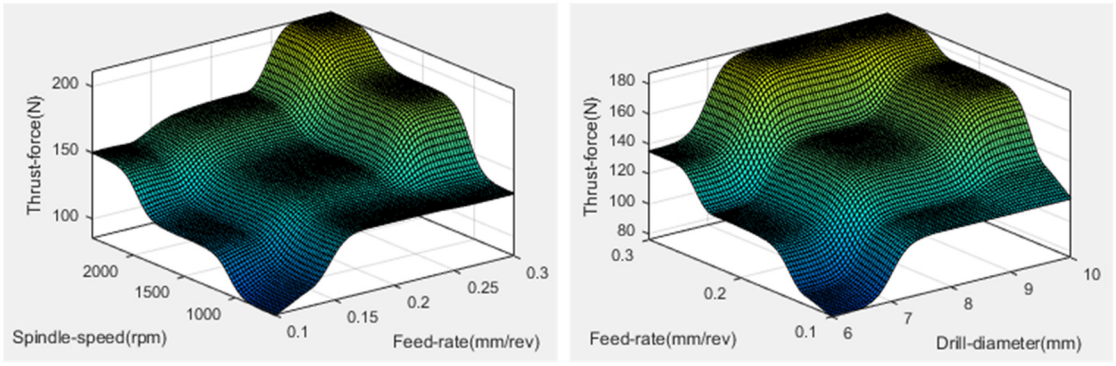

(a) Biocomposite M1 (30wt% biocarbon particles)

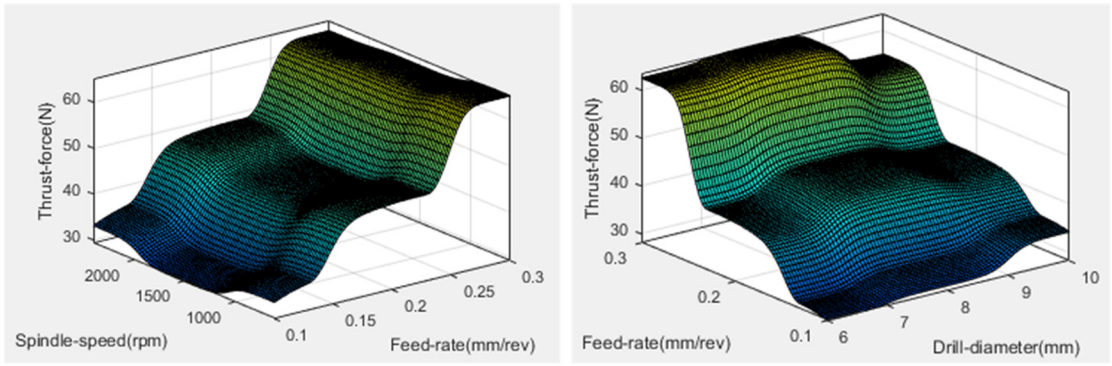

(b) Biocomposite M2 (30wt% miscanthus fiber)

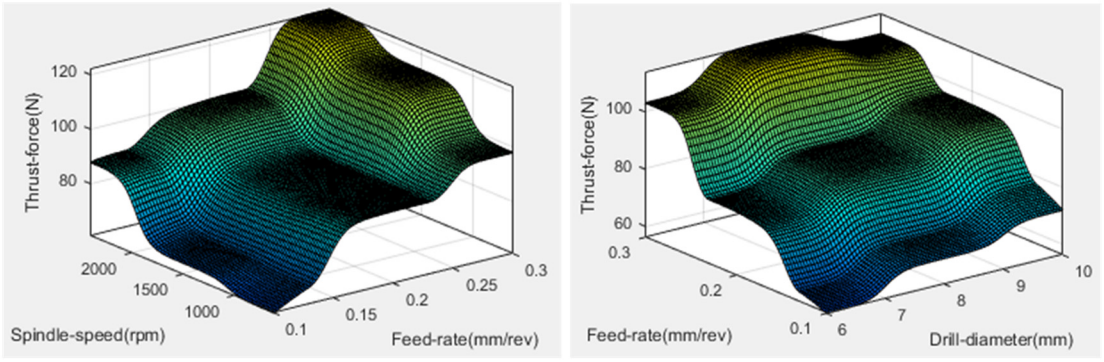

(c) Hybrid biocomposite M3 (15wt% biocarbon + 15wt% miscanthus)

Figure 5.7 ANFIS-based surface plot of thrust force in relation to input parameters

5.4.3 ANFIS based model for surface roughness R_a

Table 5.13 shows values of MAPE, RMSE, and R^2 obtained from the predictive models for surface roughness R_a, and calculated by the equations of (5.5), (5.6), and (5.25), respectively. From Table 5.13, it can be seen that the values of MAPE and RMSE received from the ANFIS model are much smaller than those of the regression model. Conversely, the R^2-value of the ANFIS model is larger than that of the regression model, respectively for each biocomposite. This means that the ANFIS models having better predictive accuracy as compared to regression models.

Figure 5.8 presented the relationship between surface roughness R_a and drilling parameters (d, f, and s) by surface plot of proposed ANFIS model. From Figure 5.8, it can be seen that the spindle speed and drill diameter have a significant influence on the surface roughness. The roughness R_a decreases with the decreased spindle speed and drill diameter for all biocomposites. The effect of feed rate on surface roughness varies with the type of biocomposite. The surface roughness R_a increases with the increased feed rate for biocomposites M2 and M3. However, the feed rate has no significant effect on the surface roughness for biocomposite M1. The surface roughness R_a of biocomposite M1 obtained is smaller than did other two biocomposites (M2 and M3) when drilling with various cutting parameters.

Table 5.12 The RMSE-values of various ANFIS structures for surface roughness R_a

Number of MF for input				**Membership functions**							
x_1	x_2	x_3	x_4	Trimf	Trapmf	gbellmf	gaussmf	gauss2mf	pimf	dsigmf	psigmf
2	2	2	2	0.111	0.111	0.111	0.111	0.111	0.111	0.111	0.111
2	2	2	3	0.099	0.099	0.090	0.099	0.099	0.099	0.094	0.094
2	2	3	2	0.103	0.103	0.103	0.103	0.103	0.103	0.103	0.103
2	2	3	3	0.086	0.086	0.086	0.086	0.086	0.086	0.086	0.086
2	3	2	2	0.092	0.092	0.092	0.092	0.092	0.092	0.092	0.092
2	3	2	3	0.075	0.076	0.075	0.076	0.077	0.075	0.075	0.075
2	3	3	2	0.079	0.079	0.079	0.079	0.079	0.079	0.079	0.079
2	3	3	3	0.053	0.053	0.053	0.053	0.053	0.053	0.053	0.053
3	2	2	2	0.108	0.108	0.108	0.108	0.109	0.108	0.108	0.108
3	2	2	3	0.092	0.092	0.082	0.092	0.092	0.092	0.084	0.084
3	2	3	2	0.099	0.099	0.099	0.099	0.100	0.099	0.099	0.099
3	2	3	3	0.076	0.073	0.063	0.075	0.074	0.074	0.075	0.075
3	3	2	2	0.085	0.085	0.085	0.085	0.086	0.085	0.085	0.085
3	3	2	3	0.061	0.061	0.061	0.061	0.061	0.061	0.061	0.061
3	3	3	2	0.067	0.067	0.067	0.067	0.068	0.067	0.067	0.067
3	3	3	3	9.7×10^{-7}	10×10^{-7}	1×10^{-6}	1×10^{-6}	9.8×10^{-7}	10×10^{-7}	9.6×10^{-7}	9.6×10^{-7}

Table 5.13 The comparison of predictive models for surface roughness R_a

Material	**Regression-based model**			**ANFIS-based model**		
	MAPE (%)	RMSE	R^2	MAPE (%)	RMSE	R^2
M1 (30wt% biocarbon)	7.41	0.08	90.26	0.2603	0.0024	99.99
M2 (30wt% miscanthus)	9.57	0.14	79.25	0.2581	0.0030	99.99
M3 (hybrid)	8.48	0.09	84.82	0.3537	0.0034	99.98

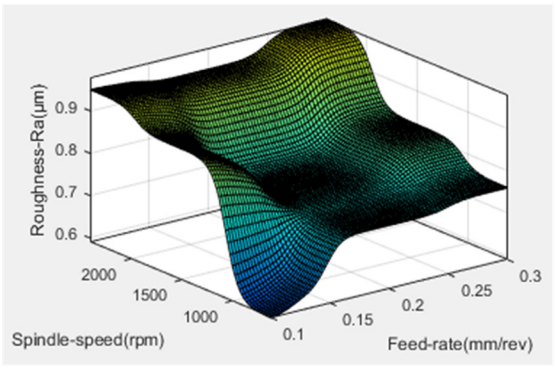

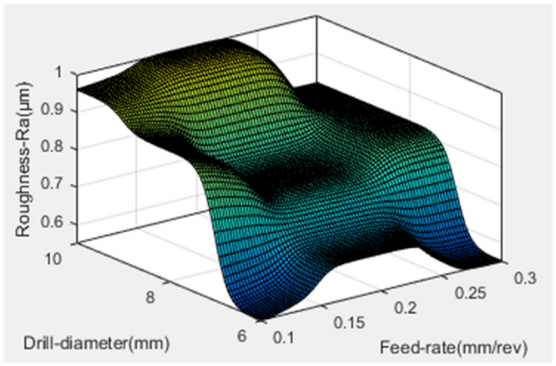

(a) Biocomposite M1 (30wt% biocarbon particles)

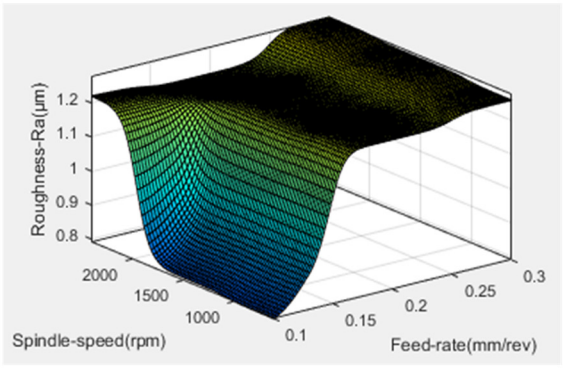

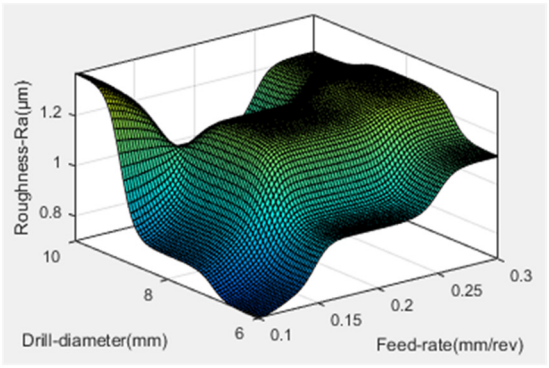

(b) Biocomposite M2 (30wt% miscanthus fibers)

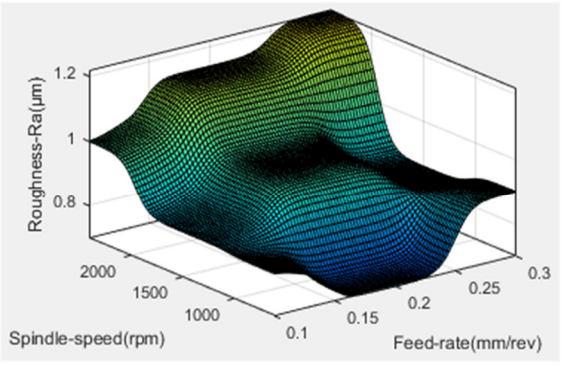

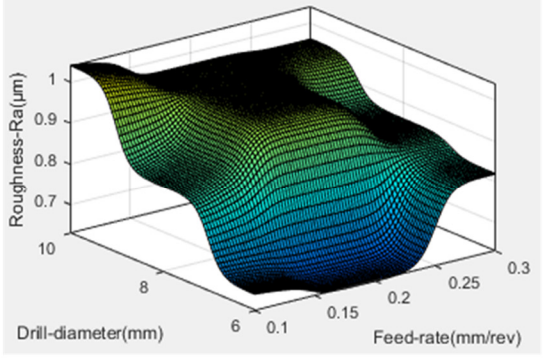

(c) Hybrid biocomposite M3 (15wt% biocarbon + 15wt% miscanthus)

Figure 5.8 ANFIS-based surface plot of surface roughness R_a related to input parameters

5.5 Conclusions

In this study, the predictive models for thrust force and surface roughness were established based on empirical data obtained during dry drilling of biocomposites. Some conclusions are summarized as follows.

Regression models have been established with good predictive accuracy for thrust forces and surface roughness thanks to multiple regression analysis and comparison of MAPE and RMSE to select a better model. The predictive model is used in the objective function to perform optimization using Genetic Algorithm. The optimal drilling parameters are determined to achieve the minimum values of thrust force and surface roughness R_a for the biocomposites tested.

The ANFIS model was built to predict surface roughness R_a and thrust force based on empirical data. The predicted accuracy of ANFIS model depends on the type and number of membership functions used in the ANFIS structure.

By comparing MAPE, RMSE, and R^2-values, it is shown that the proposed ANFIS models have better predictive accuracy than the regression models. The effect of drilling parameters (d, s, and f) to thrust force and surface roughness was investigated by the proposed ANFIS model. Due to the interaction between biocomposites and drilling parameters, the effects of cutting condition on surface roughness and thrust force varies according to each biocomposite. When drilling biocomposites with various cutting parameters, biocomposite M1 (PP/POE/MAPP + 30 wt% biocarbon) was found to have the smallest surface roughness and the highest thrust force compared to other biocomposites (M2-(PP/POE/MAPP + 30 wt% miscanthus) and M3- (PP/POE/MAPP + 15 wt% biocarbon + 15 wt% miscanthus)).

CHAPTER 6

DISCUSSIONS

6.1 Introduction

In this section, the influence of the cutting speed and the material removal rate on the machining process performance indicators (thrust force, specific cutting energy, surface finish, fine particle emission) is discussed in regards to the reinforcements.

6.2 Assumptions and observations on tested biocomposites

Figure 4.1 shows SEM images of biocomposites M1 (30wt% biocarbon) and M2 (30wt% miscanthus). From Figure 4.1, it can be observed that the distribution of biocarbon particles in the matrix is relatively uniform. The matrix-biocarbon debonding was not found in these images (Figure 4.1a). From Figure 4.1 b, it is seen that there is a lack of adhesion between the miscanthus fibers and the matrix. The fiber-matrix debonding phenomenon of biocomposite M2 is observed in SEM images. These observations could be explained as follow:

Biocarbon particles are relatively small in size (less than 0.4 mm) and have good wettability; This facilitates their even distribution and good adhesion with the matrix in the biocomposite. In contrast, the larger size of miscanthus fiber (about 4 mm) and its nature as a natural fiber with various shapes, leading to a lack of adhesion with the matrix in biocomposite.

The difference in nature of the biocarbon particles and the miscanthus fibers (size, nature, shape, etc.) leads to the difference in the mechanical properties of biocomposites as it can be seen in Table 4.2: the impact strength of biocomposite M1(30wt% biocarbon) is twice higher than that of biocomposite M2 (30wt% miscanthus). This fundamental difference between these two materials can explain the difference found in their machinability.

6.3 Effects of cutting speed on the machinability indicators

6.3.1 The effect of cutting speed on thrust forces (F_t)

Figure 6.1 a, c shows that cutting speed significantly affects the thrust force when drilling biocomposites M1 (30wt% biocarbon) and M3 (15wt% biocarbon), respectively. In general, for these two composites, when the cutting speed increased from 11 to 45 m/min, the thrust force fluctuates and increases slightly, then rise sharply up to 75 m/min for both biocomposites M1 and M3. Meanwhile, the influence of cutting speed on thrust force is negligible for biocomposite M2 (30wt% miscanthus). The increase in cutting speed did not result in increased thrust force (Figure 6.1 b). It should also be noted for this biocomposites M2, the thrust force is very small compared to those measured when drilling M1 and M3.

This denotes interactions between cutting speed and various biocomposites. The biocarbon particles used in biocomposites (M1, M3) considerably affect the machining behavior of biocomposites; when the cutting speed is increased, the friction between the tool and the workpiece is increased consequently thus leading to increased cutting force. Meanwhile, because miscanthus is a natural fiber (soft and less abrasive), the increase in cutting speed does not affect the friction at the tool-workpiece interface when the cutting speed is increased. Therefore, the thrust force generated from the drilling of biocomposite M2 (30wt% miscanthus) is not influenced by the cutting speed.

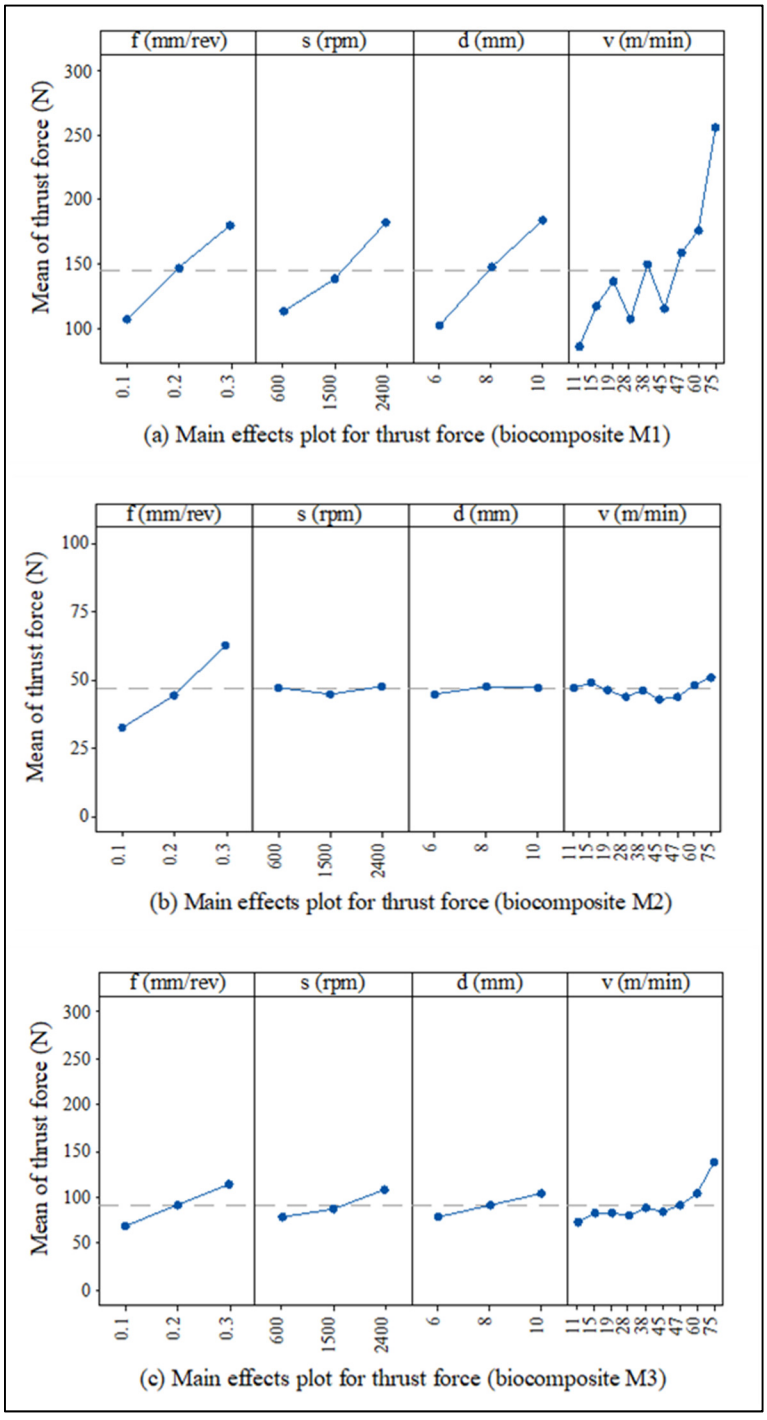

Figure 6.1 Main effects plot for thrust force

6.3.2 The effect of cutting speed on specific cutting energy (K_t)

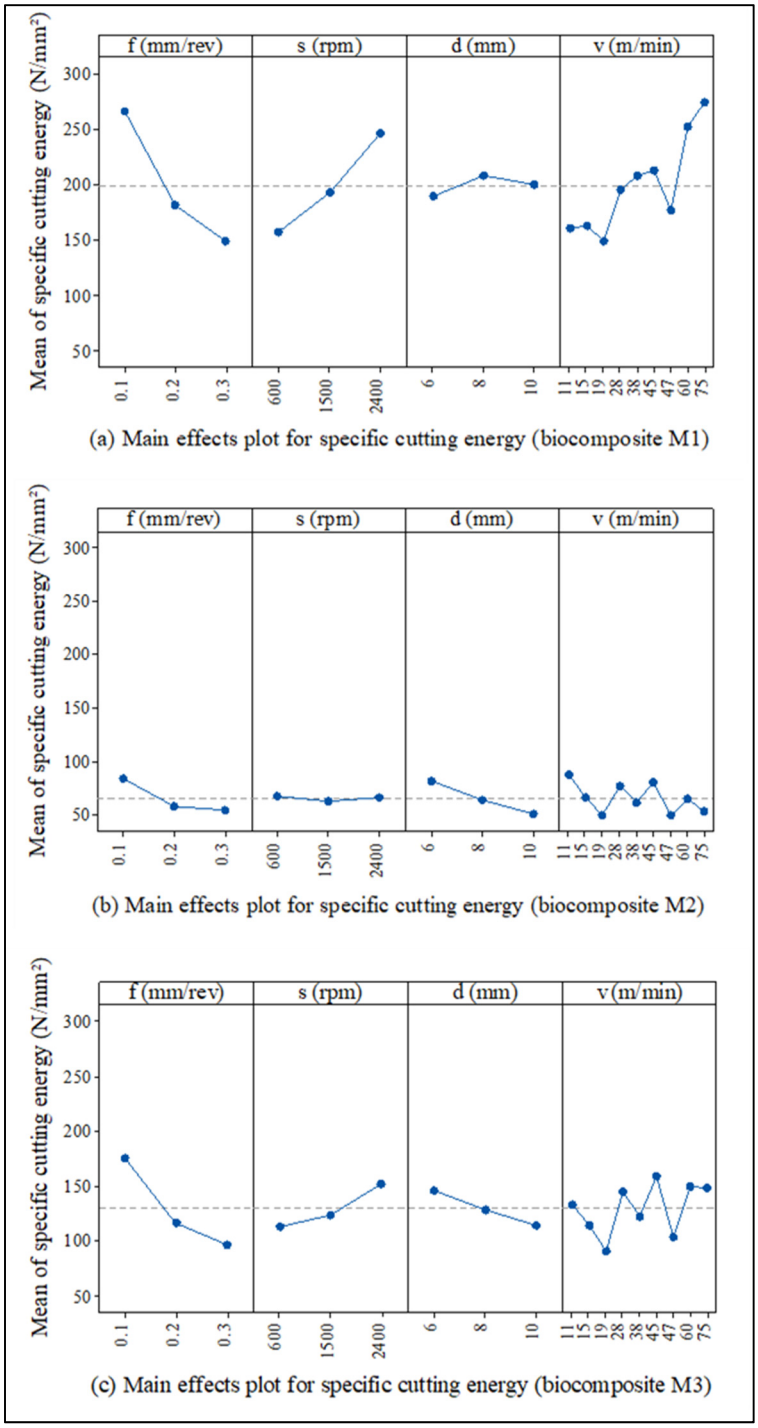

Figure 6.2 Main effects plot for specific cutting energy

Figure 6.2 shows the effect of cutting speed on the specific cutting energy for biocomposites M1, M2, and M3. From Figure 6.2a, it can be seen that in general, for biocomposites M1, the increase in cutting speed results in increased specific force. Meanwhile, the influence of cutting speed on the specific cutting energy of biocomposites M2 and M3 is negligible (Figure 6.2 b, c). It could be explained that the miscanthus fibers used in biocomposite (M2 and M3) reduced the impact strength of biocomposites. Therefore, biocomposites reinforced with miscanthus fibers have good machining behavior in cutting force.

6.3.3 The effect of cutting speed on surface roughness average R_a

Figure 6.3 shows the influential trend of cutting speed on the roughness R_a is similar for all biocomposites. The roughness R_a increases slightly and fluctuates in the range of cutting speed from 11 to 47 (m/min), then it rises sharply in a range of cutting speed between 47 and 75 (m/min) for all biocomposites tested (M1, M2, and M3).

It could be due to the rise of the cutting speed results in increased material removal rate and reduced contacting time between the tool and machined surface, thereby reduced polishing time. Furthermore, an increase in cutting speed will cause an increase in the cutting temperature and then a decrease in matrix-reinforcement bonding. It could cause some damages to the machined surface such as particles and fibers pull-out, melted matrix. It could be seen from Figure 4.17 that the failure of the machined surface occurred with the highest cutting parameters, such as debonding, particles, and fibers pull-out, leading to a rougher of the drilled hole surfaces. Consequently, the surface roughness increased with an increase in cutting speed.

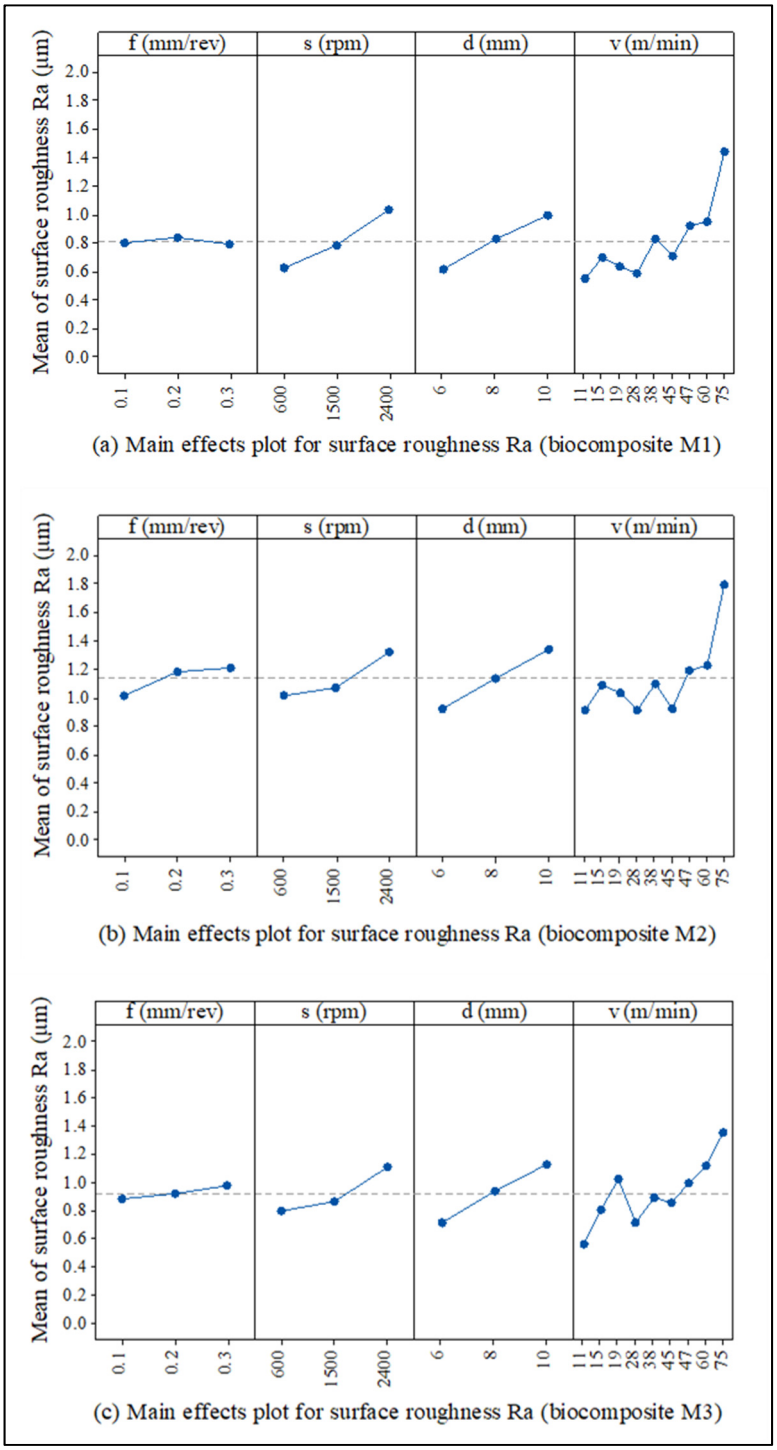

(a) Main effects plot for surface roughness Ra (biocomposite M1)

(b) Main effects plot for surface roughness Ra (biocomposite M2)

(c) Main effects plot for surface roughness Ra (biocomposite M3)

Figure 6.3 Main effects plot for surface roughness R_a

6.3.4 The effect of cutting speed on surface roughness R_t

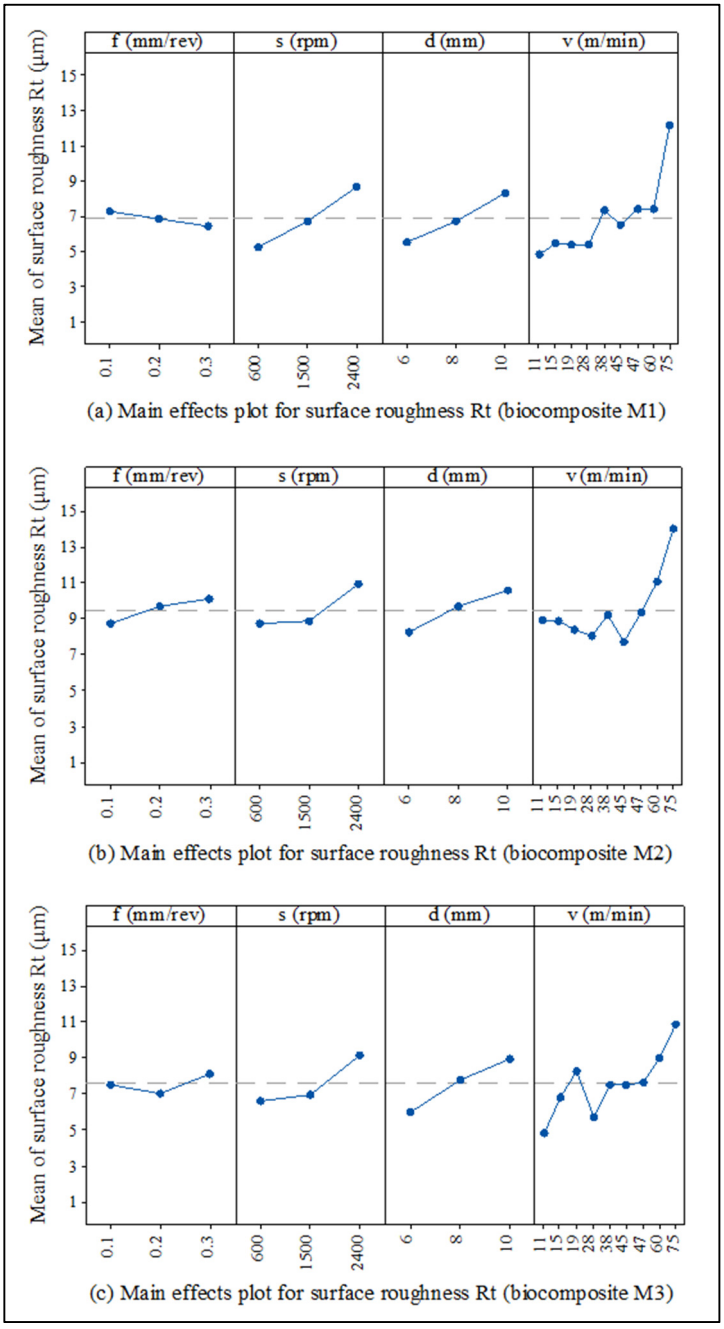

Figure 6.4 Main effects plot for surface roughness R_t

Figure 6.4 has shown that the cutting speed significantly affects the surface roughness R_t for all biocomposites. When the cutting speed increases from 11 to 47 (m/min), the roughness tends to fluctuate and increase slightly. Then, the roughness R_t increases dramatically with cutting speeds between 47 and 75 (m/min). Thus, the influence of the cutting speed on the surface roughness parameters (R_a and R_t) is the same trend for all biocomposites tested (M1, M2, and M3) and can be explained the same way.

6.3.5 The effect of cutting speed on fine particle emission

Figures 6.5 a, b, and c show the influence of cutting speed on fine particle emission during drilling of biocomposites M1, M2, and M3, respectively. From Figure 6.5 a, it can be seen that the cutting speed has almost no effect on fine particle emission for biocomposite M1, the amount of emitted fine dust is very low and almost unchanged. It is probably due to good adhesion between biocarbon and matrix in biocomposite M1 that makes less fine particles generated during drilling.

Figures 6.5 b and c show the effect of cutting speed on fine dust generated from biocomposites M2 and M3 with the same general trend. It could be observed that the number of fine particles emitted continuously fluctuates for both biocomposites M2 and M3. With exception of the lowest cutting speed for biocomposite M3, the fine particle emission fluctuates when the cutting speed was varied. It can be inferred that the amount of fine dust generated depending on the reinforcements in biocomposites (more discussion will be presented in subsection 6.4.3).

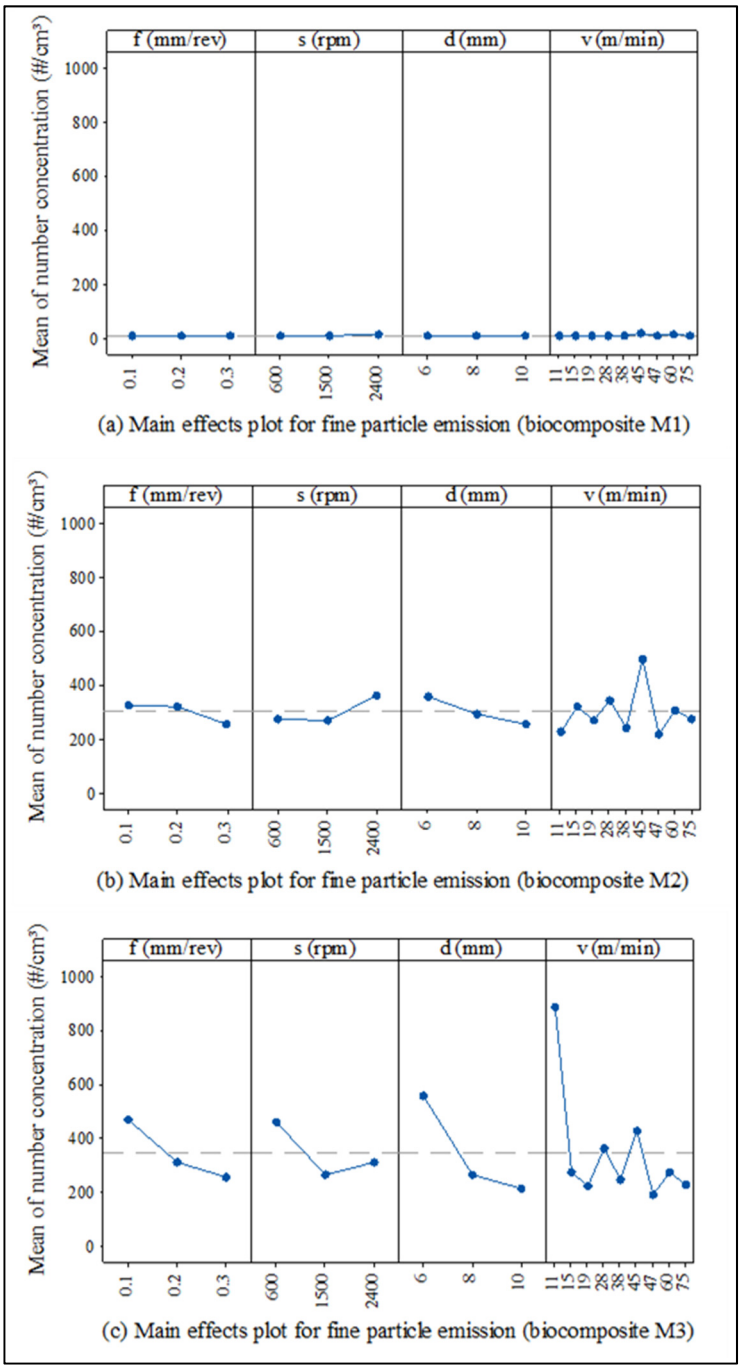

Figure 6.5 Main effects plot for fine particle emission (PM10)

6.4 Effect of reinforcements on the machinability indicators

6.4.1 The effect of reinforcements on thrust force

Figure 4.8 has shown that the highest thrust force created by biocomposite M1 (30wt% biocarbon), followed by biocomposites M3 (15wt% biocarbon, 15wt% miscanthus) and M2 (30wt% miscanthus) under the same drilling conditions. It is seen that biocomposites reinforced with miscanthus fibers have better machining behavior in terms of cutting force than biocomposites reinforced with biocarbon particles.

It could be explained by the fact that the impact strength of biocomposite M1 is twice higher than that of biocomposite M2 (Table 4.2). Moreover, as mentioned above, the bonding strength of matrix-biocarbon particles is better than the adhesion of matrix-miscanthus fibers. These last are soft and less abrasive in nature, thus are less demanding during machining. Therefore, the thrust force generated during the drilling of biocomposites reinforced with miscanthus fibers is smaller than that recorded on biocarbon particles reinforced biocomposites (M1).

6.4.2 The effect of reinforcements on surface roughness

Figure 4.15 has shown that the highest roughness is generated from the drilling of biocomposite M2, followed by biocomposite M3 and biocomposite M1 under the same cutting conditions. It could be recognized that the miscanthus fibers significantly affects the roughness of the drilled surface.

Miscanthus fibers have an irregular shape and a fibrous bundle structure. This short fiber geometry could lead to the fiber's cut resulting in a rougher surface as compared to the particle's cut surface after machining. Furthermore, a lack of adhesion of matrix-fibers results in more damages to the drilled surface, such as matrix-fibers debonding, fibers pull out (as mentioned in Figure 4.17). Therefore, the surface roughness of miscanthus fiber-reinforced biocomposite is higher than that of biocomposite reinforced with biocarbon particles under the same cutting conditions.

6.4.3 The effect of reinforcements on fine particle emission

Figures 4.25 and 4.26 have shown that the total number of fine particles generated from biocomposite M2 is much larger (about 20 times) than that from biocomposite M1 under the same cutting conditions. From Figure 4.26, it is also seen that the total number of fine particles emitted by biocomposite M3 is in the intermediate interval from that of biocomposite M1 (lower level) to that of biocomposite M2 (upper level) under the same drilling conditions. It could be observed that miscanthus fibers have a significant effect on the total number of fine particles generated when machining. The amount of fine particles emitted is proportional to the miscanthus fiber content used in biocomposite.

It could be because a lack of matrix-fiber bonding is the main factor affecting the fine particle emission when machining. Figure 4.17b has shown that the miscanthus fibers are separated from the biocomposite (fibers pull-out), leaving pores on the machined surface. It could cause an increase in the number of fine particles emitted when drilling of miscanthus fiber-reinforced biocomposites (M2). Another possible cause is the nature of miscanthus fibers, which could produce a lot of fine dust when being cut (due to the fibrous bundle structure of miscanthus).

In contrast, due to good adhesion between biocarbon and matrix, little biocarbon particles were separated from biocomposite (particles pull-out) were observed (Figure 4.17a). Therefore, the number of fine particles emitted from biocomposites reinforced with biocarbon particles (M1) is smaller.

6.5 Effects of material removal rate on the machinability indicators

6.5.1 The effect of material removal rate (MRR) on thrust force

Figure 6.6 shows the influence of the material removal rate on thrust force during the drilling of biocomposites. From Figure 6.6 it can be seen that thrust force increases with an increase in material removal rate (MRR) for biocomposites tested. In fact, when the material removal

rate increases, the energy required for material separation increase too, so the thrust force is increased.

From Figure 6.6, it is seen that the highest thrust force is generated from the drilling of biocomposite M1 (30wt% biocarbon), followed by M3 and M2 in the same material removal rate. The lowest thrust force is generated from the drilling of biocomposites M2 (30wt% miscanthus). It is also indicated that the miscanthus-reinforced biocomposite has good machining behavior in terms of cutting force.

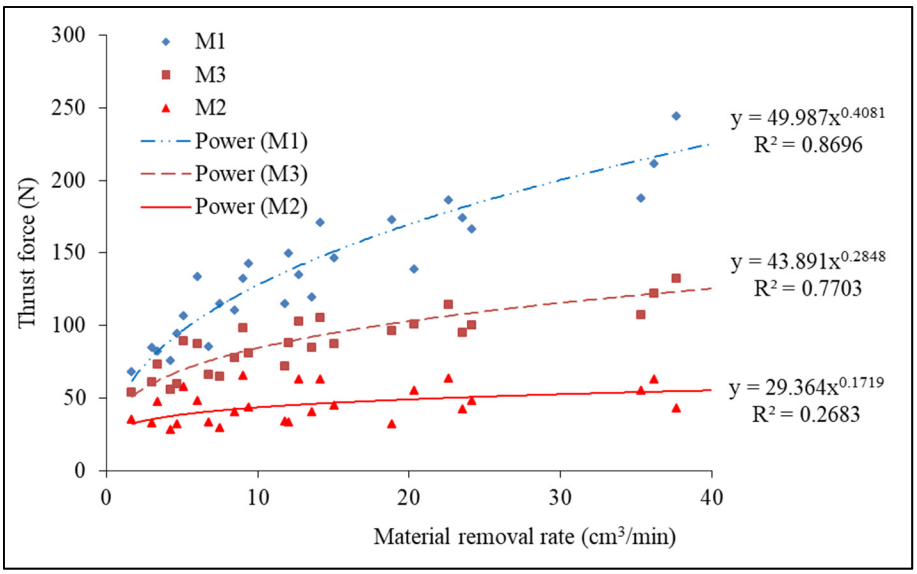

Figure 6.6 Thrust force as a function of material removal rate for all biocomposites (M1, M2 and M3)

6.5.2 The effect of material removal rate on surface roughness R_a

Figure 6.7 shows the relationship between roughness R_a and material removal rate when drilling biocomposites. It is observed that roughness increased with an increase in material removal rate for all biocomposites tested. It could be due to an increase in material removal rate leads to an increase in cutting force and temperature, and increases machined surface damages. At the same time, when the material removal rate increases, the friction between the machined surface and chips increases. Hence, surface quality decreases with increasing material removal rate.

Figure 6.7 has also shown that at the same material removal rate, biocomposite M2 presented the highest roughness, followed by M3 and M1. It is deduced that biocomposite M1 has the best machining behavior in terms of surface roughness as compared to the other two biocomposites.

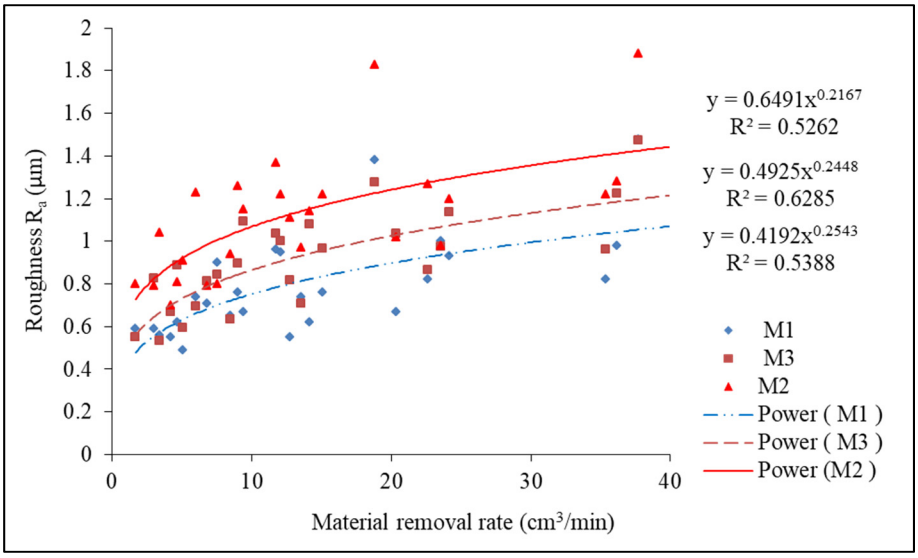

Figure 6.7 The roughness R_a as a function of material removal rate for biocomposites tested

6.6 The cutting force signals during drilling biocomposites

Figure 6.8 presents the relationship between the cutting force signals and the drilling time: F_t (M1- green line), F_t (M2- red line), and F_t (M3- blue line) are the thrust force signals when drilling biocomposite M1, M2, and M3, respectively.

From Figure 6.8, it can be seen that the thrust force signals fluctuate continuously during drilling. It is most likely due to the heterogeneous properties of biocomposite materials. The cutting forces will be changed continuously at distinct contact positions between the tool-cutting edges and the workpiece material, resulting in small vibrations during drilling.

Figure 6.8 has also shown that the cutting force signals changes drastically during the drilling of biocomposite M2 as compared to two other biocomposites (M3 and M1) in the same cutting conditions. It may be due to a higher heterogeneity of mechanical properties of biocomposites is reinforced with chopped miscanthus fibers (M2). From Figure 6.8, it is also noticed that under the same cutting conditions, biocomposite M1 has the highest thrust force, followed by biocomposite M3 and M2.

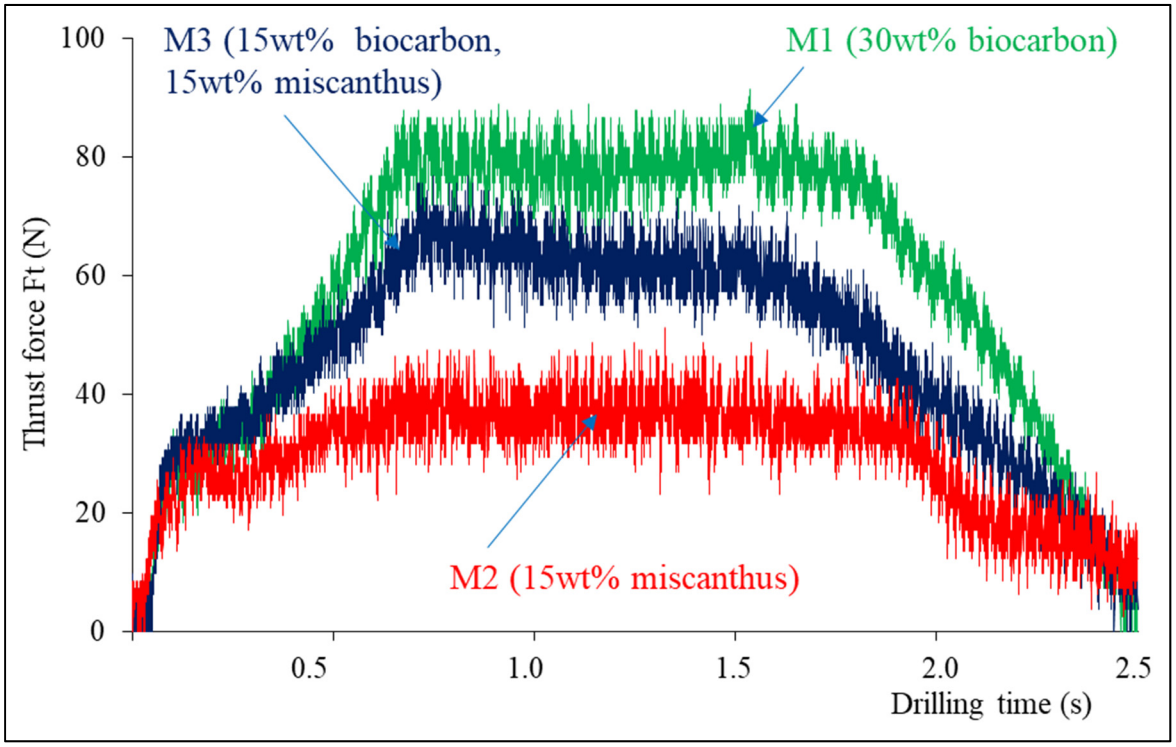

Figure 6.8 Thrust force as a function of drilling time during drilling biocomposites: (d = 6 mm, f = 0.1 mm/rev, s = 1500 rpm)

CONCLUSION

This research was thoroughly conducted to understand the machining behaviors of the three new biocomposites. The input factors to be investigated include the feed rate, the spindle speed, the drill diameter, and biocomposites. The machining process performance indicators studied during drilling biocomposites are thrust force, specific cutting energy for thrust force, surface roughness (R_a, R_t), and fine dust emissions. A full factorial design is used for the experimental design to perform the dry drilling of biocomposites. Furthermore, the predictive models are established based on the multiple regression analysis and ANFIS to predict the thrust force and the surface roughness R_a. Besides, the GA approach is applied to find the optimal drilling parameters for thrust force and surface roughness R_a during the drilling of biocomposites. From the results achieved, the main conclusions are drawn as follows.

The feed rate is recognized to be the most significant effect on the thrust force, and the specific cutting energy for thrust force during the drilling of all biocomposites (M1, M2, and M3). The increased feed rate contributes to thrust force increases, and the specific cutting energy for thrust force decreases. In addition, the feed rate is also statistically significant for fine particle emission and surface roughness R_a for biocomposite M2 (30wt% miscanthus) and hybrid biocomposite M3 (15wt% miscanthus, 15wt% biocarbon) at the 95% confidence interval. An increase in feed rate leads to a reduction in the total number of fine particles emitted (PM10), and a slight increase in surface roughness R_a for biocomposites M2 and M3.

The spindle speed and drill diameter are statistically significant for the surface roughness (R_a, R_t) for all biocomposites at the 95% confidence level. The drill diameter is the highest effect on the surface roughness, followed by the spindle speed. The increased surface roughness results from an increase in spindle speed and drill diameter for all biocomposites. Moreover, the spindle speed and drill diameter have statistical significance for thrust force for both biocomposite M1 (30wt% biocarbon) and hybrid biocomposite M3. The rise of spindle speed and drill diameter results in the increase of thrust force for both biocomposites M1 and M3. However, the spindle speed and drill diameter are not statistically significant for biocomposite M2 at the 95% confidence interval.

The influence of the spindle speed and drill diameter on the specific cutting energy for thrust force depends mainly on a particular biocomposite during the drilling process. The result has shown that the drill diameter has statistical significance on the specific cutting energy for biocomposites M2 and M3. An increase in drill diameter contributes to decreased specific cutting energy for both biocomposites M2 and M3. Meanwhile, the spindle speed is statistically significant on the specific cutting energy, and the spindle speed increased leads to the increased specific cutting energy for both biocomposites M1 and M3.

The type and the weight ratio of reinforcements used in biocomposites significantly affect the machining process performance indicators during the drilling of biocomposites. An increase in the weight ratio of miscanthus fibers used in biocomposites leads to decreased thrust force and specific cutting energy and results in increased surface roughness (R_a, R_t) and fine particle generation (PM10). In contrast, an increase in the weight ratio of the biocarbon used in biocomposites leads to an increase in thrust force and specific cutting energy and results in a decrease in surface roughness (R_a, R_t) and fine particle emission (PM10).

The material removal rate has a significant effect on thrust force and surface roughness. An increase in material removal rate leads to an increase in thrust force and surface roughness for biocomposites tested.

The surface roughness (R_a, R_t) is considerably affected by the cutting speed. The roughness increased with an increase in cutting speed for all biocomposites (M1, M2, and M3). Moreover, the cutting speed has a significant effect on thrust force and specific cutting energy for biocomposite M1.

The result has shown that the drilling parameters' effect on the fine particle emission is different for each biocomposite. The drill diameter has the most significant effect on the fine particle generation. The larger the drill diameter, the lower the number of fine particles generated for all biocomposites. Furthermore, a general trend has observed that the fine particles generated increased with increasing spindle speed and decreased with increasing feed rate. More fine particles emitted with the size are smaller than 2.5 microns.

The majority of the ultrafine particles emitted are of a size ranging from 30 nm to 100 nm, and peaks occurring at around 50 nm. It has also shown that the drilling parameters have not statistical significance for the ultrafine particle emission at the 95% confidence interval for all biocomposites. Therefore, the ultrafine particle emission is unpredictable.

The predictive models for thrust force and surface roughness R_a is established based on the regression analysis and ANFIS approach. It is shown that the predictive models have high predictive accuracy, and the ANFIS-based models have better predictive accuracy than that of the regression-based models. The optimal drilling parameters for thrust force and surface roughness R_a, for all biocomposites, were identified by the GA approach.

MAIN CONTRIBUTIONS

This study contributes to understanding the influence of the drilling parameters on the machining process performance indicators of new biocomposites. The thrust force and surface roughness R_a were predicted by the regression-based models and the proposed ANFIS models. The GA approach is applied to find the optimal drilling parameters for thrust force and surface roughness. The specific contributions of this study are summarized as follows.

- The influence of drilling parameters on the machining process performance indicators was studied, thereby helping manufacturers choose the appropriate cutting parameters to achieve the desired quality during the drilling of new biocomposites.
- The optimal drilling parameters for thrust force and surface roughness R_a were determined by the GA approach during the drilling of biocomposites.
- The regression and ANFIS-based models have been developed, which can help predict the surface roughness (R_a) and the thrust force during drilling biocomposites.
- The amount of fine dust generated could be reduced by choosing the suitable cutting parameters during the drilling of biocomposites according to data, models, and machining strategies established in this research work.

RECOMMENDATIONS

The future work related to this study will focus on the following aspects.

- Studying the effects of cutting parameters, tool geometry, and material on the machining process performance indicators during the milling (slot milling, edge trimming) of biocomposites as these are some other operations usually carried on these composites in industry.
- Studying the influence of the cutting temperature on the machining-induced damages during machining biocomposites (drilling, and milling).
- In this research work, the delamination-caused damage is not clearly recognized. It could be due to the polypropylene-based biocomposites are reinforced with short fibers and biocarbon particles and because of only a single layer (5 mm thickness) is produced by the heated press molding process. The drilling-induced failures observed in this study were matrix-reinforcement debonding, particles and fibers pull-out. Therefore, it should be taken into consideration to investigate the factors affecting these damages as well as the delamination phenomenon under specific cutting conditions (the machining process, workpiece material, cutting parameters, tools, etc.).
- More fine particles emitted during drilling biocomposites with a size smaller than 2.5 microns, which are easily inhaled into the deepest part of the lung. Therefore, it is necessary to study the harmful reinforcements used in biocomposites.

LIST OF BIBLIOGRAPHICAL REFERENCES

Abbas, A. T., Alata, M., Ragab, A. E., El Rayes, M. M., & El Danaf, E. A. (2017). Prediction Model of Cutting Parameters for Turning High Strength Steel Grade-H: Comparative Study of Regression Model versus ANFIS. *Advances in Materials Science and Engineering*, *2017*. https://doi.org/10.1155/2017/2759020

Abdelwahab, M. A., Rodriguez-Uribe, A., Misra, M., & K. Mohanty, A. (2019). Injection Molded Novel Biocomposites from Polypropylene and Sustainable Biocarbon. *Molecules*, *24*(22), 4026. https://doi.org/10.3390/molecules24224026

Abilash, N., & Sivapragash, M. (2016). Optimizing the delamination failure in bamboo fiber reinforced polyester composite. *Journal of King Saud University - Engineering Sciences*, *28*(1), 92–102. https://doi.org/10.1016/j.jksues.2013.09.004

Akampumuza, O., Wambua, P. M., Ahmed, A., Li, W., & Qin, X.-H. (2017). Review of the applications of biocomposites in the automotive industry. *Polymer Composites*, *38*(11), 2553–2569. https://doi.org/10.1002/pc.23847

Anstey, A., Vivekanandhan, S., Rodriguez-Uribe, A., Misra, M., & Mohanty, A. K. (2016). Oxidative acid treatment and characterization of new biocarbon from sustainable Miscanthus biomass. *Science of the Total Environment*, *550*, 241–247. https://doi.org/10.1016/j.scitotenv.2016.01.015

Azmi, H., Haron, C. H. C., Ghani, J. A., Suhaily, M., & Yuzairi, A. R. (2018). Machinability Study on Milling Kenaf Fiber Reinforced Plastic Composite Materials using Design of Experiments. *IOP Conference Series: Materials Science and Engineering*, *344*(1). https://doi.org/10.1088/1757-899X/344/1/012027

Babu, G. D., Babu, K. S., & Gowd, B. U. M. (2013). Effect of Machining Parameters on Milled Natural Fiber-Reinforced Plastic Composites. *Journal of Advanced Mechanical Engineering*, 1–12. https://doi.org/10.7726/jame.2013.1001

Bajpai, P. K., Debnath, K., & Singh, I. (2017). Hole making in natural fiber-reinforced polylactic acid laminates: An experimental investigation. *Journal of Thermoplastic Composite Materials*, *30*(1), 30–46. https://doi.org/10.1177/0892705715575094

Bajpai, P. K., & Singh, I. (2013). Drilling behavior of sisal fiber-reinforced polypropylene composite laminates. *Journal of Reinforced Plastics and Composites*, *32*(20), 1569–1576. https://doi.org/10.1177/0731684413492866

Balasubramanian, K., Sultan, M. T. H., Cardona, F., & Rajeswari, N. (2016). Machining analysis of natural fibre reinforced composites using fuzzy logic. *IOP Conference Series: Materials Science and Engineering*, *152*(1). https://doi.org/10.1088/1757-899X/152/1/012051

Balout, B., Songmene, V., & Masounave, J. (2007). An experimental study of dust generation during dry drilling of pre-cooled and pre-heated workpiece materials. *Journal of Manufacturing Processes*, *9*(1), 23–34. https://doi.org/10.1016/S1526-6125(07)70105-6

Basavarajappa, S., Venkatesh, A., Gaitonde, V. N., & Karnik, S. R. (2012). Experimental investigations on some aspects of machinability in drilling of glass epoxy polymer composites. *Journal of Thermoplastic Composite Materials*, *25*(3), 363–387. https://doi.org/10.1177/0892705711408166

Behazin, E., Misra, M., & Mohanty, A. K. (2017a). Sustainable biocarbon from pyrolyzed perennial grasses and their effects on impact modified polypropylene biocomposites. *Composites Part B: Engineering*, *118*, 116–124. https://doi.org/10.1016/j.compositesb.2017.03.003

Behazin, E., Misra, M., & Mohanty, A. K. (2017b). Sustainable Biocomposites from Pyrolyzed Grass and Toughened Polypropylene: Structure-Property Relationships. *ACS Omega*, *2*(5), 2191–2199. https://doi.org/10.1021/acsomega.7b00122

Bourmaud, A., & Pimbert, S. (2008). Investigations on mechanical properties of poly(propylene) and poly(lactic acid) reinforced by miscanthus fibers. *Composites Part A: Applied Science and Manufacturing*, *39*(9), 1444–1454. https://doi.org/10.1016/j.compositesa.2008.05.023

Çelik, Yahya H., Kilickap, E., & Kilickap, A. İ. (2019). An experimental study on milling of natural fiber (jute)- reinforced polymer composites. *Journal of Composite Materials*, *53*(22), 3127–3137. https://doi.org/10.1177/0021998319826373

Çelik, Yahya Hışman, & Alp, M. S. (2020). Determination of Milling Performance of Jute and Flax Fiber Reinforced Composites. *Journal of Natural Fibers*, *0478*(May). https://doi.org/10.1080/15440478.2020.1764435

Chaudhary, V., & Gohil, P. P. (2016). Investigations on Drilling of Bidirectional Cotton Polyester Composite. *Materials and Manufacturing Processes*, *31*(7), 960–968. https://doi.org/10.1080/10426914.2015.1059444

Chauhan, V., Kärki, T., & Varis, J. (2019). Review of natural fiber-reinforced engineering plastic composites, their applications in the transportation sector and processing techniques. *Journal of Thermoplastic Composite Materials*. https://doi.org/10.1177/0892705719889095

Chegdani, F., Mezghani, S., El Mansori, M., & Mkaddem, A. (2015). Fiber type effect on tribological behavior when cutting natural fiber reinforced plastics. *Wear*, *332–333*, 772–779. https://doi.org/10.1016/j.wear.2014.12.039

Chegdani, Faissal, & El Mansori, M. (2018). Friction scale effect in drilling natural fiber

composites. *Tribology International*, *119*(October 2017), 622–630. https://doi.org/10.1016/j.triboint.2017.12.006

Chegdani, Faissal, & El Mansori, M. (2019). New Multiscale Approach for Machining Analysis of Natural Fiber ReinforcedBio-Composites. *Journal of Manufacturing Science and Engineering*, *141*(1). https://doi.org/10.1115/1.4041326

Chegdani, Faissal, Mezghani, S., & El Mansori, M. (2016). On the multiscale tribological signatures of the tool helix angle in profile milling of woven flax fiber composites. *Tribology International*, *100*, 132–140. https://doi.org/10.1016/j.triboint.2015.12.014

Chegdani, Faissal, Takabi, B., El Mansori, M., Tai, B. L., & Bukkapatnam, S. T. S. (2020). Effect of flax fiber orientation on machining behavior and surface finish of natural fiber reinforced polymer composites. *Journal of Manufacturing Processes*, *54*(March), 337–346. https://doi.org/10.1016/j.jmapro.2020.03.025

Chen, Y., Yu, Q. L., & Brouwers, H. J. H. (2017). Acoustic performance and microstructural analysis of bio-based lightweight concrete containing miscanthus. *Construction and Building Materials*, *157*, 839–851. https://doi.org/10.1016/j.conbuildmat.2017.09.161

Cococcetta, N. M., Pearl, D., Jahan, M. P., & Ma, J. (2020). Investigating surface finish, burr formation, and tool wear during machining of 3D printed carbon fiber reinforced polymer composite. *Journal of Manufacturing Processes*, *March*. https://doi.org/10.1016/j.jmapro.2020.04.025

Codou, A., Misra, M., & Mohanty, A. K. (2018). Sustainable biocarbon reinforced nylon 6/polypropylene compatibilized blends: Effect of particle size and morphology on performance of the biocomposites. *Composites Part A: Applied Science and Manufacturing*, *112*(January), 1–10. https://doi.org/10.1016/j.compositesa.2018.05.018

Debnath, K., Singh, I., & Dvivedi, A. (2014). Drilling characteristics of sisal fiber-reinforced epoxy and polypropylene composites. *Materials and Manufacturing Processes*, *29*(11–12), 1401–1409. https://doi.org/10.1080/10426914.2014.941870

Debnath, K., Singh, I., & Dvivedi, A. (2017). On the analysis of force during secondary processing of natural fiber-reinforced composite laminates. *Polymer Composites*, *38*(1), 164–174. https://doi.org/10.1002/pc.23572

Dhaouadi, T. (2018). *Caractérisation et modélisation des propriétés mécaniques des biocomposites à fibres courtes aléatoires*. http://espace.etsmtl.ca/id/eprint/2187

Djebara, A., Songmene, V., & Bahloul, A. (2013). Effects of machining conditions on specific surface of PM2.5 emitted during metal cutting. *Health*, *05*(10), 36–43. https://doi.org/10.4236/health.2013.510a2005

Faruk, O., Bledzki, A. K., Fink, H. P., & Sain, M. (2014). Progress report on natural fiber reinforced composites. *Macromolecular Materials and Engineering*, *299*(1), 9–26.

https://doi.org/10.1002/mame.201300008

Fu, S. Y., Xu, G., & Mai, Y. W. (2002). On the elastic modulus of hybrid particle/short-fiber/polymer composites. *Composites Part B:Engineering*, *33*(4), 291–299. https://doi.org/10.1016/S1359-8368(02)00013-6

Girones, J., Vo, L., Arnoult, S., Brancourt-Hulmel, M., & Navard, P. (2016). Miscanthus stem fragment – Reinforced polypropylene composites: Development of an optimized preparation procedure at small scale and its validation for differentiating genotypes. *Polymer Testing*, *55*, 166–172. https://doi.org/10.1016/j.polymertesting.2016.08.023

Haddad, M., Zitoune, R., Eyma, F., & Castanie, B. (2014). Study of the surface defects and dust generated during trimming of CFRP: Influence of tool geometry, machining parameters and cutting speed range. *Composites Part A: Applied Science and Manufacturing*, *66*, 142–154. https://doi.org/10.1016/j.compositesa.2014.07.005

Ho, M. P., Wang, H., Lee, J. H., Ho, C. K., Lau, K. T., Leng, J., & Hui, D. (2012). Critical factors on manufacturing processes of natural fibre composites. In *Composites Part B: Engineering* (Vol. 43, Issue 8, pp. 3549–3562). https://doi.org/10.1016/j.compositesb.2011.10.001

Imani, L., Rahmani Henzaki, A., Hamzeloo, R., & Davoodi, B. (2020). Modeling and optimizing of cutting force and surface roughness in milling process of Inconel 738 using hybrid ANN and GA. *Proceedings of the Institution of Mechanical Engineers, Part B: Journal of Engineering Manufacture*, *234*(5), 920–932. https://doi.org/10.1177/0954405419889204

Ismail, S. O., Dhakal, H. N., Dimla, E., Beaugrand, J., & Popov, I. (2016). Effects of drilling parameters and aspect ratios on delamination and surface roughness of lignocellulosic HFRP composite laminates. *Journal of Applied Polymer Science*, *133*(7), 1–8. https://doi.org/10.1002/app.42879

Ismail, S. O., Dhakal, H. N., Popov, I., & Beaugrand, J. (2016). Comprehensive study on machinability of sustainable and conventional fibre reinforced polymer composites. *Engineering Science and Technology, an International Journal*, *19*(4), 2043–2052. https://doi.org/10.1016/j.jestch.2016.07.010

Jayabal, S., Natarajan, U., & Sekar, U. (2011). Regression modeling and optimization of machinability behavior of glass-coir-polyester hybrid composite using factorial design methodology. *International Journal of Advanced Manufacturing Technology*, *55*(1–4), 263–273. https://doi.org/10.1007/s00170-010-3030-7

Kamguem, R., Djebara, A., & Songmene, V. (2013). Investigation on surface finish and metallic particle emission during machining of aluminum alloys using response surface methodology and desirability functions. *International Journal of Advanced Manufacturing Technology*, *69*(5–8), 1283–1298. https://doi.org/10.1007/s00170-013-

5105-8

Kar, S., Das, S., & Ghosh, P. K. (2014). Applications of neuro fuzzy systems: A brief review and future outline. *Applied Soft Computing Journal*, *15*, 243–259. https://doi.org/10.1016/j.asoc.2013.10.014

Karaboga, D., & Kaya, E. (2019). Adaptive network based fuzzy inference system (ANFIS) training approaches: a comprehensive survey. *Artificial Intelligence Review*, *52*(4), 2263–2293. https://doi.org/10.1007/s10462-017-9610-2

Khettabi, R., Songmene, V., & Masounave, J. (2007). Effect of tool lead angle and chip formation mode on dust emission in dry cutting. *Journal of Materials Processing Technology*, *194*(1–3), 100–109. https://doi.org/10.1016/j.jmatprotec.2007.04.005

Khettabi, Riad, Songmene, V., & Masounave, J. (2010). Effects of speeds, materials, and tool rake angles on metallic particle emission during orthogonal cutting. *Journal of Materials Engineering and Performance*, *19*(6), 767–775. https://doi.org/10.1007/s11665-009-9551-2

Khettabi, Riad, Songmene, V., Zaghbani, I., & Masounave, J. (2010). Modeling of particle emission during dry orthogonal cutting. *Journal of Materials Engineering and Performance*, *19*(6), 776–789. https://doi.org/10.1007/s11665-009-9538-z

Kirwan, K., Johnson, R. M., Jacobs, D. K., Smith, G. F., Shepherd, L., & Tucker, N. (2007). Enhancing properties of dissolution compounded Miscanthus giganteus reinforced polymer composite systems. Part 1. Improving flexural rigidity. *Industrial Crops and Products*, *26*(1), 14–27. https://doi.org/10.1016/j.indcrop.2006.12.013

Koronis, G., Silva, A., & Fontul, M. (2013). Green composites: A review of adequate materials for automotive applications. *Composites Part B: Engineering*, *44*(1), 120–127. https://doi.org/10.1016/j.compositesb.2012.07.004

Kouam, J., Songmene, V., Djebara, A., & Khettabi, R. (2012). Effect of friction testing of metals on particle emission. *Journal of Materials Engineering and Performance*, *21*(6), 965–972. https://doi.org/10.1007/s11665-011-9972-6

Kouam, Jules, Songmene, V., Balazinski, M., & Hendrick, P. (2015). Effects of minimum quantity lubricating (MQL) conditions on machining of 7075-T6 aluminum alloy. *International Journal of Advanced Manufacturing Technology*, *79*(5–8), 1325–1334. https://doi.org/10.1007/s00170-015-6940-6

Kremer, A., & El Mansori, M. (2009). Influence of nanostructured CVD diamond coatings on dust emission and machinability of SiC particle-reinforced metal matrix composite. *Surface and Coatings Technology*, *204*(6–7), 1051–1055. https://doi.org/10.1016/j.surfcoat.2009.06.012

Kremer, A., & El Mansori, M. (2011). Tool wear as-modified by particle generation in dry

machining. *Wear*, *271*(9–10), 2448–2453. https://doi.org/10.1016/j.wear.2010.12.030

Krishnaraj, V., Prabukarthi, A., Ramanathan, A., Elanghovan, N., Kumar, M. S., Zitoune, R., & Davim, J. P. (2012). Optimization of machining parameters at high speed drilling of carbon fiber reinforced plastic (CFRP) laminates. *Composites Part B: Engineering*, *43*(4), 1791–1799. https://doi.org/10.1016/j.compositesb.2012.01.007

Kumar, R., & Hynes, N. R. J. (2019). Prediction and optimization of surface roughness in thermal drilling using integrated ANFIS and GA approach. *Engineering Science and Technology, an International Journal*, *23*, 30–41. https://doi.org/10.1016/j.jestch.2019.04.011

Latha, B., Senthilkumar, V. S., & Palanikumar, K. (2011). Influence of drill geometry on thrust force in drilling GFRP composites. *Journal of Reinforced Plastics and Composites*, *30*(6), 463–472. https://doi.org/10.1177/0731684410397681

Li, Z., Reimer, C., Wang, T., Mohanty, A. K., & Misra, M. (2020). Thermal and mechanical properties of the biocomposites of Miscanthus biocarbon and poly(3-hydroxybutyrate-co-3-hydroxyvalerate) (PHBV). *Polymers*, *12*(6). https://doi.org/10.3390/polym12061300

Lotfi, A., Li, H., Dao, D. V., & Prusty, G. (2019). Natural fiber–reinforced composites: A review on material, manufacturing, and machinability. *Journal of Thermoplastic Composite Materials*. https://doi.org/10.1177/0892705719844546

Manickam, R., & Gopinath, A. (2017). Measurement and analysis of thrust force in drilling sisal-glass fiber reinforced polymer composites. *IOP Conference Series: Materials Science and Engineering*, *197*(1). https://doi.org/10.1088/1757-899X/197/1/012056

Marani, M., Songmene, V., Kouam, J., & Zedan, Y. (2018). Experimental investigation on microstructure, mechanical properties and dust emission when milling Al-20Mg 2 Si-2Cu metal matrix composite with modifier elements. *International Journal of Advanced Manufacturing Technology*, *99*(1–4), 789–802. https://doi.org/10.1007/s00170-018-2491-y

Marani, M., Songmene, V., Zeinali, M., Kouam, J., & Zedan, Y. (2019). Neuro-fuzzy predictive model for surface roughness and cutting force of machined Al–20 Mg2Si–2Cu metal matrix composite using additives. *Neural Computing and Applications*, *6*. https://doi.org/10.1007/s00521-019-04314-6

Mata, F., Beamud, E., Hanafi, I., Khamlichi, A., Jabbouri, A., & Bezzazi, M. (2010). Multiple regression prediction model for cutting forces in turning carbon-reinforced PEEK CF30. *Advances in Materials Science and Engineering*, *2010*. https://doi.org/10.1155/2010/824098

Mohanty, A. K., Misra, M., & Hinrichsen, G. (2000). Biofibres, biodegradable polymers and

biocomposites: An overview. *Macromolecular Materials and Engineering*, *276–277*, 1–24. https://doi.org/10.1002/(SICI)1439-2054(20000301)276:1<1::AID-MAME1>3.0.CO;2-W

Moll, L., Wever, C., Völkering, G., & Pude, R. (2020). Increase of Miscanthus cultivation with new roles in materials production—a review. *Agronomy*, *10*(2), 8–11. https://doi.org/10.3390/agronomy10020308

Muthuraj, R., Misra, M., Defersha, F., & Mohanty, A. K. (2016). Influence of processing parameters on the impact strength of biocomposites: A statistical approach. *Composites Part A: Applied Science and Manufacturing*, *83*, 120–129. https://doi.org/10.1016/j.compositesa.2015.09.003

Muthuraj, R., Misra, M., & Mohanty, A. K. (2017). Biocomposite consisting of miscanthus fiber and biodegradable binary blend matrix: compatibilization and performance evaluation. *RSC Advances*, *7*(44), 27538–27548. https://doi.org/10.1039/c6ra27987b

Nagarajan, V., Mohanty, A. K., & Misra, M. (2013). Sustainable green composites: Value addition to agricultural residues and perennial grasses. *ACS Sustainable Chemistry and Engineering*, *1*(3), 325–333. https://doi.org/10.1021/sc300084z

Nassar, M. M. A., Arunachalam, R., & Alzebdeh, K. I. (2017). Machinability of natural fiber reinforced composites: a review. *International Journal of Advanced Manufacturing Technology*, *88*(9–12), 2985–3004. https://doi.org/10.1007/s00170-016-9010-9

Navaneethakrishnan, S., & Athijayamani, A. (2016). Measurement and analysis of thrust force and torque in drilling of sisal fiber polymer composites filled with coconut shell powder. *International Journal of Plastics Technology*, *20*(1), 42–56. https://doi.org/10.1007/s12588-016-9139-2

Ogunsona, E. O., Codou, A., Misra, M., & Mohanty, A. K. (2019). A critical review on the fabrication processes and performance of polyamide biocomposites from a biofiller perspective. *Materials Today Sustainability*, *5*. https://doi.org/10.1016/j.mtsust.2019.100014

Ogunsona, Emmanuel O., Misra, M., & Mohanty, A. K. (2017a). Impact of interfacial adhesion on the microstructure and property variations of biocarbons reinforced nylon 6 biocomposites. *Composites Part A: Applied Science and Manufacturing*, *98*, 32–44. https://doi.org/10.1016/j.compositesa.2017.03.011

Ogunsona, Emmanuel O., Misra, M., & Mohanty, A. K. (2017b). Sustainable biocomposites from biobased polyamide 6,10 and biocarbon from pyrolyzed miscanthus fibers. *Journal of Applied Polymer Science*, *134*(4), 1–11. https://doi.org/10.1002/app.44221

Pailoor, S., Murthy, H. N. N., & Sreenivasa, T. N. (2019). Drilling of In-Line Compression Molded Jute / Polypropylene Composites. *Journal of Natural Fibers*, *0478*.

https://doi.org/10.1080/15440478.2019.1612309

Palanikumar, K., & Valarmathi, T. N. (2016). Experimental Investigation and Analysis on Thrust Force in Drilling of Wood Composite Medium Density Fiberboard Panels. *Experimental Techniques*, *40*(1), 391–400. https://doi.org/10.1007/s40799-016-0044-6

Peças, P., Carvalho, H., Salman, H., & Leite, M. (2018). Natural Fibre Composites and Their Applications: A Review. *Journal of Composites Science*, *2*(4), 66. https://doi.org/10.3390/jcs2040066

Pickering, K. L., Efendy, M. G. A., & Le, T. M. (2016). A review of recent developments in natural fibre composites and their mechanical performance. *Composites Part A: Applied Science and Manufacturing*, *83*, 98–112. https://doi.org/10.1016/j.compositesa.2015.08.038

Prakash, S., Mercy, J. L., & Goswami, K. (2014). A systemic approach for evaluating surface roughness parameters during drilling of medium density fiberboard using Taguchi method. *Indian Journal of Science and Technology*, *7*(11), 1888–1894. https://doi.org/10.17485/ijst/2014/v7i11/51413

Ragoubi, M., George, B., Molina, S., Bienaimé, D., Merlin, A., Hiver, J. M., & Dahoun, A. (2012). Effect of corona discharge treatment on mechanical and thermal properties of composites based on miscanthus fibres and polylactic acid or polypropylene matrix. *Composites Part A: Applied Science and Manufacturing*, *43*(4), 675–685. https://doi.org/10.1016/j.compositesa.2011.12.025

Rajmohan, T., Vinayagamoorthy, R., & Mohan, K. (2019). Review on effect machining parameters on performance of natural fibre–reinforced composites (NFRCs). *Journal of Thermoplastic Composite Materials*, *32*(9), 1282–1302. https://doi.org/10.1177/0892705718796541

Rezghi Maleki, H., Hamedi, M., Kubouchi, M., & Arao, Y. (2019). Experimental investigation on drilling of natural flax fiber-reinforced composites. *Materials and Manufacturing Processes*, *34*(3), 283–292. https://doi.org/10.1080/10426914.2018.1532584

Rezghi Maleki, Hadi, Hamedi, M., Kubouchi, M., & Arao, Y. (2019). Experimental study on drilling of jute fiber reinforced polymer composites. *Journal of Composite Materials*, *53*(3), 283–295. https://doi.org/10.1177/0021998318782376

Roy Choudhury, M., Srinivas, M. S., & Debnath, K. (2018). Experimental investigations on drilling of lignocellulosic fiber reinforced composite laminates. *Journal of Manufacturing Processes*, *34*(June 2017), 51–61. https://doi.org/10.1016/j.jmapro.2018.05.032

Saidi, M. N., Songmene, V., Kouam, J., & Bahloul, A. (2015). Experimental investigation on

fine particle emission during granite polishing process. *International Journal of Advanced Manufacturing Technology*, *81*(9–12), 2109–2121. https://doi.org/10.1007/s00170-015-7303-z

Saidi, M. N., Songmene, V., Kouam, J., & Bahloul, A. (2019). Study of surface quality and dust particles emission and dispersion during dry polishing of granite. *International Journal of Advanced Manufacturing Technology*, *104*(9–12), 4675–4684. https://doi.org/10.1007/s00170-019-04166-3

Salit, M. S., Jawaid, M., Yusoff, N. Bin, & Hoque, M. E. (2015). Manufacturing of natural fibre reinforced polymer composites. In *Manufacturing of Natural Fibre Reinforced Polymer Composites*. https://doi.org/10.1007/978-3-319-07944-8

Samanta, B., Erevelles, W., & Omurtag, Y. (2008). Prediction of workpiece surface roughness using soft computing. *Proceedings of the Institution of Mechanical Engineers, Part B: Journal of Engineering Manufacture*, *222*(10), 1221–1232. https://doi.org/10.1243/09544054JEM1035

Savas, V., & Ozay, C. (2008). The optimization of the surface roughness in the process of tangential turn-milling using genetic algorithm. *International Journal of Advanced Manufacturing Technology*, *37*(3–4), 335–340. https://doi.org/10.1007/s00170-007-0984-1

Savkovic, B., Kovac, P., Dudic, B., Rodic, D., Taric, M., & Gregus, M. (2019). Application of an adaptive "neuro-fuzzy" inference system in modeling cutting temperature during hard turning. *Applied Sciences (Switzerland)*, *9*(18). https://doi.org/10.3390/app9183739

Sen, B., Mandal, U. K., & Mondal, S. P. (2017). Advancement of an intelligent system based on ANFIS for predicting machining performance parameters of Inconel 690 – A perspective of metaheuristic approach. *Measurement: Journal of the International Measurement Confederation*, *109*, 9–17. https://doi.org/10.1016/j.measurement.2017.05.050

Sheikh-Ahmad, J. Y. (2009). Machining of polymer composites. In *Machining of Polymer Composites*. https://doi.org/10.1007/978-0-387-68619-6

Shivakoti, I., Kibria, G., Pradhan, P. M., Pradhan, B. B., & Sharma, A. (2019). ANFIS based prediction and parametric analysis during turning operation of stainless steel 202. *Materials and Manufacturing Processes*, *34*(1), 112–121. https://doi.org/10.1080/10426914.2018.1512134

Snowdon, M. R., Wu, F., Mohanty, A. K., & Misra, M. (2019). Comparative study of the extrinsic properties of poly(lactic acid)-based biocomposites filled with talc: Versus sustainable biocarbon. *RSC Advances*, *9*(12), 6752–6761. https://doi.org/10.1039/c9ra00034h

Songmene, V., Kouam, J., & Bahloul, A. (2018). Effect of minimum quantity lubrication (MQL) on fine and ultrafine particle emission and distribution during polishing of granite. *Measurement: Journal of the International Measurement Confederation*, *114*(June 2017), 398–408. https://doi.org/10.1016/j.measurement.2017.10.012

Songmene, V., Balout, B., & Masounave, J. (2008a). Clean machining : experimental investigation on dust formation: Part I : influence of machining parameters and chip formation. *International Journal of Environmentally Conscious Design & Manufacturing*, *14*(1), 1–16.

Songmene, V., Balout, B., & Masounave, J. (2008b). Clean machining : experimental investigation on dust formation: Part II : influence of machining strategies and drill condition. *International Journal of Environmentally Conscious Design & Manufacturing*, *14*(1), 17–33.

Subramanian, M., Sakthivel, M., Sooryaprakash, K., & Sudhakaran, R. (2013). Optimization of cutting parameters for cutting force in shoulder milling of Al7075-T6 using response surface methodology and genetic algorithm. *Procedia Engineering*, *64*, 690–700. https://doi.org/10.1016/j.proeng.2013.09.144

Szwajka, K., Zielińska-Szwajka, J., & Trzepiecinski, T. (2019). Experimental study on drilling MDF with tools coated with TiAlN and ZrN. *Materials*, *12*(3). https://doi.org/10.3390/ma12030386

Tran, D. S., Songmene, V., Ngo, A. D., Kouam, J., Rodriguez-Uribe, A., Misra, M., & Mohanty, A. K. (2020). Experimental investigation on machinability of polypropylene reinforced with miscanthus fibers and biochar. *Materials*, *13*(5). https://doi.org/10.3390/ma13051181

Venkateshwaran, N., & ElayaPerumal, A. (2013). Hole quality evaluation of natural fiber composite using image analysis technique. *Journal of Reinforced Plastics and Composites*, *32*(16), 1188–1197. https://doi.org/10.1177/0731684413486847

Vinayagamoorthy, R. (2017). Parametric optimization studies on drilling of sandwich composites using the Box–Behnken design. *Materials and Manufacturing Processes*, *32*(6), 645–653. https://doi.org/10.1080/10426914.2016.1232811

Vinayagamoorthy, R., & Rajmohan, T. (2018). Machining and its challenges on bio-fibre reinforced plastics: A critical review. *Journal of Reinforced Plastics and Composites*, *37*(16), 1037–1050. https://doi.org/10.1177/0731684418778356

Voss, R., Seeholzer, L., Kuster, F., & Wegener, K. (2017). Influence of fibre orientation, tool geometry and process parameters on surface quality in milling of CFRP. *CIRP Journal of Manufacturing Science and Technology*, *18*, 75–91. https://doi.org/10.1016/j.cirpj.2016.10.002

Wang, T., Rodriguez-Uribe, A., Misra, M., & Mohanty, A. K. (2018). Sustainable

Carbonaceous Biofiller from Miscanthus: Size Reduction, Characterization, and Potential Bio-composites Applications. *BioResources*, *13*(2), 3720–3739. https://doi.org/10.15376/biores.13.2.3720-3739

Yallew, T. B., Kumar, P., & Singh, I. (2016). A study about hole making in woven jute fabric-reinforced polymer composites. *Proceedings of the Institution of Mechanical Engineers, Part L: Journal of Materials: Design and Applications*, *230*(4), 888–898. https://doi.org/10.1177/1464420715587750

Zaghbani, I., Songmene, V., & Khettabi, R. (2009). Fine and ultrafine particle characterization and modeling in high-speed milling of 6061-T6 aluminum alloy. *Journal of Materials Engineering and Performance*, *18*(1), 38–48. https://doi.org/10.1007/s11665-008-9265-x

Zain, A. M., Haron, H., & Sharif, S. (2010). Application of GA to optimize cutting conditions for minimizing surface roughness in end milling machining process. *Expert Systems with Applications*, *37*(6), 4650–4659. https://doi.org/10.1016/j.eswa.2009.12.043

Zhang, K., Nagarajan, V., Zarrinbakhsh, N., Mohanty, A. K., & Misra, M. (2014). Co-injection molded new green composites from biodegradable polyesters and miscanthus fibers. *Macromolecular Materials and Engineering*, *299*(4), 436–446. https://doi.org/10.1002/mame.201300189